Molecular and Functional Characterization of a Novel Alcohol Oxidase From *Aspergillus terreus* MTCC6324

A Thesis

Submitted by

MITUN CHAKRABORTY

For the award of the degree

Of

DOCTOR OF PHILOSOPHY

Department of Biotechnology
Indian Institute of Technology Guwahati
Guwahati 781039, Assam, India

March, 2014

Dedication

I hereby dedicate my PhD thesis to my beloved Parents……

Department of Biotechnology

Indian Institute of Technology Guwahati

STATEMENT

I do hereby declare that the matter embodied in this thesis is the result of investigations carried out by me in the Department of Biotechnology, Indian Institute of Technology Guwahati, India, under the supervision of Prof. Pranab Goswami and co-supervision of Prof. Siddhartha Sankar Ghosh.

In keeping with the general practice of reporting scientific observations, due acknowledgements have been made wherever the work described is based on the findings of other investigators.

March, 2014

Mitun Chakraborty

(Roll No: 09610601)

Acknowledgement

"All power is within you, you can do anything and everything…believe in that." – Swami Vivekananda. Swamiji's preachings had always motivated me since childhood. My mother first gave me a photograph of him to keep along as a moral support, little did I know then that the much unwanted gesture of my mother with a simple picture and a two line proverb of Swamiji can have the potential to change and motivate my life in such a positive way.

Yes!.. Finally I have completed my Ph.D and earned my Doctoral degree. The journey of a common mediocre student to India's premiere engineering institute "Indian Institute of Technology Guwahati (IITG)" involved well wishes and blessings of family, friends, teachers and people who have motivated me even for once in my career. I wish to express my deep sense of gratitude to my supervisor Prof. Pranab Goswami for his constant encouragement, time, ideas and above all freedom to do research work in a state-of-the-art research laboratory which was a productive and stimulating experience. His optimistic overlook to research and teaching is truly inspiring for me. I am also grateful to my co-supervisor Prof. Siddhartha Sankar Ghosh for his Support throughout my research work. Down to earth student friendly nature made him approachable for suggestions even for minute problems. I am much thankful to my Doctoral committee chairman Dr. Anil Mukund Limaye for his interesting questions and critically evaluating my research work. I am extremely grateful to my other distinguished Doctoral committee member Dr. Biplab Bose. His dedication, critical reasoning and troubleshooting a research problem makes him a true researcher. His valuable suggestions often gave a whole new perception to my work. Apart from being my Doctoral committee member he also taught me an exciting new field of system's biology during my Ph.D coursework. Last but not the least Prof. Anil Kumar Saikia for his constant support as a doctoral committee member during the entire tenure of my Ph.D work.

The thesis would not have come to a successful completion without the help and support of my lab seniors Dr. Preety Vatsyayan and Dr. Urmila Saxena. Their Selfless support, co-

operation and help during the initial phase of my phd made me accustomed to the lab environment and research work. I am highly indebted to my lab members, Seraj, Madhuri, Somashekhar, Ankana, Santhosh, Babina, Priyamvada, Priyanki, Mrinal, Sharbani, Naveen and Danish for their kind co-operation and making my research in lab memorable and fun loving. I am grateful to Mr. Manish Goel (B-Tech project student) and Ujjwal Ranjan Dahiya (M-Tech project student) for their significant contribution in completing my Ph.D thesis work. I am thankful to my co-supervisor's students Kokila, Amit, Subhamoy, Amaresh, Nidhi, Chokalingam, Archita, Sharmila, Asif, Neha and Upashi as well for extending a helping hand during the tenure of my research work and making me feel as a part of their own research group. During a man's journey to achieve his dreams, there come friends who motivates you and become part of life forever. Few friends starting from B.Tech college life, Aziz-ur-Rahman; M.Tech college life, Nillohit and PhD mates, Paramartha, Digar, Ayan, Soumyadeep, Arghya and Dipendra are worthy to be acknowledged. Being Friends, batchmates and juniors each one had a different role to play during my ups and downs in campus life. Time spent with them in campus was excellent and will always be treasured. Lokesh had been a great friend in IIT Guwahati, worthy of being acknowledged as "a friend in need a friend indeed". He is a humble, caring and over-all a great human being, I will continue to cherish his friendship throughout my life.

My sincere thanks goes out to Ms. Deeplina for being a good friend since my M-Tech days and also as a Ph.D batch mate in IIT Guwahati. I am indebted to my past and present seniors, Dr Ashim Bikash Das, Mr. Manab Deb Adhikary and Mr. Pojul Loying for their useful suggestions and helping me out initially with some critical experiments. It would be unfair, not to mention nice conversations during evening snacks with a cup of hot tea, discussing from academics to politics with Sukhamoy (Ph.D Scholar). It was surely a refreshing moment after a daylong tiring work schedule. I pass my hearty gratitude to Rakesh and Pranjal for being great friends throughout and showing their concern during difficult times in IIT Guwahati. Time was different with Rohit Gaurav (B-Tech student), my wall mate during his doubt solving sessions on different aspects of biotechnology.

I would not have achieved my dream of getting a Doctoral degree lagging proper guidance provided by my teachers. I would like to convey my gratitude to Late Shri. Kishalaya

Ghosh, my arts teacher from 7th - 10th standard who taught me to dream big and accomplish the dream through honesty and dignity. I would like to pay my respect to Prof. Chandralekha Dutta Gupta (Ex. H.O.D, Dept. of Biotechnology, Institute of Technology and Marine Engineering, West Bengal, India) of my B-Tech college for initiating my interest in biotechnology and arousing in me the awareness to do quality research for betterment of mankind. I am highly indebted to Dr. Sharmila Chattopadhyay (Senior Scientist, Indian Institute of Chemical Biology, a C.S.I.R lab, Kolkata, West Bengal, India) for giving me an opportunity, to do my B-Tech summer internship in her lab, where I learned to do systematic and serious research work for the first time. My sincere thanks to Dr. Provash Chandra Sadhukhan (Scientist B, Indian Council of Medical Research Virus Unit, Kolkata, West Bengal, India) for his inspiration which installed in me the strength to do my M-Tech and Ph.D degree. I extend my deep sense of gratitude to my M-Tech supervisor Dr. Nandan Kumar Jana (Assistant Professor, Dept. of Biotechnology, Heritage Institute of Technology, Kolkata, West Bengal, India) and co-supervisor Prof. Subrata Sau (Professor, Dept. of Biochemistry, Bose Institute, Kolkata, West Bengal, India) for guiding my M-Tech project work which was a true learning experience.

Last but not the least, I express my deepest gratitude to my parents, Mr. Shyamal Chakraborty and Mrs. Chhanda Chakraborty for bringing me onto this earth and teaching me the values of honesty, hard work and sincerity. Their undying love, support and encouragement throughout my life, installed in me the spirit of overcoming any obstacle and heightened my strength to achieve my dream in life. Above all I thank God almighty for blessing me throughout my career till date. I would like to end with few lines from one of the prominent literary work "Geetanjali"; which gave me immense strength all throughout my Ph.D and will continue to do so in future.

"Where the mind is without fear and the head is held high;
Where the mind is lead forward by thee into
Ever-widening thought and action;
Into that heaven of freedom, my Father,
Let my country awake…" -Rabindranath Tagore.

March, 2014 Mitun Chakraborty

Contents

List of Abbreviations and Symbols..... **i**

List of Figures…… **vii**

List of Tables…….. **xii**

Abstract…… **xiii**

Chapter 1: Introduction…… **1**

Chapter 2: Literatue Review…… **4-15**

2.1: Alcohol oxidase: Discovery and detection methods..... **4**

2.2: Types of alcohol oxidases……. **4**

2.2.1: Short chain alcohol oxidase……..... **5**

2.2.2: Long chain alcohol oxidase……..... **7**

2.2.3: Aromatic alcohol oxidase……. **9**

2.2.4: Secondary alcohol oxidase……. **12**

2.3: Characteristics of *Aspergillus terreus*……... **13**

2.4: Current protocols to characterize novel genes in filamentous fungi…….. **14**

Chapter 3: Materials and Experimental Methodologies……..... **16-61**

3.A: Materials…….. **16**

3.B: Experimental Methodologies……. **16-61**

3.B.1: Molecular characterization of alcohol oxidase gene from *Aspergillus terreus*

MTCC6324……..... **16-36**

3.B.1.1: Growth and maintenance of microorganisms…. **16**

3.B.1.2: Isolation and optimization of total RNA from *A.terreus* MTCC6324……. **17**

3.B.1.3: Quantification of RNA..…….. **18**

3.B.1.4: Formaldehyde denaturing agarose gel electrophoresis……..... **18**

3.B.1.5: Reverse-transcriptase polymerase chain reaction (RT-PCR) based first strand cDNA synthesis……..... **19**

3.B.1.6: Checking the integrity of RNA…… **20**

3.B.1.7: Preparation of *A. terreus* MTCC6324 microsomal protein extracts……..... **20**

3.B.1.8: Activity assay of alcohol oxidase…… **22**

3.B.1.9: Protein estimation by Bradford assay…….. **23**

3.B.1.10: Two dimentional (2D) gel electrophoresis…….. **23**

3.B.1.11: Mass spectrometry compatible silver staining of SDS-PAGE gel……. **24**

3.B.1.12: Target protein identification from 2D gel spots……..... **24**

3.B.1.13: Peptide mass fingerprinting database search….. **26**

3.B.1.14: Multiple sequence alignment (msa) of reported AOxs from fungal and yeast species……... **27**

3.B.1.15: Designing overlapping PCR primer probes to amplify the coding sequence of AOx…….. **27**

3.B.1.16: Overlapping PCR……. **28**

3.B.1.17: Agarose gel electrophoresis of DNA…….. **29**

3.B.1.18: Elution of DNA samples from agarose gel……. **29**

3.B.1.19: Cloning PCR amplicons in pGEM-T Easy T/A vector system…….. **30**

3.B.1.20: Quantification of DNA…… **31**

3.B.1.21: Competent *E.coli* cells preparation…….. **31**

3.B.1.22: Transformation of competent *E.coli* cells…..... **32**

3.B.1.23: Plasmid DNA isolation…… **33**

3.B.1.24: Digestion of DNA by restriction enzymes…….. **34**

3.B.1.25: Characterization of full length ORF of AOx from overlapping PCR product……..... **34**

3.B.1.26: DNA sequencing of cloned fragments……. **35**

3.B.2: Sub-cloning, and expression of recombinant alcohol oxidase protein in *E.coli*…… 37-41

3.B.2.1: PCR amplification of AOx fragment from AOx cloned pGEM-T Easy vector……..... **37**

3.B.2.2: Ligation of PCR amplified AOx fragment to pET28a(+) bacterial expression system……..... **38**

3.B.2.3: Expression of histidine tagged rAOx as apoenzyme in *E.coli* BL21(DE3)…….. **39**

3.B.2.4: SDS-PAGE of protein……..... **40**

3.B.3: Isolation, solubilization and purification of apo-rAOx from inclusion bodies and reconstitution with co-factor FAD……..... 42-46

3.B.3.1: Isolation, purification and solubilization of

	apo-rAOx from inclusion bodies…….....	**42**
3.B.3.2:	Purification of solubilized rAOx by nickel affinity chromatography…….....	**43**
3.B.3.3:	Western blot analysis…….....	**44**
3.B.3.4:	In-vitro refolding and reconstitution of apo-rAOx with co-factor FAD…….	**45**
3.B.4:	**Biophysical characterizations of rAOx**.....	**47-53**
3.B.4.1:	MALDI-TOF/TOF mass spectrometry of apo-rAOX……..	**47**
3.B.4.2:	Determining isoelectric point (pI) of rAOx by 2-D electrophoresis……...	**49**
3.B.4.3:	Determining isoelectric point (pI) of rAOx by Zeta potential……	**49**
3.B.4.4:	Fluorimetric identification of free FAD and rAOx-FAD holoenzyme in refolding buffer……....	**50**
3.B.4.5:	Circular dichroism (CD) spectroscopy measurement……..	**51**
3.B.4.6:	Studying the aggregation potential through Dynamic Light Scattering (DLS) analysis of rAOx……..	**52**
3.B.5:	***In-silico* studies of recombinant alcohol oxidase**……...	**54-57**
3.B.5.1:	*In-silico* sequence analysis of AOx from *A.terreus* MTCC6324……	**54**
3.B.5.2:	*Ab-initio* based rAOx protein structure	

prediction……..... **54**

3.B.5.3: Checking the stereo-chemical quality of predicted rAOx through Ramachandran plot….. **55**

3.B.5.4: Molecular docking studies with predicted model of rAOx……... **56**

3.B.6: Functional characterization of recombinant bioactive alcohol oxidase..... **58-61**

3.B.6.1: Determining enzyme activity and kinetics…….. **58**

3.B.6.2: Determining the Activation energy (E_a), enthalpy (ΔH), free energy (ΔG) and entropy (ΔS) of rAOx…… **59**

3.B.6.3: Measuring the half life and decimal reduction values of rAOx…… **61**

Chapter 4: Results and Discussions..... **62-110**

4.A: Results..... **62-106**

4.A.1: Identification of AOx gene from *A.terreus* MTCC6324 ……..... **62-72**

4.A.1.1: mRNA isolation and preparation of cDNA …… **63**

4.A.1.2: Designing primers from the peptide sequences of AOx protein …….. **63**

4.A.1.3: Construction of full length AOx gene by overlapping PCR approach…… **65**

4.A.2: Over-expression of apo-rAOx in *E.coli* BL21(DE3) and subsequent *in- vitro* refolding of the purified apo-protein

isolated from the inclusion bodies..... **73-77**

4.A.2.1: Sub-cloning AOx gene into bacterial expression system pET28a (+)…….. **73**

4.A.2.2: Expression, purification and in-vitro activation of rAOx……..... **73**

4.A.3: Characterizations of physicochemical properties of rAOx…….. **78-87**

4.A.3.1: Characterization of apo-rAOx mass…….. **78**

4.A.3.2: Isoelectric point (p*I*) of rAOx……..... **78**

4.A.3.3: Reconstitution of apo-rAOx with co-factor FAD through fluorescence spectrophotometry……. **79**

4.A.3.4: Analysis of secondary structure of the rAOx... **79**

4.A.3.5: Studies on the aggregating nature of rAOX…. **79**

4.A.4: *In-silico* studies on rAOx for sequence to structure and function paradigm ……..... **88-98**

4.A.4.1: *In-silico* sequence analysis of rAOx……. **88**

4.A.4.2: Molecular modeling and docking studies of rAOx……..... **89**

4.A.5: Steady state kinetics and thermo-inactivation studies of rAOx ……. **99-106**

4.A.5.1: Enzyme activity and kinetic studies of AOx…….. **99**

4.A.5.2: Activation energy of rAOx……... **100**

4.A.5.3: Thermoinactivation studies of rAOx…… **100**

4.B: Discussions..... **107-110**

Chapter 5: Conclusion and Future Directions of Research …..….. **111-112**

5A: Conclusion……. **111**

5B: Future Direction of Research……. **112**

Bibliography……... **113-127**

Appendix……. **128-136**

Publications……... **137-138**

List of Abbreviations and Symbols

×*g*……..	Relative centrifugal force
µA……..	Microampere
µg……..	Microgram
µl……...	Microliter
µmol……...	Micromoles
2,6DCPIP……...	2,6-dichlorophenol-indophenol
6xHis……..	Six histidine residues
Å……	Angstrom
AAO……..	Aromatic alcohol oxidase
ABTS…….	2,2′-azino-bis[3-ethylbenzothiazoline-6-sulphonic acid]
ADH……..	Alcohol dehydrogenase
AOx…….....	Alcohol oxidase enzyme
apo-rAOx……	Apoenzyme recombinant alcohol oxidase
bp……..	Base pair
BSA……...	Bovine serum albumin
CAD……...	*Cis*-aconitic acid decarboxylase
cAOx……..	Commercial alcohol oxidase
CD…….	Circular dichroism

cDNA…….	Complementary DNA
CHAPS……...	3-[(3 Cholamidopropyl) dimethylammonio]-1-propane sulfonate
CHCA…….	α-Cyano-4-hydroxycinnamic acid
ChOx/ COX ……	Cholesterol oxidase
CPK……	Corey-Pauling-Koltun
C-score…….....	Confidence score
CTAB…….	Cetyl trimethylammonium bromide
Cyt P450…….	Cytochrome P450
Da……..	Daltons
DAB……...	3, 3'-Diaminobenzidine
DEPC…….	Diethylpyrocarbonate
DLS……	Dynamic light scattering
DMSO…….....	Dimethyl sulfoxide
DNA……..	Deoxyribonucleic acid
dNTP……..	Deoxyribonucleotide triphosphate
DTT…….....	Dithiothreitol
EC …….	Enzyme Commission
FAD…….....	Flavin adenine dinucleotide
FAO……...	Fatty alcohol oxidase
GAPDH……..	Glyceraldehyde 3 phosphate dehydrogenase
GI ……..	Gene identification number
gla1……	Glucoamylase

GMC……..	Glucose-methanol-choline
GOX……...	Glucose oxidase
GSSG…….	Glutathione oxidized
h……	Hour
His-tag……	Histidine tagged
HRP……	Horse radish peroxidase
IgG…….	Immunoglobulin G
IPTG……...	Isopropyl β-D-1-thiogalactopyranoside
J……	Joules
K……	Kelvin
k_{cat}…….	Catalytic turn-over number
kDa……	Kilo Dalton
kJ……...	Kilojoules
K_m……..	The Michaelis-Menten constant
LCAO……....	Long chain alcohol oxidase
LMF……...	Light mitochondrial fraction
ln……...	Natural logarithm
m/z……	Mass by charge
MALDI-TOF-MS…….	Matrix assisted laser desorption ionization-time of flight-mass spectrometry
MF……	Microsomal fraction
mFAD…….	Modified Flavin adenine dinucleotide
mg……..	Milligram

min…….	Minute
ml……...	Milliliter
mM…….	Millimolar
MOPS…….	3-(*N*-morpholino) propane sulfonic acid
msa…….	Multiple sequence alignment
MTCC…….	Microbial type culture collection
mV…….	Millivolt
M_w…….	Molecular weight
NAD^+…….	Nicotinamide adenine dinucleotide (oxidized)
NADH……	Nicotinamide adenine dinucleotide (reduced)
NADP+……...	Nicotinamide adenine dinucleotide phosphate (oxidized)
NADP…….	Nicotinamide adenine dinucleotide phosphate
NADPH……..	Nicotinamide adenine dinucleotide phosphate (reduced)
NCBI……..	National Center for Biotechnology Information
ng……...	Nanogram
NIH……...	National Institute of Health
nm……..	Nanometer
O.D…….....	Optical density
ORF……	Open reading frame
PAO……...	Polyvinyl alcohol oxidase
PBS……	Phosphate buffer saline
PBS-T…….	Phosphate buffer saline-Tween 20

PCMB…….	*ρ*-chloromercuribenzoate
PCR……	Polymerase chain reaction
PDB……	Protein Data Bank
p*I*……...	Isoelectric point
Pmf……	Peptide mass fingerprint
pmol……...	Picomoles
PMSF…….	Phenylmethanesulfonyl fluoride
PVA……...	Polyvinyl alcohols
PVDF…….	Polyvinylidene difluoride
rAOx……..	Recombinant alcohol oxidase
RMSD……	Root mean square deviation
RNA……..	Ribonucleic acid
rpm…….	Revolutions per minute
RT……..	Room temperature
SAO……...	Secondary alcohol oxidase
SCAO…….....	Short chain alcohol oxidase
SDS……	Sodium Dodecyl Sulphate
SDS-PAGE…….	Sodium dodecyl sulphate-polyacrylamide gel electrophoresis
TAE……...	Tris-acetate EDTA
TM-score…….	Template modeling score
TSS……	Transformation and storage solution
u……	Units

v/v……	Volume by volume
VAO……..	Vanillyl alcohol oxidase
V_{max}……	Maximal rate of the reaction
w/v……	Weight by volume
X-Gal……..	5-bromo-4-chloro-3-indolyl-beta-D-galacto-pyranoside
λ ……	Wavelength
µM……	Micro molar

List of Figures

Figure no.	Title	Page
1	Reaction mechanism of AOx and ADH as catalyst……	**2**
3.1	Schematic overview of differential centrifugation approach for the isolation of *A.terreus* microsomal protein extract ……..	**21**
3.2	Schematic of horseradish peroxidase based coupled assay method for detecting AOx activity ……	**22**
3.3	An experimental overview of steps involved in target protein identification from 2D gel by MALDI-TOF-MS…….....	**26**
3.4	An overall schematic diagram highlighting the proteomics and genomics approach undertaken to characterize AOx cDNA……...	**28**
3.5	An overview of overlapping PCR approach ……...	**32**
3.6	Schematic showing the experimental methodology to confirm the orientation of the individual PCR fragments cloned in T/A vector and ligation cloning in T/A vector……..	**35**
3.7	An overview of sub-cloning full length AOx fragment from pGEM-T Easy to *E.coli* expression system pET28a (+)…….	**39**
3.8	Experimental overview of inclusion body isolation, purification and solubilization of over-expressed rAOX……...	**43**
3.9	A schematic overview showing *in*-vitro refolding of apo-rAOx with its co-factor FAD in refolding buffer……...	**46**

3.10	An overview of experimental steps involved in identification of mass and sequence coverage of rAOx by MALDI-TOF/TOF mass spectrometry…….....	**48**
3.11	Diagram showing the ionic concentration and potential difference as a function of distance from the charged surface of a protein…….	**50**
3.12	A schematic overview of studying the aggregation pattern of rAOx while it's refolding in refolding buffer after a regular interval of 24 h for 96 h duration…….....	**53**
3.13	A schematic representation of I-TASSER algorithm for protein structure and function prediction…….....	**55**
3.14	An overall schematic of the algorithm followed by Molegro Virtual Docker for our docking simulation studies……..	**57**
3.15	A schematic overview of determining the rAOX activity and kinetic parameters……	**59**
3.16	Activation energy plot of an enzyme……...	**60**
4.1	Formaldehyde agarose gel electrophoresis of total RNA isolated from *A.terreus* MTCC6324 following five standard isolation techniques…...	**68**
4.2	GAPDH house-keeping gene amplicons by PCR amplification from the total RNA……...	**68**
4.3	(A) 2D electrophoresis of microsomal membrane bound proteins and (B) multiple sequence alignment of highly similar AOx proteins from filamentous fungi and yeast species showing the primers for overlapping PCR……..	**69**
4.4	Amplicons obtained by overlapping PCR using cDNA of *A. terreus* MTCC 6324 as a template……...	**70**

4.5	Checking the orientation of the cloned PCR fragments (PCR 1 & 2) in T/A cloning vector through double restriction……	**70**
4.6	Restriction digestion pattern of ligated overlapping PCR fragments in T/A vector with *EcoR*I restriction enzyme……..	**71**
4.7	Pair-wise sequence alignment of primer walking DNA sequence with the hypothetical, unreviewed AOx sequence information from *A. terreus* NIH strain at nucleotide and amino acid level……	**71**
4.8	Nucleotide and deduced amino acid sequence of AOx from *A.terreus* MTCC6324……..	**72**
4.9	Qualitative agarose gel for PCR amplification of full length AOx from T/A vector……	**75**
4.10	Confirmation of full length clone of AOx in pET28a (+) with double digestion……...	**75**
4.11	SDS-PAGE profile on expression of rAOx in *E.coli* BL21 (DE3) under different (A) IPTG concentration, time and (B) temperature of induction……..	**76**
4.12	(A) Purification profile of apo-rAOx and (B) western blot analysis…...	**77**
4.13	MALDI–TOF/TOF analysis of rAOx……..	**82**
4.14	Determination of the isoelectric point (p*I*) of rAOx through (A) 2D electrophoresis and (B) Zeta potential studies…….	**83**
4.15	Fluorescence emission maxima ($\lambda_{\sim 527\ nm}$) of free FAD and FAD reconstituted holoenzyme (rAOx) at an excitation of λ_{443nm}…….	**84**
4.16	Dichroic spectra of rAOx in different pH environment after incubating the samples for ~80 h at 16 °C…….	**84**

4.17	DLS analysis of rAOx, cAOx from *Pichia pastoris* and BSA for (A) 0 h, (B) 24 h, (C) 48h, (D) 72 h and (E) 96 h incubation, respectively at 16 °C……	**85-87**
4.18	NCBI conserve domain search with rAOx amino acid sequence as a query input……...	**92**
4.19	(A) N-terminal multiple sequence alignment of AOx coding amino acid sequences from 11 species of filamentous fungi and yeast species and (B) Phylogenetic tree of the corresponding AOxs by Neighbour - Joining method……	**92**
4.20	mRNA to genomic alignment using NCBI spidey……..	**93**
4.21	The best 3D model of rAOx as predicted by I-TASSER online protein structure prediction software……...	**93**
4.22	Ramachandran plot of predicted AOx model by PROCHECK……..	**94**
4.23	I-TASSER predicted *ab-initio* model of apo-rAOx docked with its co-factor FAD……...	**95**
4.24	(A) 3D superimposition of best pose of FAD predicted in our docking simulation with modeled AOx and (B) Protein 3D superimposition of FAD bound crystal structure of aryl AOx (PDB id: 3FIM) with FAD docked modeled AOx…….	**96**
4.25	FAD bound AOx docked with (A) *ρ*-methoxybenzyl alcohol, (B) *m*-methoxybenzyl alcohol (C) 3,4 dimethoxybenzyl alcohol and (D) benzyl alcohol……..	**97**
4.26	Docking view of aromatic alcohols (A) *ρ*-methoxybenzyl alcohol, (B) *m*-methoxybenzyl alcohol (C) 3,4 dimethoxybenzyl alcohol and (D) benzyl alcohol, as substrates with FAD docked apo-rAOx holoenzyme	

complex..... **98**

4.27 Studies on (A) temperature, (B) pH optima, (C) thermal and (D) pH stability of rAOx…….. **104**

4.28 Effect of temperature on purified refolded rAOx activity from 20-65 °C showing Arrhenius plot (A) as inset……... **105**

4.29 Temperature dependence of the thermo-inactivation constant of purified refolded rAOx…… **105**

4.30 Temperature dependence of the decimal reduction value (*D*-value) of the purified rAOx……. **106**

List of Tables

Table no.	Title	Page
4.1	Quantification of total RNA isolated from *A.terreus* MTCC 6324 by different protocols……	**66**
4.2	Identification of internal conserved amino acid sequence blocks by homology study between the pmf fragments and NCBI database of AOx hypothetical peptide sequences……..	**66**
4.3	Secondary structural profile of rAOx under different pH environment……	**81**
4.4	A Comparison of Ramachandran plots of the crystal structures used as templates in predicting the best 3D model structure of rAOx……..	**91**
4.5	Steady-state kinetic parameters of *in-vitro* refolded rAOx……..	**102**
4.6	Elucidation of deactivation kinetic parameters at different incubation temperature in range from 30 °C to 70 °C of the purified rAOx……	**103**

Abstract

A novel flavin based alcohol oxidase (AOx) has been successfully cloned, sequenced and characterized from a hydrocarbon degrading filamentous fungi *Aspergillus terreus* MTCC 6324. The cDNA encoding AOx was constructed from mRNA of *n*-hexadecane induced cells of *A.terreus* MTCC6324 and expressed successfully as recombinant AOx (rAOx) in *Escherichia coli*. A combined proteomics and genomics approach was successfully performed to characterize an AOx coding open reading frame (ORF). Proteomics approach starts with the isolation of microsomal protein extract following a well established differential centrifugation protocol. Thereafter, the microsomal protein extract was resolved through 2D electrophoresis and the resolved 2D spots were manually processed for MALDI MS based peptide mass fingerprinting (pmf). Successful identification of target protein (AOx) through pmf database search was achieved. Two internal PCR primers were designed based on the wild type AOx internal peptide sequence match from pmf database search. Two internal PCR primers in combination with two PCR primers designed corresponding to the 5' and 3' end of hypothetical nucleotide sequence information of AOx from *A.terreus* NIH2624 in NCBI, proved successful in picking up two overlapping PCR amplicons flanking the full length coding region of AOx from *A.terreus* MTCC6324. The two overlapping PCR products were ligated at a common restriction endonuclease site present in its overlapping region to attain the full length 2001 bp ORF of AOx confirmed through double stranded primer walking which corresponds to 666 amino acid residues and the same had been submitted to NCBI Genbank with an accession no JX139751. The nucleotide and deduced amino acid sequence showed high sequence homology with un-reviewed hypothetical AOx from *A. terreus* NIH2624 strain and maximum structural homology with chain B of aryl alcohol oxidase (AAO) from *Pleurotus eryngii* (PDB id: 3FIM).

The full length coding region was successfully sub-cloned into *E.coli* expression vector and over-expressed as a recombinant histidine-tagged-AOx protein (rAOx). Due to the lack of proper post-translational modification in prokaryotic expression system, the over-expressed rAOx was found to be associated as highly aggregated, inclusion bodies present in the pellet

fraction of the bacterial cell lysate. Inclusion body isolation, purification and solubilization had been successfully demonstrated by minor modification of an existing protocol from the literature. Approximately, 10 mg protein per 2.4 g wet cell weight per liter of induced culture was achieved after one step purification of Histidine-tagged-rAOx using Ni^{2+} affinity chromatography. Western blot of the purified fraction with anti-histidine antibody confirmed the expression of rAOx as a histidine tagged fusion protein. *In-vitro* re-folding to a functionally active AOx holoenzyme with its co-factor FAD was achieved after incubation of apo-rAOx (~ 10µg ml^{-1}) for ~ 80 h at 16 ºC in refolding buffer (20 mM Tris-HCl buffer, pH 9.0, 2.5 mM glutathione oxidized, 1mM dithiothreitol, 35 % glycerol, 0.6 M urea and 0.08 mM FAD).

Successful incorporation of FAD into the protein matrix was confirmed through fluorescence spectroscopy. The apoenzyme p*I* as predicted by 2D-electrophoresis and Zeta potential was 6.5±0.1 and mass as determined by MALDI-TOF/TOF was ~74 kDa, which was in good co-relation with the theoretical studies. Circular dichroism (CD) data of the refolded rAOx confirmed its ordered structure with α-helix, β-strand and random/non-regular structures as 28 ± 1%, 33 ± 2 % and 39 ± 2 %, respectively as predicted through CD spectra analysis program. The high aggregating nature of the rAOx had been demonstrated through dynamic light scattering studies and a significant shift in peak of the hydrodynamic radius to ~1000 nm within 24 h incubation in refolding condition was evident in our observation.

Docking studies with an *ab-initio* protein model as predicted though online protein structure prediction software I-TASSER, demonstrated the presence of a conserved FAD binding domain with an active substrate binding site. The modeled rAOx was found to be specific for aryl alcohols and the order of its substrate preference with its total binding energy in parenthesis was evaluated as follows: 4-methoxybenzyl alcohol (-82.87 kJ mol^{-1}) > 3-methoxybenzyl alcohol (-74.12 kJ mol^{-1})> 3, 4 dimethoxybenzyl alcohol (-71.75 kJ mol^{-1})> benzyl alcohol (-56.45 kJ mol^{-1}).

Thermal and pH stability of rAOx were studied. A range of alcohol substrates for activity of the rAOx was studied and found that only the aryl alcohol substrates showed detectable activity for the recombinant enzyme. Enzyme kinetics pertaining to its specific activity, K_m, K_{cat} were evaluated which validated *in-silico* docking simulations. Thermo-inactivation studies pertaining to activation and deactivation energies were studied based on Arrhenius type equation.

Enthalpy (ΔH), free energy (ΔG) and entropy (ΔS) of bioactive rAOx were investigated and reported in this thesis.

This thesis highlights the molecular characterization of a full length coding nucleotide sequence of AOx from filamentous fungi following a combined proteomics and genomics approach. The significant sequence variation of the characterized *A.terreus* rAOx protein from the prevailing AOxs demonstrated the novelty of the protein although functionally it is closer to the reported aryl alcohol oxidase from a lignin degrading filamentous fungi. The work demonstrated in this thesis would advance the knowledge on the molecular characteristics of AOxs from filamentous fungi and will open the scope for the production of this industrially useful enzyme through recombinant DNA technology.

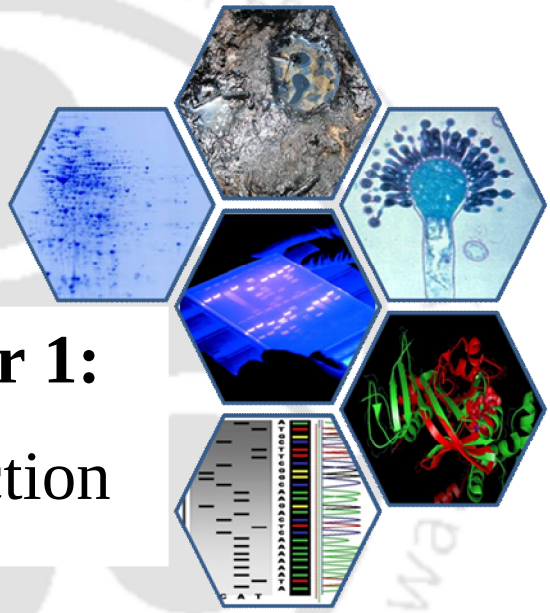

Chapter 1:

Introduction

Chapter 1

Introduction

In nature, the direct conversion of alcohols to their corresponding carbonyl compounds are catalyzed largely by two groups of enzymes: alcohol oxidase (AOx) (Alcohol: O_2 Oxidoreductase; EC 1.1.3.X) and alcohol dehydrogenase (ADH) (Alcohol: NAD^+ oxidoreductases; EC 1.1.1.1). The AOx catalyzes only the forward reactions leading to the formations of hydrogen peroxide (**Fig. 1B**) and the FAD (flavin adenine dinucleotide) based cofactor is involved in the catalysis. Unlike NAD (nicotinamide adenine dinucleotide) co-factor in ADH, the FAD in AOx is strongly associated with the redox center of the enzyme. During the reaction the oxidized state of the co-factor (FAD) is auto-regenerated in the reactive centre of the enzyme without engaging any additional metabolic co-operation for continuous oxidation of the substrate alcohols. AOx-based catalysis being employed for the bio-catalytic processes thus obviates the need of supplementing the cofactor into the reaction medium. Moreover, this group of redox enzymes is widely available in nature because of their production by various aerobic microorganisms, thus offering the scope for their large scale production through simple aerobic cultivation of the source microorganisms. These interesting treats of the FAD based AOx enzymes are widely acclaimed in the scientific literature during recent past for their prospective applications in developing various products and processes. The potential areas of applications of the AOxs as witnessed from the steeply growing publications in global science on the subject are biocatalytic synthesis of flavor, fragrance and optically pure compounds, biosensors and biofuel cells.

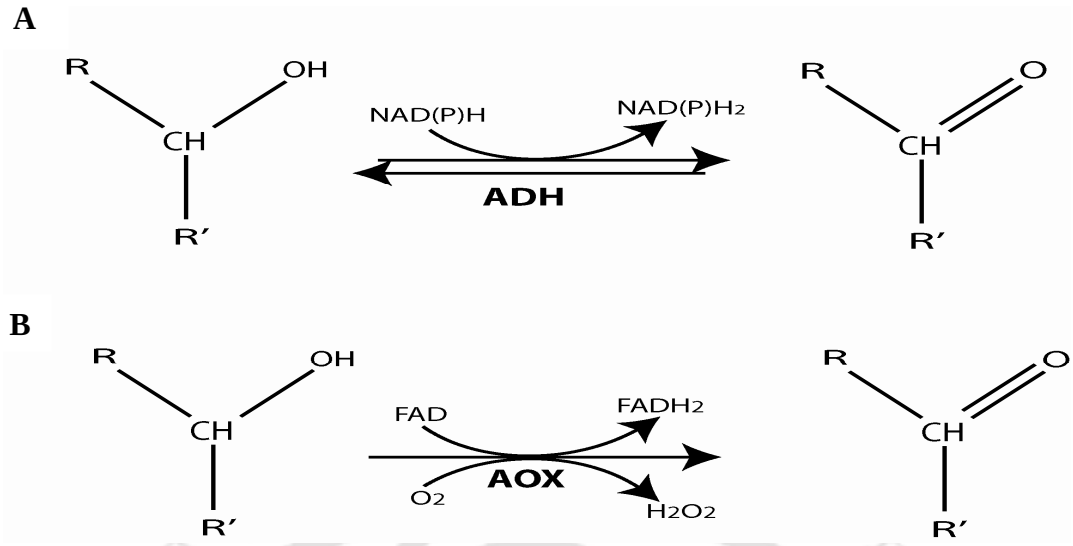

Figure 1. (**A**) Alcohol dehydrogenase (ADH) as catalyst and (**B**) Alcohol oxidase (AOx) as catalyst; R′= -H or any other alkyl/aryl group

Based on the substrate specificity, AOxs are categorized broadly into four groups: Short chain alcohol oxidase (SCAO), Long chain alcohol oxidase (LCAO), Aromatic alcohol oxidase (AAO) and Secondary alcohol oxidase (SAO). The molecular characteristics of these groups of enzymes are not adequately known due to their multifaceted molecular architecture and complex biogenesis in the cells. The sources reported for these enzymes are mostly limited to bacteria, yeast, fungi, plant, insect, and mollusks. However, the quantum of reports for each category of enzymes considerably varies across these sources. The enzymes belonging to SCAO and LCAO are intracellular in nature whereas, AAO and SAO are mostly secreted to the growth medium.

Previous work from our laboratory on a filamentous fungus, *Aspergillus terreus* MTCC6324 revealed an interesting fact that the strain exhibits all the four categories of AOx activities in the cells during the growth on hydrocarbon substrates. However, the exact metabolic role of these AOx enzymes induced in the cells during hydrocarbon degradation by *A. terreus* is yet to be clearly elucidated. The different AOx activities were located in the microsomal membrane of the cells and all activities were confined to a highly aggregated protein particles purified from the cell homogenate by chromatographic means. Characterization of the individual AOx enzymes following the conventional purification protocols was a challenge posed by the very high aggregating tendency of the isolated complex enzyme assembly and low protein yield.

This perplexed protein conglomerate of the enzymes, their intriguing metabolic role in the cells of *A. terreus*, and the importance of AOx enzyme for their potential applications in bioprocesses and in emerging fields like, biosensors and biofuelcell inspired us to investigate further on the line to unveil the characteristics of this enzyme through molecular biotechnology approaches.

Molecular characterization and cloning of *A.terreus* genes for commercially significant enzymes are, however limited primarily due to the lack of its available reliable genome sequence and inadequate information in annotated, non-redundant protein database. The current research work thus utilizes a combinatorial approach of proteomics and genomics to elucidate a full length *A.terreus* MTCC6324 cDNA for the AOxs. Here we report for the first time the molecular characteristics, cDNA cloning, and expression of an alcohol oxidase gene from *n*-hexadecane induced *A terreus* MTCC 6324. Heterologous cloning and expression of the characterized gene in *E.coli* leads to the production of recombinant apoenzyme, which was subsequently transformed into a functionally active protein following an *in-vitro* flavin adenine dinucleotide reconstitution approach. In a parallel work, *ab-initio* based alcohol oxidase protein structure and function was investigated using the translated peptide sequence of the characterized gene and predicted aryl alcohols as the substrates, which were validated by the follow-up experiments using the recombinant alcohol oxidase. The high aggregating nature, kinetic and thermo-inactivation characteristics of the recombinant enzyme were also analyzed and compared with the native enzyme and reported in this thesis.

Chapter 2:

Literature Review

Chapter 2

Literature Review

2.1 Alcohol oxidase: Discovery and detection methods

Activity of AOx was initially reported by Farmer *et al*. (1960) in a culture of *Polystictus versicolor* (a synonym of *Trametes versicolor*). In a later report, Janssen *et al*. (1965) described the isolation of an enzyme from a basidiomycete that catalyzes the oxidation of methanol and other lower primary alcohols to the corresponding aldehydes and H_2O_2. Subsequently, they designated the enzyme as 'alcohol oxidase, purified it to the crystalline state, and discovered FAD as the prosthetic group of the enzyme (Janssen and Ruelius 1968).

Blasig *et al*., (1988) first proposed the quantitative detection of AOx activity in a sample by monitoring stoichiometric consumption of oxygen in the reaction mixture containing alcohol substrates. Latter on the concentration of H_2O_2, which is formed as the co-product of the alcohol oxidase catalyzed reaction, was used to measure the enzyme activity. The H_2O_2 so formed, was colorimetrically measured by the use of horseradish peroxidase (HRP) that oxidizes chromogenic substrates during the reduction of H_2O_2. The chromogenic substrate most commonly used to measure AOx activity is 2, 2′-azinobis (3-ethylbenzothiazoline-6-sulphonic acid) as developed by Kemp *et al*. (1988). HRP catalyzed co-oxidation of phenol-4-sulfonic acid and 4-aminoantipyrine was also reported to assay H_2O_2 (Vojinovic *et al*. 2004) for measuring AOx activity (Azevedo *et al*. 2004).

2.2 Types of alcohol oxidases

Based on the substrate specificity, AOxs (EC 1.1.3.x) may be categorized broadly into four groups (Kumar and Goswami, 2006): (a) Short chain alcohol oxidase (SCAO) (b) Long chain alcohol oxidase (LCAO) (c) Aromatic alcohol oxidase (AAO) and (d) Secondary alcohol oxidase (SAO).

2.2.1 Short chain alcohol oxidase

Alcohol oxidase (EC 1.1.3.13), methanol oxidase, or ethanol oxidase that catalyzes the oxidation of lower chain length alcohol substrates in the range of C_1-C_8 carbons belongs to the category of SCAO (review: Tani *et al*. 1972; Sahm,1977; Woodward,1990; van der Klei *et al*. 1991; Ozimek *et al*. 2005). Yeasts and fungi are wellknown sources of SCAOs. There are also limited reports on SCAOs from mollusk (Grewal *et al*., 2000). Among the various sources, *Pichia pastoris, Pichia putida, Pichia methanolica, Hansenula polymorpha, Poria contigua, Candida boidinii, Candida methanosorbosa, Cladosporium fulvum, Aspergillus ochraceus, Aspergillus terreus, Gloeophyllum trabeum, Achatina achatina, Achatina fulica, Arion ater, Helix aspersa, Polyporus obtuses, Peniophora* gigantea, and Thermoascus aurantiacus are prominent, and some of them are also reported in the last decade (Alvaradocaudillo *et al*., 2002; Ko *et al*., 2005; Srisuk *et al*., 2006; Kumar and Goswami, 2006; Isobe *et al*., 2007; Daniel *et al*., 2007; Gvozdev *et al*., 2010).

SCAOs are intracellular enzymes located mostly in the microbody/peroxisome of yeasts and in membranous locations of mollusks. The enzyme is an octameric protein with the exceptions of *A. ochraceus* AIU 031 where tetrameric nature has been demonstrated (Isobe and Kawakami, 2007). The subunit molecular masses of the SCAOs range from 65 to 80 kDa. The co-factor FAD is non-covalently bound to the protein. In the methanol oxidases from methylotrophic yeasts, the mFAD, a modified analog of FAD, is also additionally present. mFAD is assumed to be formed by the spontaneous modification of FAD in the active center of the enzyme and differs from FAD in the stereo-position of the hydroxylic group in acyclic carbohydrate chain (Kellogg *et al*., 1992). This modification of FAD slightly decreases the V_{max} however significantly reduces the K_m of the enzyme for the substrate methanol. These effects are of significant physiological relevance in the cultures of low methanol concentration.

SCAO are usually active over a pH range of 6–9 with few exceptions bearing activity up to pH 10. The optimum temperatures widely reported for the activity of SCAO are 25 to 30 and 37 °C with deviation to 50 °C and 50–55 °C for the enzyme from *C. methanosorbosa* (Suye, 1997) and *A. ochraceus* AIU031 (Isobe *et al*., 2007), respectively.

The AOx protein and the regulation of the genes encoding AOx have been studied for several reasons (Holzmann *et al*., 2002; Gurkan *et al*., 2004). The promoter that controls AOx

expression is one of the strongest and tightly controlled promoters in yeasts (Review: Hartner and Glieder, 2006). Several genes encoding AOx proteins that have been cloned to date are mostly from the *Pichia* species such as, *Pichia angusta*, *P. pastoris*, *P. methanolica*, and *Pichia pinus*. Other sources reported in a later period are *C. boidinii* (Sakai and Tani., 1992), *C. fulvum* (Segers *et al*., 2001), *Helminthosporium victoriae* (Soldevila and Ghabrial., 2001), *Penicillium chrysogenum* (Holzmann et al., 2002) and *Aspergillus nidulans* (GenBank GI:40747510). Although AOx proteins from filamentous fungi show a high degree of homology (65–70 % identity) to those of methylotrophic yeast species, their function is not related to methanol metabolism as in yeasts. AOx activity in the cells of *A. terreus* is induced by non-methanolic growth substrates (Kumar and Goswami 2006). Expression of AOx gene is subject to strong carbon catabolite repression. Under such conditions, the AOx promoter sequence is organized into nucleosomal structures (Costanzo *et al*., 1995). Prior to initiation of AOx synthesis, the gene needs to be liberated from nucleosomal packaging by a chromatin remodeler. The ultimate level of AOx expression strongly depends on the cultivation conditions, and differences exist in the regulation of AOx expression in different yeast species. Moreover, the components involved in the regulation of AOx catabolite repression have been identified which includes a hexose transporter (Stasyk *et al*., 2004), a glucokinase, and a hexokinase (Kramarenko *et al*., 2004; Laht *et al*., 2002; Karp *et al*., 2003).

The AOx proteins, which belong to the group of glucose-methanol-choline (GMC) family, have an FAD-binding domain, a flavin attachment loop, and a substrate binding domain. In addition to these domains, there are two minor domains, namely an FAD-covering loop and an extended FAD-binding domain. The FAD-binding domain is the most conserved region and consists of an ADP-binding motif (βαβ) and a characteristic nucleotide-binding site GXGXXG (amino acids 13–18 of AOx) (Ozimek *et al*., 2005). Two inserts have also been identified in the substrate-binding domain that is probably involved in AOx-octamer formation. Boteva *et al*, (1999) created a model of AOx based on the known structure of glucose oxidase (GOX) from *Aspergillus niger* which shares maximum homology with *Hansenula polymorpha* AOx (25 % identity). The conformation of AOx is irreversibly changed following the dissociation of FAD which is deeply buried in the protein matrix (Zlateva *et al*., 2001).

Multiple AOx isoforms have been reported in several strains of *P. methanolica*. In a study, a total of nine isoforms were identified based on their electrophoretic mobility which have identical subunit molecular weights but differ in their p*I* (4.1–5.2). The reason for such molecular heterogeneity has been attributed to the occurrence of two AOx genes (Nakagawa *et al*., 1996) differing in some amino acids in the encoded proteins. Gruzman *et al*, (1996) confirmed the occurrence of two types of subunits in the enzyme and demonstrated that the octameric AOx isozymes are formed as a result of different combinations of the subunits. In some past studies, two highly homologous genes with different promoters and transcription levels in *P. pastoris* were documented. These two genes, however, did not result in AOx isozyme formation, instead are correspondingly expressed into major and minor proteins with AOx activity. The minor protein is the product of one of the genes transcribed on a much lower level than the other gene (Koutz *et al*., 1989). Notably, although *H. polymorpha* and *C. boidinii* are known to have only one AOx gene, two AOx active proteins are expressed in these strains (Lee and Komagata 1983). Effort has been made to elucidate the crystal structure of AOX from *P. pastoris.* The spatial structure of the enzyme could not be further refined, and the possible reason for failure is ascribed to the intermolecular micro-heterogeneity of the enzyme (Gvozdev *et al*., 2010).

2.2.2 Long chain alcohol oxidase

Several terminologies namely, fatty alcohol oxidase (FAO), long chain fatty acid oxidase, long chain fatty alcohol oxidase, have been reported for LCAO (EC:1.1.3.20). These enzymes catalyze alcohol substrates with carbon chain length of usually above C_6. The existence of LCAO was first established in *T. candida* (Ilchenko, 1984) and *C. guilliermondii* (Krauzova *et al*., 1984). The purification and properties of a LCAO that oxidizes both the long chains of saturated and unsaturated alcohol substrates from a plant source, *T. vulgare* was reported by Banthorpe *et al*., (1976). The cotyledons of *S. chinensis* containing FAO and fatty alcohol dehydrogenase (Moreau and Huang, 1979) also oxidize fatty alcohols formed from the hydrolysis of stored wax esters during germination. The plant species, *A. thaliana* (Cheng *et al*., 2004) and *L. japonicas* (Zhao *et al*., 2008) have also been reported as sources of LCAO. However, FAOs are mostly reported from yeast species, such as *C. Bombicola* (Hommel and

Ratledge, 1990), *C. cloacae* (Vanhanen *et al*., 2000), *C. tropicalis* (Hommel *et al.*, 1994; Kemp *et al*., 1988), *Y. lipolytica* (Kemp *et al*., 1990). The LCAO from *Candida* species catalyze the oxidation of long chain alcohols in mono-terminal, di-terminal and sub-terminal positions (Blaisig *et al*., 1988; Kemp *et al.*, 1988). Many filamentous fungi such as *A. terreus* (Kumar and Goswami, 2006), *Cladosporium* species (Goswami and Cooney, 1999), *Aspergillus* species (Savitha and Ratledge, 1991), and YR-1 strain (Robelo *et al*., 2004) *Mucor circinelloides* YR-1 (Silva-Jiménez and Zazueta-Sandoval, 2005) produce LCAO during growth on hydrocarbon substrates. The LCAO has been reported in different subcellular locations such as, mitochondrial, microsomal and glyoxisomal membrane fractions (Mauersberger *et al*., 1987; Sahm, 1977; Krauzova *et al*., 1985, Kumar and Goswami, 2006; Goswami and Cooney, 1999; Moreau and Huang, 1979; 1981). The presence of FAO activities in either particulate or soluble fractions from a cell-free extract was also reported (Silva-Jiménez and Zazueta-Sandoval, 2009).

The molecular mass and the subunit number of LCAO were found to largely differ from SCAO, being lower than the latter. The LCAO from *C. cloacae*, (Vanhanen *et al*., 2000) *C. tropicalis*, (Kemp *et al*., 1988; Dickinson and Wadford, 1992), *T. vulgare* (Banthorpe *et al.*, 1976) are dimeric in nature with sub-unit molecular masses ranging from 70–94 kDa. The enzymes are heterodimeric in nature with the exception of *C. tropicalis* AOX, which is homodimeric. The AOX isolated from the microsome of n-hexadecane grown *A. terreus* showed highest affinity for n-heptanol (K_m = 0.498 mM, K_{cat} = 2.7×102 s−1) and high aggregating properties (Kumar and Goswami, 2008). In this flavoenzyme, flavin is non-covalently associated with the AOx protein where two FAD binding domains have been identified (Kumar and Goswami, 2009).

The activity of LCAO above 45ºC is generally not known and has been described as highly sensitive to temperature (Kumar and Goswami, 2006). The enzymes are usually active within the range of neutral pH value to around pH 9 with a wider range of pH (4.8-10) for AOx from *T. vulgare* (Banthorpe *et al.*, 1976). LCAO activities from *n*-alkane-grown *C. tropicalis* and *Y. lipolytica* rapidly decreased on exposure to light. The rate of inactivation of the enzyme depended upon the intensity and wavelength of the incident light (especially λ_{405nm}), but was diminished under anaerobic conditions (Kemp *et al*., 1990). In addition to light other inhibitors have been also reported for the LCAO from different sources such as, O_2 for *C. tropicalis* (Kemp

et al., 1988) and PCMB for *S. chinensis* (Moreau and Hong, 1981). Apart from flavin based co-factors, few reports on NAD (P) $^{+}$, riboflavin, 2,6DCPIP, potassium ferricyanide (Moreau and Huang, 1979; 1981) as cofactors are also available for LCAOs.

Cloning and sequencing of two FAO genes from *C. cloacae* (FERM O-736) and a single FAO gene from *C.tropicalis* (NCYC 470) have been reported (Vanhanen *et al*., 2000). The ORFs of FAO1 and FAO2 from *C. cloacae* were 2094 and 2091 bp, respectively while the ORF of FAO from *C. tropicalis* (NCYC 470) was 2,112 bp. FAO of *C. tropicalis* shared 60.6 and 61.7% nucleotide identities and 74.8 and 76.2% amino acid sequence similarities with *C. cloacae* FAO1 and FAO2, respectively. The FAO1 gene was successfully expressed in *E. coli* by Slabas *et al*, (1999). Full length cDNA of *L. japonicus* FAO (LjFAO1) protein has been also expressed in *E.coli* (Zhao *et al*., 2008). The gene contains 3 exons and 2 introns and was expressed in the whole plant, with the highest expression level in the apex. The LCFAO responded to cold stress. The active LjFAO1 protein showed substrate specificities toward 1-dodecanol, 1-hexadecanol, and 1, 16-hexadecanediol with K_m values ~59.6 (μM), ~40.9 (μM) and ~19.4 (μM), respectively. Cheng *et al*, (2004) had purified the His-tagged recombinant protein from *A. thaliana* expressed in *E. coli*. Several other LCAO from plant *T. vulgare* and in yeast *C. cloacae* were purified to homogeneity. Partial purification of LCAOs was done in yeast *C. tropicalis*, plant *S. chinensis*, fungi *Y. lipolytica* (Moreau and Huang, 1979) and *A. terreus* (Kumar and Goswami, 2008).

2.2.3 Aromatic alcohol oxidase

Aromatic alcohol oxidase or aryl alcohol oxidase (AAO; aryl-alcohol:oxygen oxidoreductase**:** EC 1.1.3.7) catalyzes the oxidation of aromatic primary alcohol to aromatic aldehyde (review: Hernández-Ortega *et al*., 2012a). Veratryl alcohol oxidase and vanillyl alcohol oxidase (VAO; EC: 1.1.3.38) also belong to this oxidoreductase family (reviews: van den Heuvel *et al*., 2001a). Notably, the VAO is active over a wide range of phenolic compounds and catalyzes oxidation, deamination, demethylation, dehydrogenation, and hydroxylation reactions.

AAO is mostly isolated and characterized from several fungal strains such as, *B. adusta*, *P.eryngii*, *P. osreatus*, *P. sajor-caju*, *P. pulmonarius*, *P. simplicissimum*, *G.candidum*, *P. chrysosporium*, *B.fulva*, *T. versicolor*, *F. solani*, *R. microporus*, *B. cinerea*, *P.cultures* and *Sphingobacterium sp.* The other well known sources of this enzyme are insects such as, *C.*

papuli, *P. vitellinae*, and a land slug such as *A. ater*. AAOs from different fungi are involved in the ligninolytic system together with peroxidase or laccase by providing H_2O_2 produced from the oxidation of benzyl alcohols (Ruiz-Duenas and Martinez, 2009**)**. AAO and laccase/peroxidase cooperate in the production of hydroxyl radical, which is thought to be involved in the initial attack of lignocellulose. Further, it is suggested that AAO prevents repolymerization of laccase oxidation products and sustained the lignin degradation process. Many of the lignin-degrading fungi produce soluble AAOs. The important characteristic of AAO is its extra cellular production except from few cases such as, *A. ater*, where the enzyme is present in the membrane. Veratryl alcohol, anisyl alcohol and 4-(methoxymethyl) phenol are reported as inducer of many VAOs. Under anaerobic conditions, certain *Pseudomonas* species produce a VAO analog with a tetrameric $\alpha_2\beta_2$ structure. These flavocytochromes share similar substrate specificity with VAO and are involved in the biodegradation of different phenolic compounds. These enzymes use their heme-containing subunit instead of natural oxygen as the terminal electron acceptor.

Optimum temperature for AAO activity from many microorganisms falls in the range of 37°C to 40°C (Ruiz-Duenas *et al*., 2006; Kumar and Rapheal, 2010; Tamboli *et al*., 2011) with few exception from fungal AAO which showed the ptimum at 55°C (Guillen *et al*., 1990). Majority of the AAO are active within a neutral to slightly acidic pH range (5.5 – 7.5), whereas few are active in a more alkaline range.

AAOs from most of the fungal sources are monomeric glycoprotein with molecular weights in the range of 65.3 to 78 kDa. The enzyme from *P. simplicissimum* however, is an inducible intracellular homooctamer, with holoenzyme molecular mass of 510 kDa (Fraaije *et al*., 1995). Wheres, the enzyme from *C. papule* and *P. vitellinae* are homotetramers with subunit molecular mass ~79 kDa (Bruckmann *et al*., 2002).

Initially the AAO protein sequences were analyzed from *P. eryngii*, *P. pulmonarius* (Varela *et al*., 2000a; 2001) and *B.adusta* (Romero *et al*., 2010). Cloning and characterization of AAO from *A. terreus* is the main focus of this thesis and discussed in following chapters. The number of sequences however, rapidly increased with the increasing basidomycetes genome in data bases including around 50 sequences annotated as putative AAO. Hernández-Ortega *et al*. (2012a) compared 112 GMC oxidoreductase sequences from 31 basidomycetes species including 40 AAO and 37 methanol oxidase sequences and demonstrated phylogenetic distance of AAO

from other GMC enzymes types including methanol oxidases. Recombinant AAO from *P. eryngii* has been expressed and purified from both bacterial and fungal expression systems (Varela *et al*., 2001; Ruiz-Duenas *et al*., 2006). Native or recombinant AAO has also been purified or partially purified from *A. terreus* (Kumar and Goswami, 2009), *C. tremulae*, *C. populi* (Michalski *et al*., 2008) and *P. sajor-caju* (Bourbonnais and Paice,1988). The cDNA sequence of *P. pulmonarius* AAO consisted of 593 amino acids including a signal peptide. Comparison with other AOXs showing highly conserved amino acid sequences in the N-terminal and C-terminal regions, in spite of differences in substrate specificities.

Two prominent crystal structures AAOs from *P. simplicissimum* (Mattevi *et al*., 1997) and *P. eryingii* (Fernandez *et al*., 2009) are available in the Protein Data Bank (PDB) with id of 1VAO and 3FIM, respectively. The crystal structure of *P. eryingii* AAO revealed the highest similarity to the crystal structures of choline oxidase from *A. globiformis* (Quaye *et al*., 2008) and *A. niger* GOX and little similarities with other GMC oxidoreductases, including bacterial ChOx (Lario *et al*., 2003). FAD and substrate-binding domains are the two different domains and The FAD molecule interacts with the protein through a network of H-bonds predominantly involving the main-chain NH and CO groups of residues located at the N-terminus and several water molecules. The FAD is stabilized by some important residues located in the βαβ fold adapted by the N terminal region in the protein. The putative active-site cavity is located in the vicinity of the FAD isoalloxazine ring and near two histidines that could contribute as catalytic bases to activate alcohol. Moreover, the active site of the native enzyme is solvent inaccessible and controls substrate specificity by providing a 'size exclusion mechanism'. The additional two structural elements existing in the surroundings of its active site that modulate the access of substrates are absent in the structure of GOX (Fernandez *et al*., 2009). From the molecular docking studies on AAO crystal structure the reason for its inability to bind secondary alcohols efficiently was identified (Hernández-Ortega *et al*.,2011a). The small space available at the bottom part of the active site cavity restricts large substituents at the C_α position. The cofactor, flavin or FAD, in AAO is either covalently or non-covalently bound to the protein. The covalent flavinylation enhances the oxidative power of VAO (Fraaije *et al*., 2003).

Analysis of crystal structures of AAO, GOX, ChOx, and choline oxidase showed a highly conserved catalytic site, suggesting a similar oxidation mechanism. The mechanism of AAO

catalyzed alcohol oxidation was revealed from kinetic studies, which was defined as the hydride transfer from substrate to flavin N_5 concerted with proton abstraction from ∞ hydroxyl by a catalytic base (Ferreira *et al*., 2009). Specific His residues have been identified as the most likely catalytic bases in AAO and choline oxidase (Hernandez-Ortega *et al*., 2011a; Hernandez-Ortega *et al*., 2012a, Ghanem and Gadda, 2005). The substrate specificity studies on *P. eryngii* AAO demonstrated that the extension of the aromatic system in the substrate benzyl alcohol favors the enzyme action. Moreover, the oxidation rates are strongly affected by the nature, position, and number of the aromatic-ring substituents. In this line, β-naphthylmethanol was identified as the most readily oxidized substrate (Ferreira *et al*., 2005). Generally, electron donor substituents promote the alcohol oxidation, whereas electron-withdrawing substituents produce the reverse effect. An interesting functional activity of AAO is its minor activity towards aromatic aldehydes (Guillen *et al*., 1992). It was noted that electron-withdrawing substituents promoted aldehyde oxidation by AAO, while electron donors caused the opposite effect, in contrast to that observed for alcohols. The enzyme activity on these aldehydes is correlated with their hydration degree in water, which is identified as the activating molecule in the oxidation (Ferreira *et al*., 2010). Aldehyde is also accepted as substrate by choline oxidase, which also, belongs to GMC oxidoreductase family in which case betaine aldehyde formed as the oxidation product of its primary substrate choline is the substrate (Fan *et al*., 2006).

2.2.4 Secondary alcohol oxidase

AOXs s such as, polyvinyl alcohol oxidase (PAO) and cholesterol oxidase (COX) which catalyze the oxidation of secondary alcohols to the corresponding ketones falls under this category. PAO (polyvinyl-alcohol: oxygen oxidoreductase: EC 1.1.3.30) activity was initially reported in the culture supernatant of polyvinyl alcohols (PVA)-degrading *Pseudomonas* strains by Suzuki, (1976) and Watanabe *et al*, (1976). Since then many PAO has been reported from *Pseudomonas* species (Morita *et al*., 1979; Shimao *et al*., 1985; Kawagoshi and Fujita, 1997). The other sources for the enzyme are limited such as, *Penicillium sp* (Qian *et al*., 2004), *Sphingopyxis* sp. (Yamatsu *et al*., 2006). The enzyme oxidizes PVA to form diketone structures in PVA (Sakai *et al*., 1986; Kawai and Hu, 2009). Two different oxidative pathways involved in PAO catalyzed degradation of PVA were proposed (Suzuki 1976; Morita and Watanabe, 1977).

Both PVA inducible and constitutive PAOs are reported from the *Pseudomonas* strains. PVA-degrading enzymes are monomeric in nature and are reported as extracellular, periplasmic or membrane bound (Shimao *et al*., 1983; 1985; Zhang *et al*., 2006). A PAO with M_w of ~40 kDa and p*I* of 4.5 was purified from a bacterial symbiotic mixed culture (Sakai *et al*., 1985). The enzymes are active within the pH range of 5 - 10. One atom of non-heme iron was detected per molecule of the enzyme and the enzyme catalyzes the oxidation of various low molecular weight secondary alcohols as well. A SAO activity detected in the microsome of *A. terreus* was active against various secondary alcohol substrates such as, isopropanol, isoamyl alcohol, 2-octanol, cyclooctanol, 3-octanol, and 2-dodecanol (Kumar and Goswami 2006, Kumar and Goswami 2008). Until now limited literatures are available on the basic biochemical characteristics and properties of PAO.

2.3 Characteristics of *Aspergillus terreus*

The work presented in this thesis is based on a strain of *Aspergillus terreus* indigenously isolated from a petroleum oil contaminated soil of Assam, India and subsequently identified and confirmed as *Aspergillus terreus* with an accession no MTCC6324 (Kumar and Goswami, 2006; Kumar *et al*., 2009). *A.terreus* is a saprophytic, asexual fungus (mold) belonging to the kingdom fungi and division of ascomycota. The class and order of this filamentous fungus belongs to eurotiomycetes and eurotiales, respectively and comes under the family of trichocomaceae (Mycota: a fungal database, www.mycota-crcc.mnhn.fr). The species predominantly grow on wood, air-conditioners, leathers, atmospheric dusts, paper and paper pulp, decayed vegetable matter, cultivated or un-cultivated soil, etc (Mycota: a fungal database, www.mycota-crcc.mnhn.fr). The species are prevalent to the tropical and sub-tropical climatic conditions. It is also a known pathogen causing aspergillosis, otomycosis, onchomycosis, abscesses of the aortic root and various skin infections in severe immune-compromised individuals.

The strain of *A.terreus* used in this investigation degrades a wide variety of petroleum hydrocarbons, alcohols and long chain primary alkanols, secondary alcohols including cholesterols and chlorinated aliphatic hydrocarbons (Kumar *et al*, 2009). Morphologically, *A.terreus* MTCC6324 is light yellow to brownish in color and becomes darker as it progressively ages in fungal agar at 28°C. The colonies grow rapidly and produce suede like soft tufts. The

hyphael network can penetrate deep into its substrate, thus can degrade contaminants from sub-surface anaerobic environment. The growth under laboratory conditions was optimized with *n*-hexadecane as a sole carbon source and requires approximately 96 h of incubation at 28°C to reach stationary phase of growth (Kumar *et al*., 2009). High cellular lipid content in the cell was also reported and was co-related to the metabolic consequences of assimilation of high energy hydrophobic substrates by the fungal strain. A considerably high amount of unsaturated fatty acids with chain length C_{32} and C_{33} were confirmed by ESI/MS and reported in Kumar *et al*, (2009). The hypothesis for the induction of high amount of palmitic acid (C_{16}) in *n*-hexadecane grown cells of *A.terreus* was also discussed and was co-related as an end product of terminal oxidation of *n*-hexadecane substrate, catalyzed by integral membrane associated enzymes primarily Cyt P450, AOx and ADH. The existence of Cyt P450 and AOx in the cells of *A.terreus* MTCC6324 had also been reported by our lab (Kumar and Goswami, 2006; Vatsyayan et al., 2008).

Reports on different genes that are cloned and characterized from *A.terreus* are gla1 gene encoding glucoamylase (Ventura *et al.*, 1995), CAD gene encoding cis-aconitic acid decarboxylase (Kanamasa *et al*., 2008), gene encoding a multi-copper blue enzyme dihydrogeodin oxidase (Huang *et al*., 1995), blasticidin S deaminase gene (Kimura *et al*., 1994), lovastatin biosysnthetic genes (Barrios-González *et al*.,2008), 6-methylsalicylic acid synthase gene (Fujii *et al*., 1996), genes for sulfate assimilation pathway (Schierová *et al*., 2000). Attempt to characterize and clone alcohol oxidase gene from *A. terreus* is limited because of unavailability of annotated nucleotide sequence of this enzyme in NCBI database. Although, a vast group of scientists from The Broad Institute Genome sequencing platform (USA), The University of Manchester (UK) and The Institute of Genomic Research (USA) have submitted the conceptually translated amino acid sequence data of alcohol oxidase (data unpublished) from the draft genome sequence of *A. terreus* NIH2624 strain available in NCBI database on 2005, but the current status dictates that the record has not yet been subjected to final NCBI review and needs further verification.

2.4 Current protocols to characterize novel genes in filamentous fungi

Finding a novel protein coding gene from filamentous fungi whose genome sequence is not available or had not undergone a final annotation in public whole genome database is a

challenging task involving strategies not relying blindly on the hypothetical protein and /or draft genome sequence. A vast array of hypothetical, conceptually translated protein sequences are readily available for filamentous fungi in the DNA databases, without any reference to its whole genome sequence. As part of the Fungal Genome Initiative by MIT and Broad Research Institute about 50 fungal genomes are sequenced or are being sequenced (www.broadinstitute.org). Till date only 8 *Aspergillus* species had been sequenced however, only a draft genome sequence exists for *A.terreus* and *A.nidulans* and had not underwent a comprehensive review by the database curators. Thus strategies to characterize novel genes remains a challenging task for the researchers working on these above two important *Aspergillus* strains.

However, the introduction of molecular biology technique involving expression cloning, molecular screening, protein engineering, have augmented the novel gene identification, but these methods rely extensively on cDNA and expressed sequence tag (EST) mapped onto the genomic DNA or aligned to closely related genome, which are not abundantly reported in databases (Dalbøge and Lange,1998; Lomsadze *et al*., 2005). Rapid amplification of cDNA ends (RACE) for determining the 5′ and 3′ ends of mRNAs and cloning full-length cDNAs by a double-stranded (ds) adaptor ligated to both ends of a library of ds cDNA by T4 DNA ligase, revolutionized the novel gene characterization protocol (Chenchik *et al*., 1996). Few researchers had utilized the knowledge of proteomics to decipher the novel target gene characterization. A recent successful application of the above proteomics approach had been utilized by Ng *et al*, (2013) to characterize laccase and porin genes from bacteria *P.hauseri*, circumventing the expensive RACE, DNA-probe, conserved domain primer design and hybridization techniques as described by the authors (Ng *et al*., 2013; Wilm *et al*., 1996). However, similar reports on characterization of genes from filamentous fungi are limited. A report on molecular cloning of an aryl-alcohol oxidase from fungus *Pleurotus eryngii* demonstrated the application of wild type novel protein purification to homogeneity through chromatographic means followed by tryptic digestion and N-terminal sequencing of individual tryptic peptides to generate degenerate primer probes for gene characterization (Varela *et al*., 1999). Thus, the work in this thesis highlights for the first time the combinatorial proteomics and genomics approach to characterize a novel gene (AOx) from filamentous fungi *A.terreus* MTCC6324.

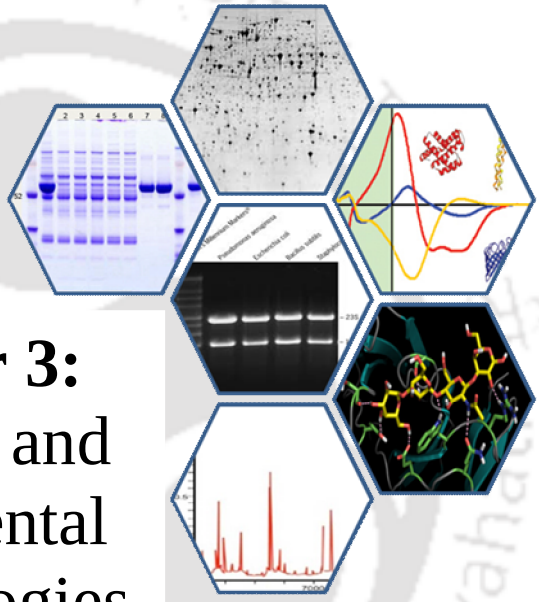

Chapter 3:
Materials and Experimental Methodologies

Chapter 3

Materials and Experimental Methodologies

3.A Materials

Standard molecular biology and mass spectrometry kits, fine chemicals and chromatography grade reagents were purchased from Sigma Aldrich (USA) unless and otherwise mentioned. Restriction enzymes were procured from New England Biolabs (USA).TA cloning was performed using pGEMT Easy cloning kit (Promega, USA) and expression in *E.coli* was carried out using pET28a (+) expression vector (Novagen, Merck, Germany). Standard molecular biology kits were purchased from Sigma Aldrich (USA). Common laboratory reagents used in this research work had been described in the appendix section of this thesis and appropriately cited in the experimental methodology section, wherever necessary.

3.B Experimental Methodologies

3.B.1 Molecular characterization of alcohol oxidase gene from *Aspergillus terreus* MTCC6324.

3.B.1.1 Growth and maintenance of microorganisms

The culture conditions and maintenance of *A. terreus* MTCC 6324 used in this study were described previously by Kumar and Goswami, (2006). *A.terreus* culture was maintained on fungal agar slants at 28 °C with periodic transfer to a fresh slant after every 15 days. For long term storage the fungal culture was maintained in paraffin sealed slants at 4 °C. For growth on *n*-hexadecane media, pure mycelium were transferred from fungal slant in 500 ml Erlenmeyer

flasks containing 2 % (v/v) *n*-hexadecane in 50 ml basal medium, the composition and pH of which is given in the appendix (**Table A2**). The pH adjusted and autoclaved culture media was incubated in static condition after aseptic inoculation with fungal mycelia at 28 ºC.

E.coli strains used as bacterial host for clone maintenance and expression were stored at -80 °C as 30 % glycerol. To revive the bacterial clones they were cultured in LB medium containing suitable antibiotics. *E.coli* strains and the composition of the culture medium are given in the appendix section of the thesis (**Table A1**).

3.B.1.2 Isolation and optimization of total RNA from *A.terreus* MTCC6324

Thin, papery, translucent mycelium from 4 day old static culture of *A. terreus* MTCC6324 were harvested and washed thoroughly with chilled double distilled water to remove excess of *n*-hexadecane and media components. The cells were pretreated with benzyl chloride (Li *et al*., 2010). 100-200 mg wet weight of mycelium were dabbed with fresh filter paper to remove excess of water and placed in mortar pestle pre-chilled with liquid nitrogen. All the necessary labwares, including tips, eppendorfs, spatulas and mortar pestle were pretreated with diethylpolycarbonate (Sigma Aldrich, USA) to minimize the effect of RNase contamination. The cells were homogenized thoroughly with liquid nitrogen in a mortar pestle. 2 ml of TRI reagent (Sigma Aldrich, USA) were immediately added without allowing the homogenized cells to thaw. The set up was allowed to incubate at room temperature until the TRI reagent thaws completely. The cell lysate were passed several times through a 5 ml syringe with needles intact until the cell homogenate becomes viscous and passes easily through the needle. In the subsequent steps of total RNA isolation, manufacturer's protocol for plant RNA isolation was optimized with TRI reagent.

Total RNA isolation protocol was optimized for its yield and purity and was compared with other standard RNA isolation techniques. The protocols followed for comparative study are (a) Extraction of total RNA by modified CTAB-based method (Zeng and Yang, 2002). (b) Extraction of total RNA by TRI reagent with an additional pretreatment with benzyl chloride. (c) A rapid isolation of total RNA by acid guanidinium thiocyanate-phenol-chloroform extraction (Chomczynski and Sacchi, 1987) (d) Extraction of total RNA by TRI reagent following manufacturer's protocol for plant tissue. (e) Extraction of total RNA by a commercial lipid tissue

isolation kit following manufacturer's protocol. RNA samples were dissolved in RNase-free water and their concentration and purity were determined through spectroscopy.

3.B.1.3 Quantification of RNA

The concentration and purity of the isolated RNA was measured by spectrophotometry. Samples were diluted in RNAase-free water at a ratio of RNA: water of 1:1000 and the ratio of optical density (O.D) at a wavelength of 260 nm and 280 nm (A_{260}/A_{280}) were calculated. Similar ratio of a blank sample having only RNAase-free water was estimated as a control in the study. An O.D value of 1 at 260 nm (A_{260} =1.0) was considered to represent 40 µg ml^{-1} of RNA. The RNA concentration was calculated using the equation as given below:

RNA concentration (µg μl^{-1}) = $O.D_{260}$ (1:1000) X dilution factor X 40

The ratio of the O.D values at 260 nm and 280 nm (A_{260}/A_{280}) provides an estimate of the purity of RNA samples with respect to the contaminants that absorb in the UV region, such as protein and phenol. A value of the ratio in range from 1.9 to 2.1 indicates the purity of the RNA.

3.B.1.4 Formaldehyde denaturing agarose gel electrophoresis

RNA samples were resolved by 1.5 % agarose gel containing 1X 3-(*N*-morpholino) propane sulfonic acid (MOPS) electrophoresis buffer supplemented with 2.2 M of formaldehyde (Green and Sambrook, Molecular Cloning: a Laboratory Manual). To set up a RNA sample for gel loading, a denaturing reaction in a sterile, DEPC treated, RNAase free microcentrifuge tube was prepared by adding the following components:

Components	Amount
RNA (5-10 µg)	5.0 µl
MOPS electrophoresis buffer (10 X)	2.0 µl
Formaldehyde (37 %)	4.0 µl
Formamide	8.0 µl

The gel was submerged in 1 X MOPS electrophoresis running buffer (composition in appendix **Table A4**) at 80 V until the desired resolution was achieved. The RNA fragments were visualized on a UV-Tran-illuminator and imaged using gel documentation system (ChemiDoc XRS+ Imaging System, BIO RAD).

3.B.1.5 Reverse-transcriptase polymerase chain reaction (RT-PCR) based first strand cDNA synthesis

Approximately, 1 µg of total RNA was used for the first strand cDNA synthesis using H minus reverse transcriptase (RT) and random hexamer primer following manufacturer's protocol (RevertAid H Minus first strand cDNA synthesis kit, Fermentas life sciences). The following components were added to an RNase free sterile PCR tube in a total reaction volume of 12 µl:

Components	Amount
Total RNA (~1.012 µg μl^{-1})	1.0 µl (~1.0 µg)
Random hexamer primer (100 pmol ul^{-1})	1.0 µl
Nuclease free water	10.0 µl
Total Volume	**12.0 µl**

The sample was mixed gently by tapping, centrifuged briefly and incubated at 65°C for 5 min to disrupt GC-rich RNA secondary structures and chilled on ice immediately for ~5 min. To the above heat treated RNA sample, the following components were added in the indicated order:

Components	Amount
RT reaction buffer (5 X)	4.0 µl
RiboLock RNase inhibitor (20 U μl^{-1})	1.0 µl
dNTP mix (10 mM)	2.0 µl
H minus reverse transcriptase (200 U μl^{-1})	1.0 µl
Total Volume	**20.0 µl**

The reaction mixture was mixed gently, centrifuged and incubated at 25 °C for 5 min followed by 45 °C for 60 min. The cDNA synthesized was used as template for further downstream PCR amplification studies. For long-term storage the cDNA was aliquoted in 1 µl volume in a sterile nuclease free PCR tube and stored at -80 °C.

3.B.1.6 Checking the integrity of RNA

To evaluate the suitability of the synthesized cDNA for further gene specific PCR amplifications, a control PCR was performed using template cDNA synthesized and the control GAPDH primers (appendix **Table A6, Sl no 1 & 2**) provided with the kit. The composition of the PCR reaction mixture was as follows.

Components	Amount
Synthesized cDNA (1:1000 diluted in autoclaved sterile water)	2.0 µl
PCR buffer (10 X)	5.0 µl
dNTP mix (10 mM each)	1.0 µl
25 mM $MgCl_2$	3.0 µl
GAPDH forward primer (10 µM)	1.5 µl
GAPDH reverse primer (10 µM)	1.5 µl
Taq DNA polymerase (5 u μl^{-1})	0.5 µl
Nuclease free water	35.5 µl
Total Volume	**50.0 µl**

PCR amplification was performed by initial denaturation at 94 °C for 5 min, followed by 35 cycles of amplification [a denaturing step at 94 °C for 30 sec, annealing at 58 °C for 30 sec and an extension at 72 °C for 45 sec]. A 5.0 µl of the above PCR product was resolved on 1 % ethidium bromide pre-stained agarose gel to check the quality of the synthesized cDNA adjudged through the amplification of glyceraldehyde 3 phosphate dehydrogenase (GAPDH) as a housekeeping gene.

3.B.1.7 Preparation of *A. terreus* MTCC6324 microsomal protein extracts

A.terreus MTCC6324 cells were harvested from the early stationary phase of its growth in a static culture. The harvested mycelium were separated from the culture broth and washed with chilled double distilled water followed by chilled 50 mM Tris/HCl buffer (pH 8). The cells were briskly washed with n-hexane to prepare substrate free cell mass following the protocol described by Goswami and Cooney, (1999). The cells were macerated in mortar pestle using lysis buffer (Appendix **Table A2**). The macerated cells were further homogenized in French press (Constant cell disruption Systems, UK) at 30 kpsi. The cell homogenate formed after disruption was processed to isolate the supernatant of the microsomal fraction following the

differential centrifugation procedure as described in Kumar and Goswami, (2006). **Figure 3.1** shows the differential centrifugation procedure to isolate the microsomal protein from *A.terreus*. Briefly, the cell homogenate formed after disruption was mixed with 1 mM DTT and then centrifuged at 10,000×*g* for 15 min to pellet the disrupted cells and nuclei. The supernatant (Sup-1) was collected and subjected to 20,000×*g* for 30 min. The supernatant (Sup-2) collected was again centrifuged at 114,000×*g* for 3 h (Beckman Ultracentrifuge, USA) to sediment the microsomal fraction. The microsomes were separated and suspended in 50 mM Tris/HCl buffer (pH 8.0). The supernatant (Sup-3) formed was retained for further downstream enzymatic study. All the steps in the procedure were performed at 4 °C, unless specified.

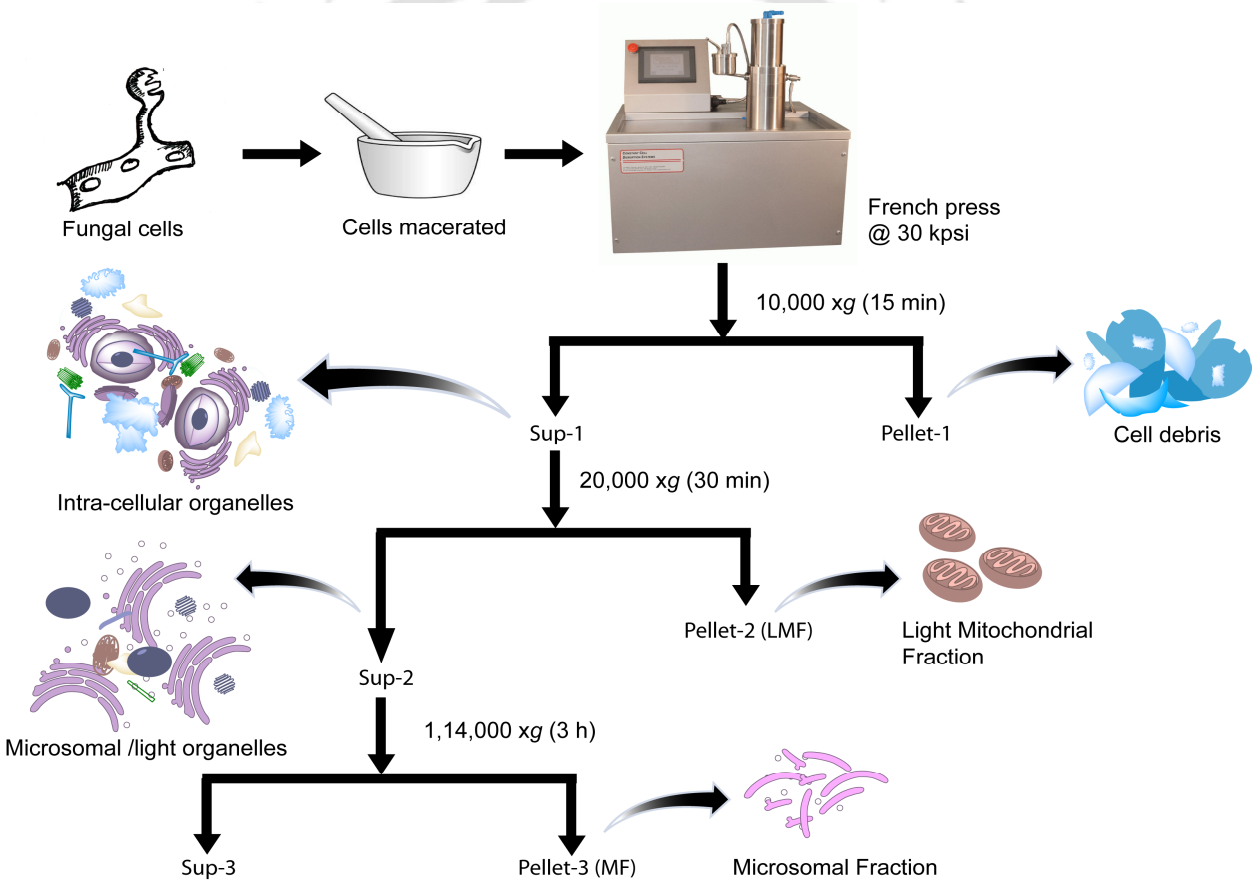

Figure 3.1. Schematic overview of differential centrifugation approach for the isolation of *A.terreus* microsomal protein extract.

3.B.1.8 Activity assay of alcohol oxidase

AOx activity was assayed spectrophotometrically using horseradish peroxidase based coupled assay method of Kemp *et al*, (1988) measuring H_2O_2 generation. Briefly, extinction co-efficient (ε) of 18.4 at 405 nm was used for 1 mM cation radical of 2,2′-azino-bis[3-ethylbenzothiazoline-6-sulphonic acid] diammonium salt (ABTS) (Werner *et al*.,1970), which is equivalent to 0.5 mM oxidized substrate (*n*-heptanol). One unit of enzyme activity was defined as the amount of enzyme required to consume 1µM O_2 per min at 30°C. The overall schematic of the assay method is show in **Figure 3.2**.

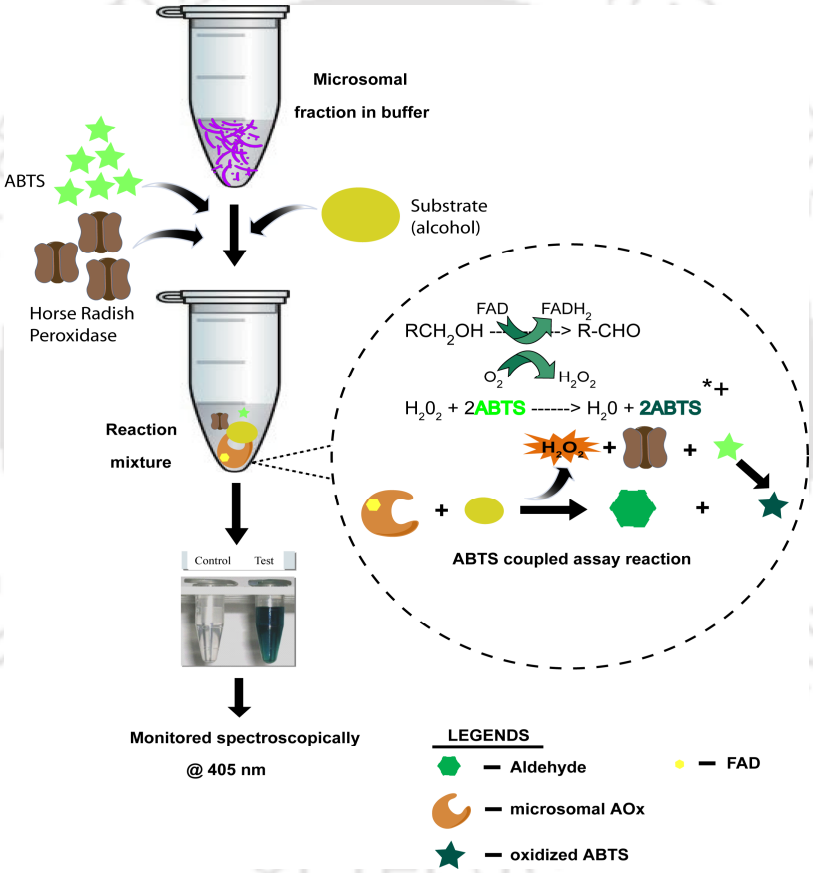

Figure 3.2. Schematic of horseradish peroxidase based coupled assay method for detecting AOx activity.

3.B.1.9 Protein estimation by Bradford assay

Microsomal protein extract was dissolved in 50 mM Tris/HCl buffer (pH 8.0), was dialysed against ice cold 20 mM Tris/HCl buffer (pH 8.0) supplemented with 0.1 mM PMSF for 4 h and was estimated of its total protein concentration by standard Bradford assay (Bradford, 1976) using Bovine serum albumin as a standard protein. A rapid protein quantification kit was purchased from Sigma Aldrich, USA and manufacturer's protocol for 96 well plate based protein estimation was followed. Total protein concentration was estimated by taking the optical density (O.D) values at 595 nm in 2030 Multilabel reader (PerkinElmer, USA).

3.B.1.10 Two dimentional (2D) gel electrophoresis

An experimental overview of 2D electrophoresis of *A.terreus* microsomal protein is shown as schematic in **Figure 3.3**. The dialyzed active supernatant from microsomal fraction (**Fig. 3.3 step 1**) was concentrated with poly (ethylene) glycol 6000 until the protein concentration by Bradford assay (Bradford, 1976) reached ~1mg ml^{-1}. 2D gel electrophoresis was performed (**Fig. 3.3, step 2 & 3**) according to the method described by Gőrg *et al*, (2000). Approximately, 150 µg per 150 µl protein sample was mixed with 250 µl of rehydration solution containing 8 M urea, 2 % (w/v) 3-[(3 Cholamidopropyl) dimethylammonio] -1-propanesulfonate (CHAPS), 0.002 % (v/v) bromophenol blue (1% w/v stock). DL-Dithiothreitol (DTT) and pH 3-10 IPG buffer or Pharmalyte (GE Healthcare, Sweden) were added just prior to use. Sample with rehydration buffer was reduced and alkylated using ProteoPrep Reduction and Alkylation kit (Sigma, USA) following kit's procedure. Sample was then passively rehydrated onto immobiline dry pH gradient strips (linear pH gradient 3-10, 18 cm, GE Healthcare, Sweden) for 16 h at 20 ºC. Strips were overlaid with mineral oil to prevent dehydration. The strip was focused at 500 V for 5 h (step and hold), 1000 V for 1h 30 min (gradient), 10,000 V for 3 h, 10,000 V for 1h (step and hold) using Ettan IPGphor 3 isoelectric focusing unit (GE Healthcare, Sweden). Focused strip was equilibrated in two steps for reduction and alkylation using ProteoPrep Reduction and Alkylation kit (Sigma Aldrich, USA) following kit's procedure. Strip was then loaded onto a vertical polyacrylamide gel and run in second dimension without stacking gel, using 18 cm X 16 cm, 12 % polyacrylamide gel. A blotting paper soaked in protein molecular weight marker was loaded onto the gel. The gel was sealed with agarose sealing solution having 0.5 % (w/v) agarose (Sigma Aldrich, USA) and 0.002 %

(v/v) bromophenol blue (1 % w/v stock) in 1X Sodium Dodecyl Sulphate (SDS) electrophoresis buffer. Electrophoresis was carried out following standard protocol of Laemmli, (1970) in vertical electrophoresis unit (SE 600 Ruby, GE Healthcare).

3.B.1.11 Mass spectrometry compatible silver staining of SDS-PAGE gel

Mass spectrometry compatible silver staining of polyacrylamide gel after second dimension was carried out following the protocol of Chevallet *et al*, (2006). Depending on the downstream application for sensitive detection of target protein spot and maximum sequence coverage in peptide mass fingerprinting, ultrafast silver nitrate staining protocol was adopted, amongst the five optimized protocols reported in the article. The gel was scanned using Image Scanner III (GE Healthcare, Sweden) and gel analysed using labScan 6.0 software (GE Healthcare, Sweden). Spot detection and excision was done manually.

3.B.1.12 Target protein identification from 2D gel spots

Silver stained 2D gel was manually investigated for protein spots and subsequently excised (**Fig. 3.3 step 4**) and digested by trypsin following an optimized in-gel digestion protocol of Shevchenko *et al.*, (2007) (**Fig. 3.3 step 5**). Each spots were cut into cubes of approximately 1 X 1 mm and 500 µl per spot of acetonitrile was used to shrink the gel pieces for 10 min followed by a brief spin. The liquid above the gel pieces were removed and discarded. 30-50 µl of DTT solution (10 mM DTT in 100 mM ammonium bicarbonate) were added to completely submerge the gel pieces and incubated at 56 ºC for 30 min in a water bath. The tubes were chilled at room temperature (RT) (22 ºC) and 500 µl of acetonitrile were added to each tube and incubated for 10 min and the liquid was pipetted out. 30-50 µl of iodoacetamide solution (55 mM in 100 mM ammonium bicarbonate) were added to completely cover the gel pieces and incubated in dark at RT for 20 min. The gel pieces were finally dehydrated with acetonitrile and all the liquid was removed. DTT and iodoacetamide solutions were prepared shortly before use. The gel pieces were covered with 50 µl of trypsin buffer [50 mM ammonium bicarbonate containing 10 % (v/v) acetonitrile] and incubated on ice for 30 min. 20 µl of freshly prepared trypsin stock solution (20 µg ml^{-1} in trypsin buffer supplemented with 1 mM HCl) was added to the gel samples so as to cover the gel pieces completely and incubated overnight at 37 ºC. After incubation, all the liquid above the gel pieces were transferred to a fresh sterile tube and gels were again incubated with

peptide extraction buffer (1:2 v/v 5 % formic acid/acetonitrile) for 30 min at 37 ºC in water bath. The peptide extraction solution was removed and combined with the liquid in the previous step.

Target protein identification by Matrix Assisted Laser Desorption Ionization Time of Flight-Mass Spectrometry (MALDI-TOF-MS) (4800 plus MALDI TOF/TOF Analyzer, AB SCIEX, USA) was carried out for each of the 2D gel spots (**Fig. 3.3 step 6**). Samples for MALDI-TOF-MS was prepared by mixing 6 µl of saturated α-cyano-4-hydroxycinnamic acid matrix (10 mg ml^{-1} of 50 % acetonitrile and 0.05 % trifluoroacetic acid in 0.2 micron filtered water) with 6 µl of eluted peptide solution for each spot. The samples were prepared immediately and vortexed to make a homogenous solution and 1µl of the mixture was dropped onto the metal target plate. The samples were air-dried completely. The plate was properly aligned and calibrated using calibration mixture (4700 proteomics analyzer calibration mix, AB SCIEX, USA). Samples for calibration were made according to the manufacturer's instructions. Samples were analyzed using MS mode to obtain the peptide mass fingerprint (pmf) of each 2D spot. For each sample 2D spot, peak list was generated using 4000 series explorer software package (AB SCIEX, USA).

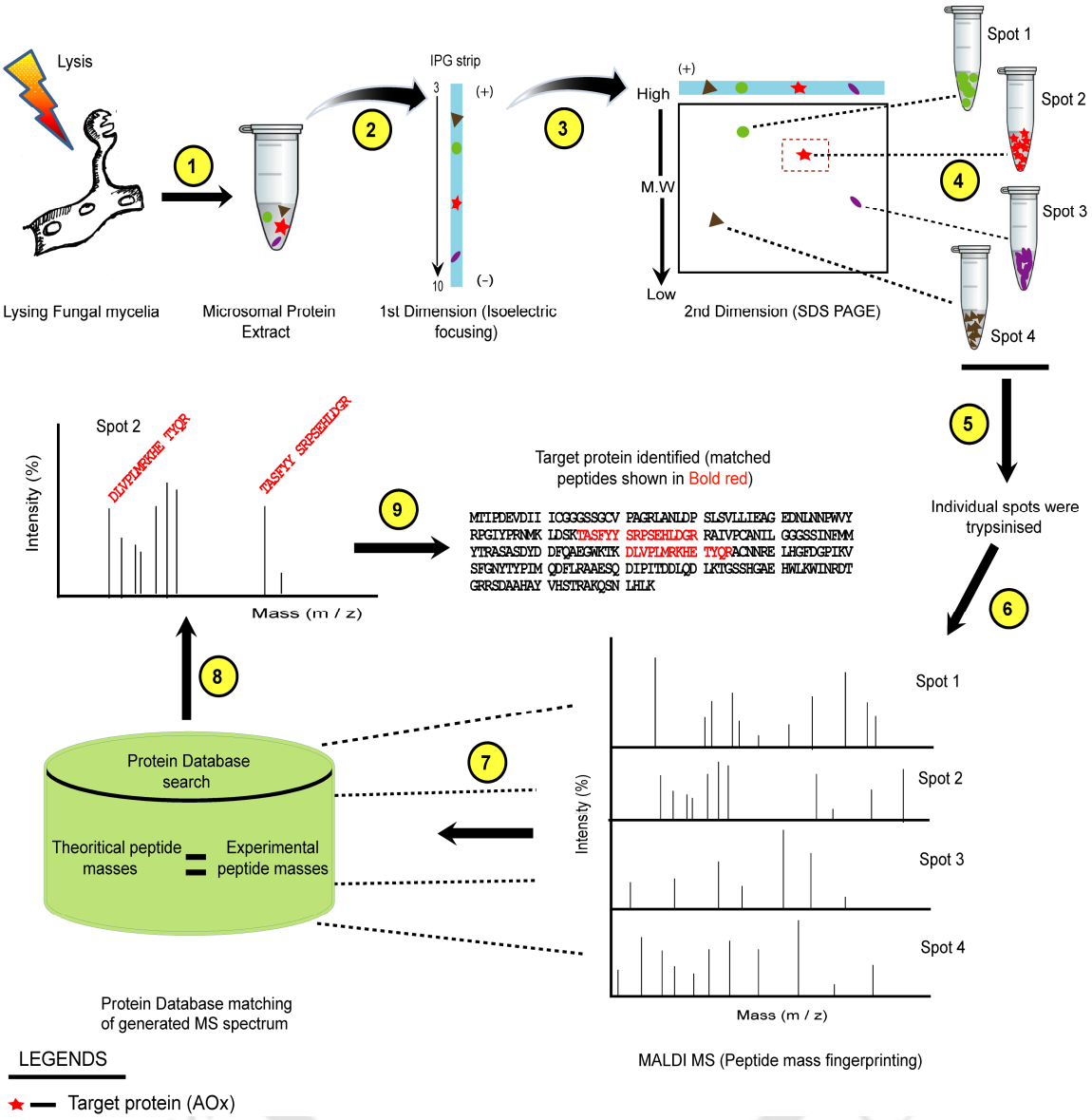

Figure 3.3. An experimental overview of steps involved in target protein identification from 2D gel by MALDI-TOF-MS.

3.B.1.13 Peptide mass fingerprinting database search

Pmf peak lists generated from each MALDI-TOF-MS sample corresponding to each 2D gel spots were analyzed for detectable m/z values (**Fig. 3.3 step 7**). One out of the seven spots that were analyzed was found to contain detectable m/z peak values after analyzing through FindPept (Gattiker *et al.*, 2002) online mass spectrometry database search tool (ExPasy Bioinformatics resourse portal) (**Fig. 3.3 step 8**). The peptide masses resulting from specific and

unspecific cleavage of the protein were matched with the theoretical masses generated from the peptides of hypothetical alcohol oxidase protein sequence (*Aspergillus terreus* NIH2624, GI: 115437438). Target protein match was confirmed through database search of pmf data corresponding to each 2D spot analyzed (**Fig. 3.3 step 9).**

3.B.1.14 Multiple sequence alignment (msa) of reported AOxs from fungal and yeast species

Multiple amino acid sequence alignment of AOxs from different filamentous fungi and yeast species were done with ClustalX version 2.1 (Jeanmougin *et al*., 1998) and the data file generated were visualized and analyzed through GeneDoc software tool (Nicholas *et al*., 1997). Unreviewed hypothetical AOx protein sequence from *A.terreus* NIH2624 (GI: 115437438) was taken as a query sequence in NCBI protein BLAST. Different filamentous fungi and yeast species coding for AOx enzyme, having 60 % or more amino acid sequence homology with the query were taken for protein multiple sequence alignment. Highly conserved amino acid sequence motifs were used for further sequence analysis for designing overlapping PCR primer probes.

3.B.1.15 Designing overlapping PCR primer probes to amplify the coding sequence of AOx

Primer probes for full length amplification of AOx gene from cDNA of *A.terreus* MTCC6324 were designed based on the peptide sequence information retrieved from the pmf and msa data generated previously. A top down proteomics based gene identification strategy (**Fig. 3.4)** was undertaken to characterize full length AOx coding sequence from cDNA of *A.terreus* MTCC6324. Two overlapping PCR amplicons covering the entire coding sequence were performed. For the first PCR (PCR 1), the forward primer (AOx-FP1) (Appendix **Table A6, Sl no 3**) was designed from the 5' end (start codon) of AOx coding sequence of *A.terreus* NIH2624 and the reverse primer (AOx-RP1 (Appendix **Table A6, Sl no 4**) was designed based on the internal peptide fragment (Fragment 1) from pmf in sync with the conserved region of msa data. The second overlapping PCR amplicon (PCR 2) was generated using the forward primer (AOx-FP2) (Appendix **Table A6, Sl no 5**) designed from internal peptide fragment

(Fragment 2) of pmf data corresponding to the conserved region of msa, and reverse primer (AOx-RP2) (Appendix **Table A6, Sl no 6**) designed from 3' end of AOx sequence information of *A.terreus* NIH2624 available in NCBI database.

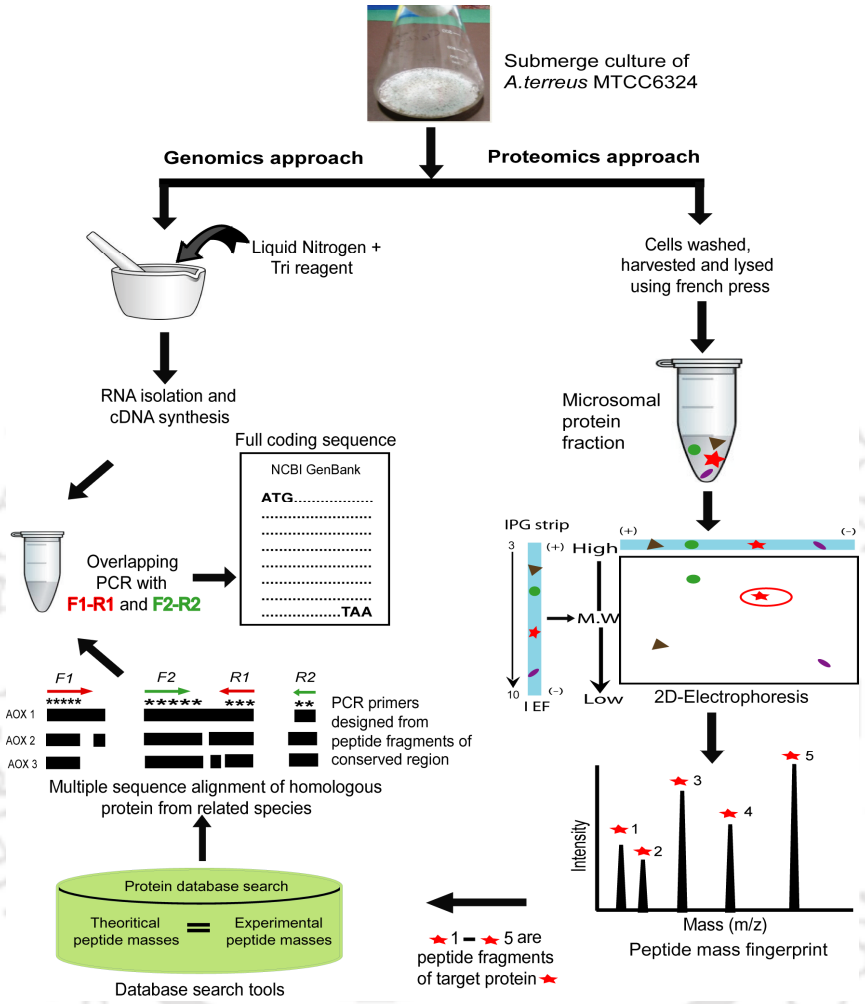

Figure 3.4. An overall schematic diagram highlighting the proteomics and genomics approach undertaken to characterize AOx cDNA. Target protein is marked in red star. AOX 1, AOX 2 and AOX 3 represent the amino acid sequences of different AOxs. F 1, F 2, R 1 and R 2 represent the PCR primers AOx-FP1, AOx-FP2, AOx-RP1 and AOx-RP2, respectively.

3.B.1.16 Overlapping PCR

The above two overlapping PCRs (PCR 1 and 2) were optimized in 50 µl reaction volume, using ~10 ng of cDNA of n-hexadecane induced *A. terreus* MTCC6324 as a template

and high fidelity taq DNA polymerase (BIO-X-ACT Long DNA polymerase, Bioline, UK). The compositions of both the PCR reaction mixtures were as follows.

Components	Amount
OptiBuffer (10 X stock)	5.0 µl
$MgCl_2$ solution (50 mM stock)	1.0 µl
dNTP (100 mM stock)	1.0 µl
DMSO	2.5µl
Forward primers (AOx-FP1/ AOx-FP2) (~ 20 pmol/ul stock)	1.0 µl
Reverse primers (AOx-RP1/ AOx-RP2) (~ 20 pmol/ul stock)	1.0 µl
cDNA (~10 ng μl^{-1})	1.0 µl
High fidelity *Taq* DNA polymerase (4 u μl^{-1})	1.0 µl
Nuclease free water	36.50 µl
Total Volume	**50.0 µl**

PCR amplifications for both the overlapping PCR products were performed using GeneAmp PCR system 9700 (Applied Biosystems, USA) following the optimized conditions of initial denaturation at 94 ºC for 5 min; 35 cycles of amplification [a denaturation step at 94 ºC for 30 sec, annealing at (60 ºC for PCR 1 and 63 °C for second overlapping PCR 2) for 45 sec, initial extension at 72 ºC for 1.5 min]; final extension at 72ºC for 10 min.

3.B.1.17 Agarose gel electrophoresis of DNA

DNA samples were resolved by agarose gel electrophoresis (Green and Sambrook, 2012) using agarose gel (0.8-1.5 % w/v agarose concentration supplemented with 0.5 µg ml^{-1} of ethidium bromide) in 1X TAE (Appendix **Table A4**) at 70 V until the desired resolution was achieved. The DNA fragments were visualized on a UV-Transilluminator and imaged using gel documentation system (ChemiDoc XRS+ Imaging System, BIO RAD).

3.B.1.18 Elution of DNA samples from agarose gel

PCR amplified products and digested plasmids and inserts used for downstream ligation cloning in pGEM-T Easy T/A vector or in other expression vectors were eluted out of agarose gel by using GenElute Gel Extraction kit (Sigma Aldrich, USA) by following the kit

manufacturer's protocol. DNA fragment of interest was excised out of the agarose gel by using a sterile, sharp scalpel. Care was taken to trim out the excess of agarose around the DNA band. Gel solubilization was performed in 2 ml sterile eppendorf tube by adding 3 gel volumes of gel solubilization solution to the excised DNA-agarose gel piece (i.e.:100 mg agarose gel + 300 µl gel solubilization solution) and allowed to incubate for 10 min at 50-60 °C, until the gel slice is completely dissolved. The mixture was vortexed briefly during incubation to help dissolve the gel, completely. GenElute binding column was placed in one of the 2 ml sterile collection tube provided with the kit and equilibrated with 500 µl of column preparation solution (supplied with the kit) and centrifuged for 1 min at 14,000 x *g*. The flow through was discarded. The agarose solubilized DNA sample solution was checked for yellowish color and 1 gel volume of 100% molecular biology grade iso-propanol was added and mixed until homogenous. The sample DNA solution was then loaded onto the pre-equilibrated binding column in maximum volume not exceeding 700 µl at one time and centrifuged for 1 min at 14,000 x *g*. The flow through liquid was discarded and the binding column was placed back into the same collection tube and 700 µl of wash solution (prepared as described in the manufacturer's protocol) was added and centrifuges for 1 min at 14,000 x *g* followed by discarding the flow through and placing back the binding column in the same collection tube. A blank centrifuge of the binding column-collection tube assembly was performed at 14,000 x *g* for 1 min to remove excess ethanol, without adding any more wash solution to it. The DNA was eluted by adding 50 µl of elution solution (provided with the kit) pre-heated to 65 °C at the center of the binding column placed in a fresh sterile eppendorf tube (provided with the kit) and centrifuged at 14,000 x *g* for 1 min. The eluted DNA solution was checked quantitatively and qualitatively through UV visible spectroscopy and DNA agarose gel electrophoresis, respectively for further downstream application.

3.B.1.19 Cloning PCR amplicons in pGEM-T Easy T/A vector system

Overlapping PCR amplicons were cloned into T/A cloning vector pGEM-T-Easy vector system (Promega, USA) (Appendix **Table A16** and appendix **Fig. A1.A)** for clone maintenance, sequencing and other downstream applications (**Fig. 3.5**). Briefly, the PCR amplicons were gel eluted following the protocol described in section **3.B.1.18** and cloned into pGEM-T-Easy vector following the manufacturer's instruction. The ligation mixture was prepared in a sterile 0.5 ml tube as follows

Components	Amount
2X Rapid ligation buffer	5.0 µl
pGEMT-T Easy vector (50 ng μl^{-1})	1.0 µl
Insert DNA (PCR products/digested plasmids)	25.0 ng (approx)
T4 DNA ligase (3 Weiss unit μl^{-1})	1.0 µl
Nuclease free water to final volume	10.00 µl

The reaction mixture was pipetted and allowed to incubate at 4 °C in circulating water bath for overnight and the ligated mixture was transformed into competent *E.coli* DH5α cells by standard heat shock method described in **section 3.B.1.22** (Green and Sambrook, 2012) and plated on LB agar /ampicillin/IPTG/X-Gal plates.

3.B.1.20 Quantification of DNA

The concentration and purity of DNA samples were measured spectrophotometrically. Samples were diluted in nuclease free water at a ratio of DNA: water of 1:1000 and the ratio of optical density (O.D) at a wavelength of 260 nm and 280 nm (A_{260}/A_{280}) were calculated. Similar ratio of a blank sample having only nuclease free water was estimated as a control in the study. An O.D value of 1 at 260 nm (A_{260} =1.0) for double stranded DNA and single stranded DNA was considered to represent 50 ng μl^{-1} and 20-33 ng μl^{-1} , respectively. The DNA concentration was calculated using the equation as given below:

DNA concentration ($\mu g\ \mu l^{-1}$) = $O.D_{260}$ (1:1000) X dilution factor X 50 or 20-33

The ratio of the O.D values at 260 nm and 280 nm (A_{260}/A_{280}) provides an estimate of the purity of the DNA samples with respect to the contaminants that absorb in the UV region, such as protein and phenol. A value of the ratio in range from 1.8 to 2.0 indicates the purity of the DNA.

3.B.1.21 Competent *E.coli* cells preparation

A one-step competent *E.coli* DH5α / BL21 (DE3) cell preparation protocol was adopted in this thesis for transformation and storage of competent bacterial cells in the same solution by Chung *et al.* (1989). Briefly, a single colony of bacterial cell was inoculated aseptically in 5 ml of LB broth (HIMEDIA, India) (Appendix **Table A1**) as a primary culture and allowed to incubate overnight at 37 °C in an incubator shaker under constant shaking at 180

rpm. A 1 % primary culture was charged aseptically in a 25 ml LB broth and grown till early exponential phase until the optical density (O.D) at 660 nm wavelength reads 0.4-0.5. The culture was then centrifuged at 3000 x *g* for 10 min at 4°C. The bacterial pellet was then resuspended aseptically in 2.5 ml of sterile ice-cold transformation and storage solution (TSS solution) (Appendix **Table A5**) and aliquoted in an appropriate volume and frozen immediately at -80 °C for long term storage.

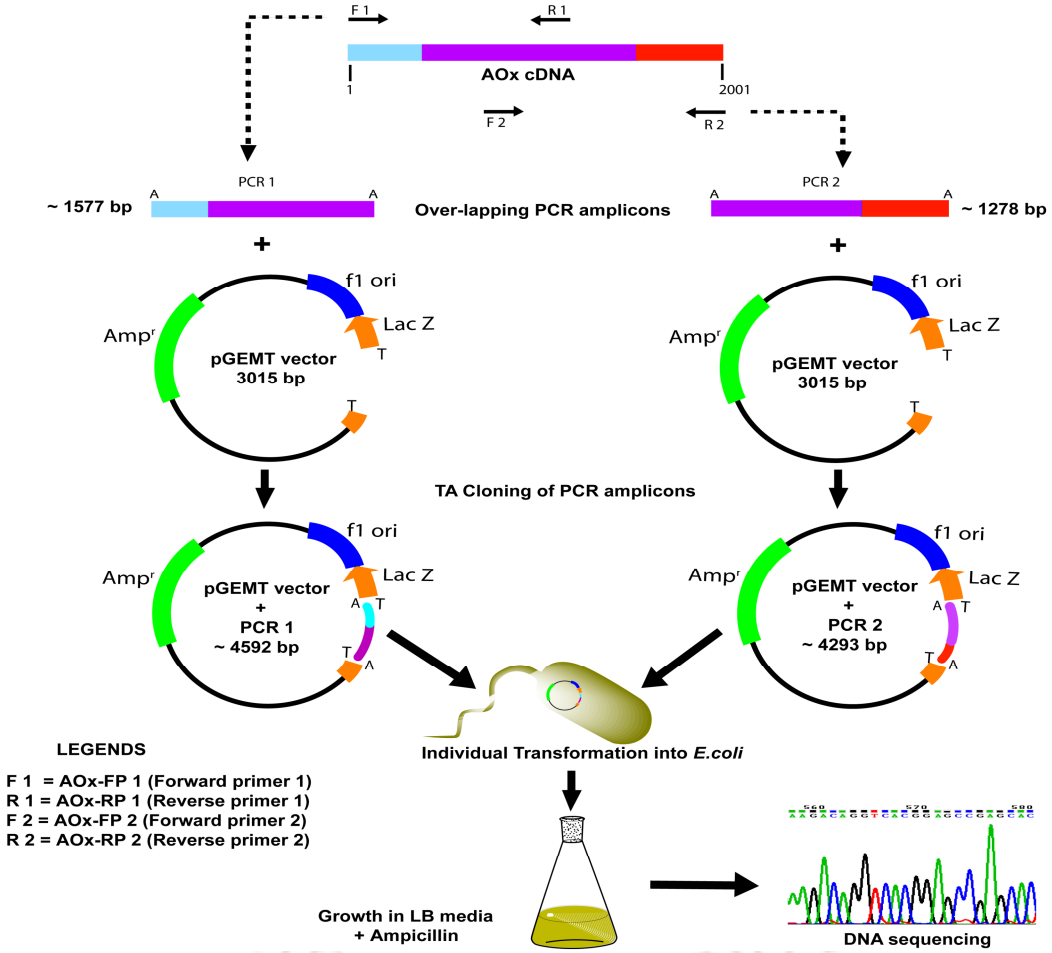

Figure 3.5. An overview of overlapping PCR approach.

3.B.1.22 Transformation of competent *E.coli* cells

For transformation, a 100 µl aliquot of the competent bacterial suspension in TSS solution prepared in **section 3.B.1.21** was transferred aseptically into a prechilled sterile 0.5 ml tube stored in ice and to it 10 µl of the ligation mixture from **section 3.B.1.19** were mixed aseptically by pipetting and dispensing. The mixture was allowed to incubate on ice for 30 min.

The competent cells were then subjected to heat shock at 42 °C in a circulating water bath for 90 sec and chilled on ice immediately. 800 µl of pre-warmed sterile LB broth at ~37 °C was added aseptically to the cells and allowed to incubate for 1 h at 37 °C with constant shaking at ~180 rpm. The cells were then harvested by centrifugation at 3000 x *g* for 10 min at 4 °C and ~ 700 µl of the supernatant was discarded aseptically and the remaining ~ 200 µl was mixed with the transformed bacterial cell pellet to form a homogenous mixture by pipetting aseptically. The resuspended cells were pour-plated on LB agar/IPTG/X-Gal plates containing appropriate antibiotic and incubated at 37 °C for 12-16 h. Subsequently, the colonies were screened for positive clones either by blue-white screening (T/A cloning in pGEM-T Easy vector) or manual screening of colonies (in case of cloning in other vectors). The cloned insert DNA fragment was also confirmed through restriction digestion with appropriate restriction endonuclease enzymes for fragment release when resolved on agarose gels.

3.B.1.23 Plasmid DNA isolation

Plasmid DNA was isolated from 5 ml of overnight grown, transformed bacterial culture by alkaline lysis method following the mini preparation protocol (Green and Sambrook, 2012). Reagents used in this method are enlisted in appendix **Table A7** at the back of the thesis. A single *E.coli* colony harboring a recombinant plasmid was grown in LB broth with appropriate antibiotic for 14-18 h at 37 °C under constant shaking at 180 rpm. The culture was harvested at 12,000 x *g* for 1 min at 4 °C and the cell pellet was resuspended in 100 µl of ice-cold solution I by pulse vortexing. The cell suspension was lysed with 200 µl of freshly prepared solution II by inverting the content of the tube gently for 5-6 times. Any vortexing at this point was completely avoided and the content was allowed to incubate on ice for 5 min. Contamination of plasmid preparation by genomic DNA and cell debris were precipitated by adding 150 µl of ice-cold solution III. The viscous bacterial lysate was mixed by gently inverting the tube 6-8 times and incubated on ice for 3-5 min followed by centrifugation at 12,000 x *g* for 10 min at 4 °C. The supernatant was transferred to a fresh tube and an equal volume of Tris saturated (pH 8.0) phenol: chloroform: iso-amyl alcohol (25:24:1 v/v, Sigma Aldrich, USA) was added. The resulting organic and aqueous mixture was mixed thoroughly by vortexing and the emulsion was centrifuged at 12,000 x *g*. The aqueous upper layer of the supernatant was aspirated out to a fresh tube and 2 volumes of molecular biology grade 100 % ethanol was added to precipitate the

plasmid DNA by incubating at -20 °C overnight. After incubation the nucleic acid was precipitated by centrifugation at 12,000 x *g* for 10 min at 4 °C. The supernatant was removed gently and the DNA pellet was washed with 70 % ice-cold molecular biology grade ethanol. The plasmid DNA was recovered by centrifugation at 12,000 x *g* for 10 min at 4 °C. The ethanol as supernatant was gently aspirated out and any residual droplets of ethanol were completely removed by inverting the tube and gently tapping it against a bed of tissue paper. Desiccation under vacuum was avoided to make the DNA pellet easily soluble in water and avoid denaturation. The plasmid DNA was resuspended in appropriate amount of nuclease free water for downstream application. RNA contamination was removed by incubating the plasmid preparation with 20 µg ml^{-1} DNase-free RNase at 37 °C for 30 mins.

3.B.1.24 Digestion of DNA by restriction enzymes

PCR amplified DNA fragments, plasmid DNA and cloning vectors (except pGEM-T Easy T/A vector) were subjected to restriction endonuclease digestion (New England Biolabs, USA). An aliquot of above DNA sample (~2 µg) was digested for 5 h with required high fidelity restriction endonucleases according to the conditions specified by the manufacturer. A list of restriction enzymes used in this study along with their corresponding buffer compatibility, temperature and time of incubation and termination conditions are given in appendix Table A8. An aliquot of the digested product was analyzed qualitatively by resolving on an appropriate concentration of agarose gel by electrophoresis.

3.B.1.25 Characterization of full length ORF of AOx from overlapping PCR product

Each PCR fragments (PCR 1 and 2) cloned into T/A cloning vector (pGEM-T Easy, Promega, USA) was analyzed individually through DNA sequencing as mentioned in **section 3.B.1.26**. *Bg1*II and *Nde*I as unique restriction enzyme sites present in the overlapping region of both the PCR fragments and in the pGEMT vector backbone, respectively, were chosen for checking the proper orientation of the cloned fragments (**Fig. 3.6**). First PCR product harboring the start codon of AOx open reading frame was ligated with second PCR fragment harboring the stop codon, at the common restriction site, thus confirming the full length functional clone of AOx from *A.terreus* MTCC6324. The full length clone of AOx in TA vector was confirmed

through digestion with *EcoR*I restriction endonuclease releasing the cloned insert fragment from T/A vector backbone. The same was also confirmed through double stranded primer walking of full length AOx fragment cloned in T/A vector.

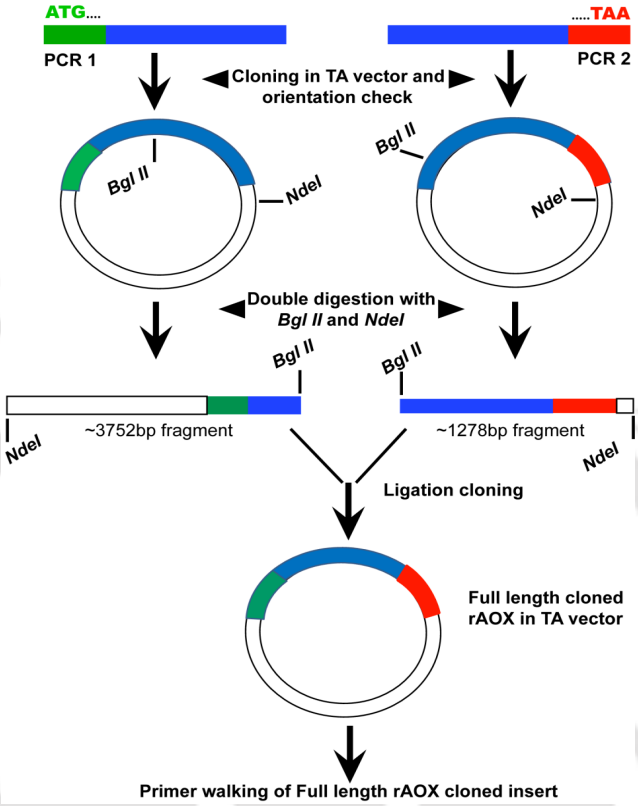

Figure 3.6. Schematic showing the experimental methodology to confirm the orientation of the individual PCR fragments cloned in T/A vector and subsequent ligation at common restriction site (*Bg1*II) to achieve full length AOx clone in T/A vector.

3.B.1.26 DNA sequencing of cloned fragments

PCR amplified products (PCR 1 and 2) cloned in pGEM-T Easy were subjected to DNA sequencing before modification and ligation experiments. Sequencing was done by dideoxy method using universal M13 forward and reverse primers, respectively and sequencing data were further analyzed by DNA Baser sequence assembly software version 4.10 (Heracle BioSoft S.R.L, Rome, Italy). Double stranded primer walking data was similarly analyzed using the software and three overlapping primer walked contigs joined by the software, gave the full length coding nucleotide sequence information of AOx from *A.terreus* MTCC6324. All the DNA

sequencing were performed by DNA sequencing facility, Department of Biochemistry, University of Delhi, South Campus using 3130xl Genetic Analyzer (Applied Biosystems, USA).

3.B.2 Sub-cloning and expression of recombinant AOx protein in *E.coli*

3.B.2.1 PCR amplification of AOx fragment from AOx cloned pGEM-T Easy vector

The full length AOx gene cloned into TA cloning vector was PCR amplified using forward (AOX-pET28a-F) and reverse (AOX-pET28a-R) primer and ligated to expression plasmid pET28a(+) (Novagen, Merck, Germany) (Appendix **Table A16** and appendix **Fig. A1.B**) using Quick ligation kit (New England Biolabs, USA) at the *EcoR*I and *Hind*III restriction site. *EcoR*I and *Hind*III restriction sites are provided in the forward and reverse primers, respectively as underlined with bold characters (appendix **Table A6, Sl no 7 & 8**).

PCR was optimized in 50 µl reaction volume using GeneAmp PCR system 9700 (Applied Biosystems, USA) using high fidelity *Taq* DNA polymerase (Bioline, UK). The PCR reaction mixture is as follows:

Components	Amount
OptiBuffer (10 X stock)	5.0 µl
$MgCl_2$ solution (50 mM stock)	1.0 µl
dNTP (100 mM stock)	1.0 µl
DMSO	2.5 µl
Forward primers (AOX-pET28a-F) (~ 20 pmol/ul stock)	1.0 µl
Reverse primers (AOX-pET28a-R) (~ 20 pmol/ul stock)	1.0 µl
pGEMT cloned AOX gene (~2.5 ng μl^{-1})	0.5 µl
High fidelity *Taq* DNA polymerase (4 u μl^{-1})	1.0 µl
Nuclease free water	37.00 µl
Total Volume	**50.0 µl**

The PCR condition was optimized with initial denaturation at 94 ºC for 5 min; 35 cycles of amplification [a denaturation step at 94 ºC for 30 sec, annealing at 61ºC for 45 sec, initial extension at 72 ºC for 2 min]; final extension at 72 ºC for 10 min. The PCR product was gel

eluted and purified for downstream experimentation using GenElute gel extraction kit (Sigma Aldrich, USA) following the manufacturer's protocol described in **section 3.B.1.18**.

3.B.2.2 Ligation of PCR amplified AOx fragment to pET28a(+) bacterial expression system.

An overall schematic showing the sub-cloning and ligation of T/A cloned AOx fragment into bacterial expression system is depicted in **Figure 3.7**. A 2001 bp PCR amplified AOx fragment having *EcoR*I and *Hind*III restriction sites from **section 3.B.1** and *EcoR*I – *Hind*III double restriction endonuclease digested bacterial expression vector, pET28a(+) was co-purified from a resolved agarose gel following the protocol described in **section 3.B.1.18.** The concentration of each was determined spectrophotometrically as described in **section 3.B.1.20.** Gel eluted vector (~50 ng) was ligated with 3-fold molar excess of gel eluted insert PCR product (~150 ng) in a sterile PCR tube, following the composition given below in a reaction volume of 20 µl :

Components	Amount
pET28a (+) vector	~50 ng
PCR AOx as Insert	~150 ng
2X Quick Ligation reaction buffer	10.0 µl
Quick T4 DNA ligase	1.0 µl
Nuclease free water to final volume	20.0 µl

The reaction mixture was mixed thoroughly by tapping or pipetting and centrifuged briefly to pull down the content at the bottom of the tube and incubated at 25 °C for 10 min in a PCR block for accurate heating.

The cloned AOx gene in pET28a (+) was transformed into competent BL21 (DE3) *E. coli* expression host by heat shock method as described previously in s**ection 3.B.1.21** and **3.B.1.22**. Successful ligation into pET28a(+) and transformation into BL21 (DE3) was confirmed through fragment release after restriction digestion with *EcoR*I and *Hind*III restriction enzymes as per the protocol described previously in **section 3.B.1.24**. Ligation of AOx gene at *EcoR*I and *Hind*III site allowed for Isopropyl β-D-1-thiogalactopyranoside (IPTG) inducible expression of apo-rAOx having both N- and C-terminal six-histidine tag for stringent affinity purification of this enzyme.

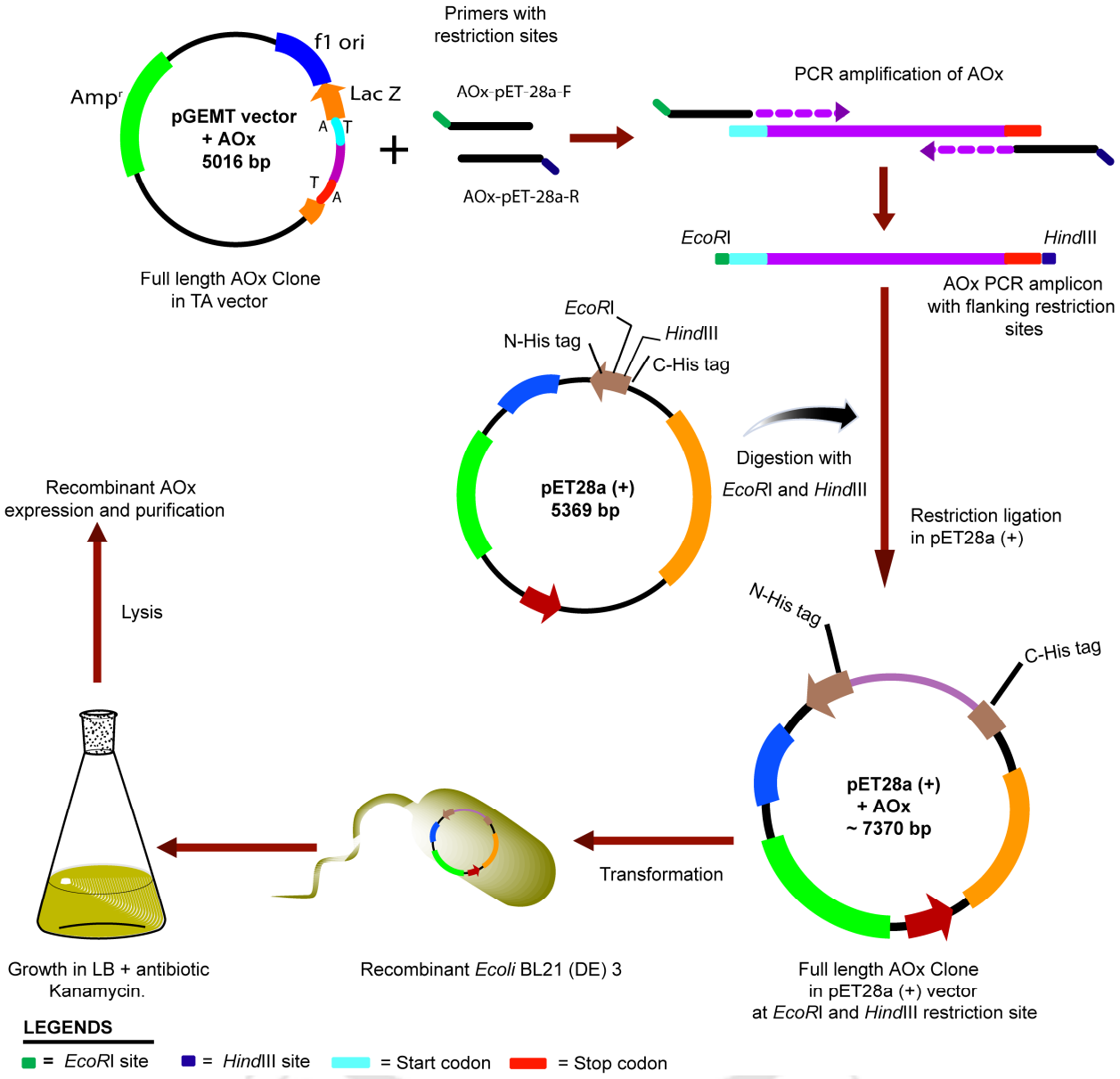

Figure 3.7. An overview of sub-cloning full length AOx fragment from pGEM-T Easy to *E.coli* expression system pET28a(+).

3.B.2.3 Expression of histidine tagged apo-rAOx in *E.coli* BL21(DE3)

Transformed *E.coli* BL21 (DE3) cells with pET28a-AOx recombinant plasmid were screened for positive clones and a single colony was grown overnight in 5 ml LB broth as primary culture supplemented with 50 µg ml^{-1} kanamycin antibiotic at 37 ºC and under constant shaking at 180 rpm. The overnight grown primary culture was given a second passage in a sterile

LB medium at a dilution of 1:100 as a secondary culture and grown at the same condition specified above until the optical density (O.D) at $\lambda_{660\ nm}$ reaches mid-log phase ($O.D_{660}$=0.6-0.8) for induction with IPTG.

To optimize small scale expression of apo-rAOx, the transformed secondary culture (5 ml volume) was induced with IPTG in concentration of 0, 0.25, 0.5 mM and a time point of 0, 4 and 8 h duration. Temperature of 15 ºC, 20 ºC, 25 ºC and 30 ºC were studied to optimize the induction temperature. Un-induced expression of apo-rAOX was also checked as a control in our studies. To check the over-expression of our protein of interest, 5 ml of IPTG induced cultures were harvested by centrifugation at 5000 x *g* for 10 min at 4 ºC in sterile 1.5 ml or 2 ml polypropylene tubes. The supernatant was discarded and the cells were resuspended in 600 to 700 µl of lysis buffer (Appendix **Table A9**) and disrupted by probe based sonication (Hielscher Ultrasonics, Germany) at amplitude of 40 % with 0.5 cycle at 4 ºC until the viscosity of the cell lysate becomes less and turns clearer when put against light source. The cell homogenate formed after sonication was clarified by centrifugation at 14,000 x *g* for 20 min at 4 ºC. The supernatants having the cell free solubilized total proteins and the pellet fractions having the proteins as inclusion bodies were simultaneously loaded onto SDS-PAGE following standard Laemmli protocol (Laemmli, 1970) to check for the over-expressed protein of interest.

3.B.2.4 Sodium dodecyl sulfate polyacrylamide gel electrophoresis (SDS-PAGE) of protein

SDS PAGE was performed to analyze the expression of recombinant proteins (rAOx in this case) and for western blot analysis. Required amount of cell free total protein, cell pellet fraction and purified soluble protein were mixed with 4X SDS-PAGE gel loading buffer (Appendix **Table A11**) with reducing agent and heated in a boiling water bath for 3-5 min. Standard SDS-PAGE protein marker for regular SDS-PAGE and pre-stained protein marker for western blots were procured from New England Biolabs (USA) and processed simultaneously as per the manufacturer's instructions. Denatured protein samples along with standard SDS-PAGE protein markers were subjected to SDS-PAGE following the method of Laemmli, (1970). The electrophoresis was carried out using 5 % stacking and 12 % separating gels of thickness 0.75 mm at a constant voltage of 120 mV in MiniVE vertical electrophoresis unit (GE Healthcare).

After the electrophoresis, the gels were stained with “Blue silver staining” protocol of Candiano *et al*, (2004), using colloidal coomassie G-250 (Sigma Aldrich, USA) (Appendix **Table A12**).

3.B.3 Isolation, solubilization and purification of apo-rAOx from inclusion bodies and reconstitution with co-factor FAD

3.B.3.1 Isolation, purification and solubilization of apo-rAOx from inclusion bodies

Pure inclusion bodies containing the over-expressed AOx protein were isolated by modifying the methodology of Schwanke *et al*, (2009) (**Fig. 3.8**). The expression was scaled up in 1 liter culture volume. IPTG induction was carried out following the optimized parameters for small scale expression. Bacterial cells were harvested by centrifugation at 6000 x *g* for 10 min at 4 ºC. *E.coli* cells of approximately 2.4 g wet weight per liter of induced culture were used for inclusion body isolation and subsequent refolding studies. *E.coli* cells were lysed in lysis buffer (appendix) and the inclusion bodies were isolated by centrifugation at 12,000 x *g* for 30 min at 4ºC. The inclusion bodies were washed extensively using sodium deoxycholate (Sigma Aldrich, USA) at a concentration of 1% (w/v) in lysis buffer and kept at mild stirring condition for 1 h at room temperature (RT) and thereafter sonicated briefly (6-7 min, 15 sec on and 10 sec off, 30 % amplitude). The inclusion bodies were pelleted at 12,000 x *g* for 30 min and resuspended in lysis buffer containing 2M urea at a final total protein concentration of ~2 mg ml^{-1}. The pH of the solution was adjusted to 11.0-12.5 with 1M NaOH and the solution was stirred at RT for 30 min. The pH was then reduced to 8.0 with 1 N acetic acid and centrifuged at 12,000 x *g* for 30 min. The supernatant containing the solubilized rAOx was collected and dialysed overnight at 4 ºC against 20 mM sodium phosphate buffer pH 7.4 supplemented with 5-10 % (v/v) glycerol to avoid protein aggregation and precipitation in the dialysis bag. In the above protocol no EDTA was used as in the original protocol by Schwanke *et al*, (2009) to avoid chelating out of nickel ions during downstream nickel affinity chromatography.

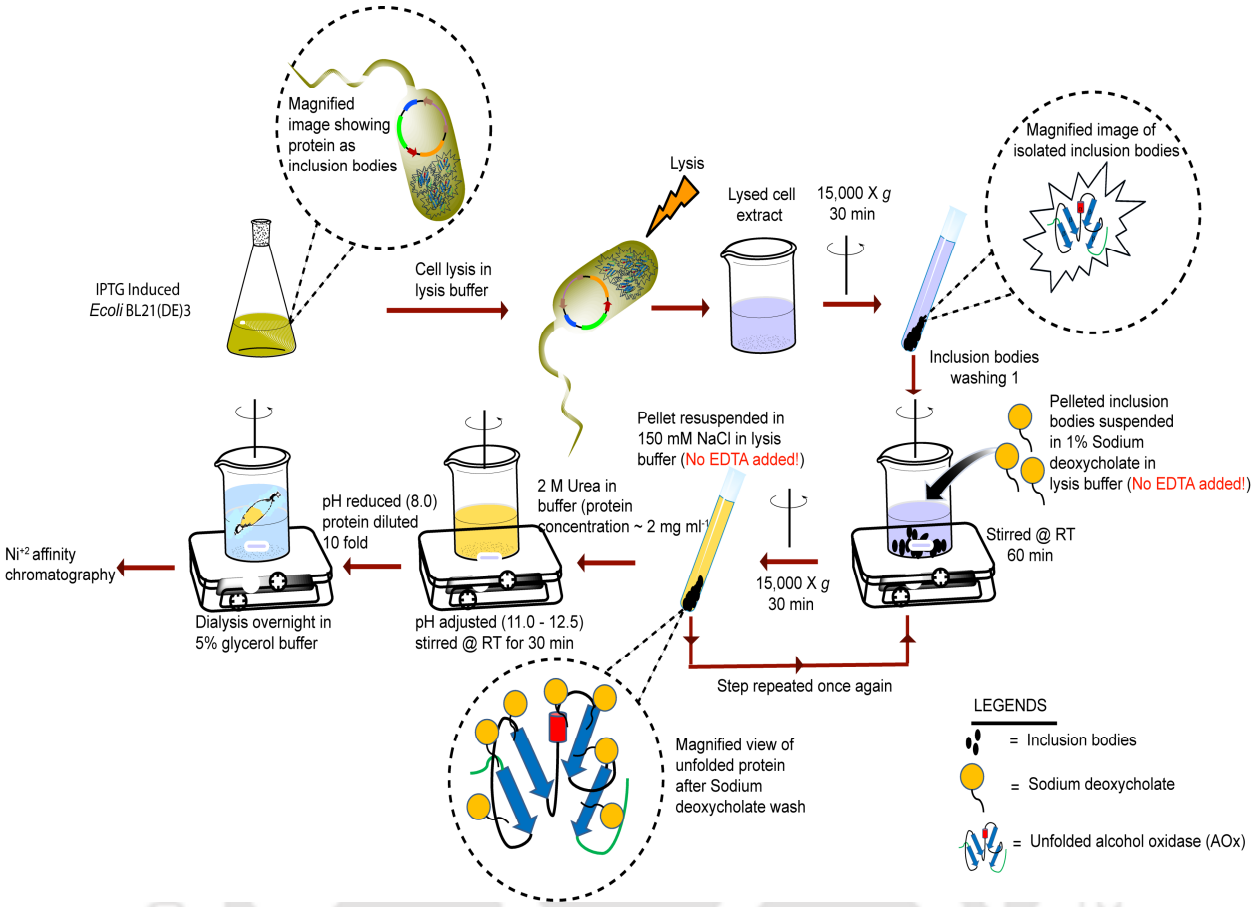

Figure 3.8. Experimental overview of inclusion body isolation, purification and solubilization of over-expressed rAOX following the modified protocol of Schwanke *et al*, (2009).

3.B.3.2 Purification of solubilized rAOx by nickel affinity chromatography

After dialysis the solubilized protein mixture was applied onto Nickel-affinity pre-packed column (HisTrap Nickel Sepharose 6 Fast Flow crude, GE Healthcare, Sweden). The column was washed thoroughly with 0.22 micron filtered distilled water for atleast 20 column volumes at a flow rate of 2 ml min^{-1}. The column was then pre-equilibrated with 10 column volumes of binding buffer (Appendix **Table A4**) at a flow rate of 2 ml min^{-1}. The solubilized protein was loaded onto the equilibrated column at a flow rate of 1 ml min^{-1}. All buffers, water and solubilized protein samples were filtered through 0.22-0.45 micron filter (Rankem, India). Column was washed once with 25 column volumes of binding buffer before the protein was

eluted with elution buffer (Appendix **Table A4**) at a flow rate of 2 ml min^{-1}. Protein was eluted in 2 ml fraction volume. SDS-PAGE of the eluted fractions were performed following standard Laemmli protocol described in **section 3.B.2.4** to check the purification of our histidine-tagged protein (N-terminal-6xHis-AOx-6xHis-C-terminal) qualitatively. The fractions having the protein of interest were pooled together and dialysed overnight against 20 mM Tris-HCl buffer, pH 9.0 supplemented with 5 % (v/v) glycerol, 5 mM DTT and 1 mM PMSF.

3.B.3.3 Western blot analysis

Eluted fractions were checked for protein concentration by Bradford method described in **section 3.B.1.9** measuring absorbance at 595 nm spectrophotometrically. Western blot was performed using purified in vitro folded protein fraction against the 6 histidine tags in our target recombinant protein. Protein samples of approximately 60 µg were loaded onto 12 % SDS-PAGE and electrophoresed until the bromophenol dye font moved out of the gel. Color plus pre-stained protein molecular weight marker (New England Biolabs, USA) was run as a standard for approximate molecular weight determination and for checking the proper target protein transfer to Polyvinylidene difluoride (PVDF) membrane (Amersham Hybond-P, GE Healthcare). Briefly, the electrophoresed protein gels were transferred to PVDF membrane at a fixed voltage of 25 volts for 3-4 h at 4 °C in Blot module (GE Healthcare). After proper transfer, the membrane was blocked in blocking buffer (Appendix **Table A13**) supplemented with 3 % bovine serum albumin (BSA) and left overnight in rocking motion at 4 °C. Membranes were then washed thoroughly for three times each for 10 min in PBS buffer (Appendix **Table A13**) containing 0.05 % Tween-20 (PBS-T). Membranes were then incubated with monoclonal anti-polyhistidine as the primary antibody (Monoclonal Anti-poly-Histidine antibody produced in mouse, Sigma Aldrich, USA) using an optimized concentration (Appendix **Table A14**) in PBS containing 1 % BSA for 2 h at room temperature. After washing the membrane three times for 5 min each in PBS-T, the membrane was treated with anti-mouse IgG (Fab specific)-peroxidase antibody as the secondary antibody (Sigma Aldrich, USA) (Appendix **Table A14**) and incubated for 1 h at room temperature. After a final 3 wash of 5 min each in PBS-T. The membrane was developed for 5 min with peroxidase substrate 3, 3'-Diaminobenzidine (DAB) tetrahydrochloride hydrate (Amresco, USA) at a concentration of 4 mg per 10 ml of PBS buffer and was

immediately poured onto the membrane and charged with 10 µl of molecular biology grade 30 % hydrogen peroxide (Sigma Aldrich, USA) and imaged using gel documentation system (ChemiDoc XRS+ Imaging System, BIO RAD).

3.B.3.4 *In-vitro* refolding and reconstitution of apo-rAOx with co-factor FAD

In-vitro activation and refolding of purified apo-rAOx with its co-factor FAD were performed following the protocol of Ruiz-Dueñas e*t al*, (2005) (**Fig. 3.9**). Briefly, an optimized protein concentration of ~ 10 µg ml^{-1} of purified apo-rAOx was used in a refolding mixture comprising of 20 mM Tris-HCl buffer, pH 9.0 containing 2.5 mM glutathione oxidized (GSSG), 1 mM DTT, 35 % glycerol, 0.3 M urea and 0.08 mM FAD. The refolding mixture was allowed to incubate at 16 °C for a period of ~ 80 h. Each of the components used in the refolding buffer were optimized for its concentration. The pH, time and temperature were also optimized for the best refolding condition. A control, containing FAD and protein in 20 mM Tris-HCl buffer pH 9.0 (no DTT and GSSG) at similar experimental conditions was also studied for *in-vitro* folding efficiency.

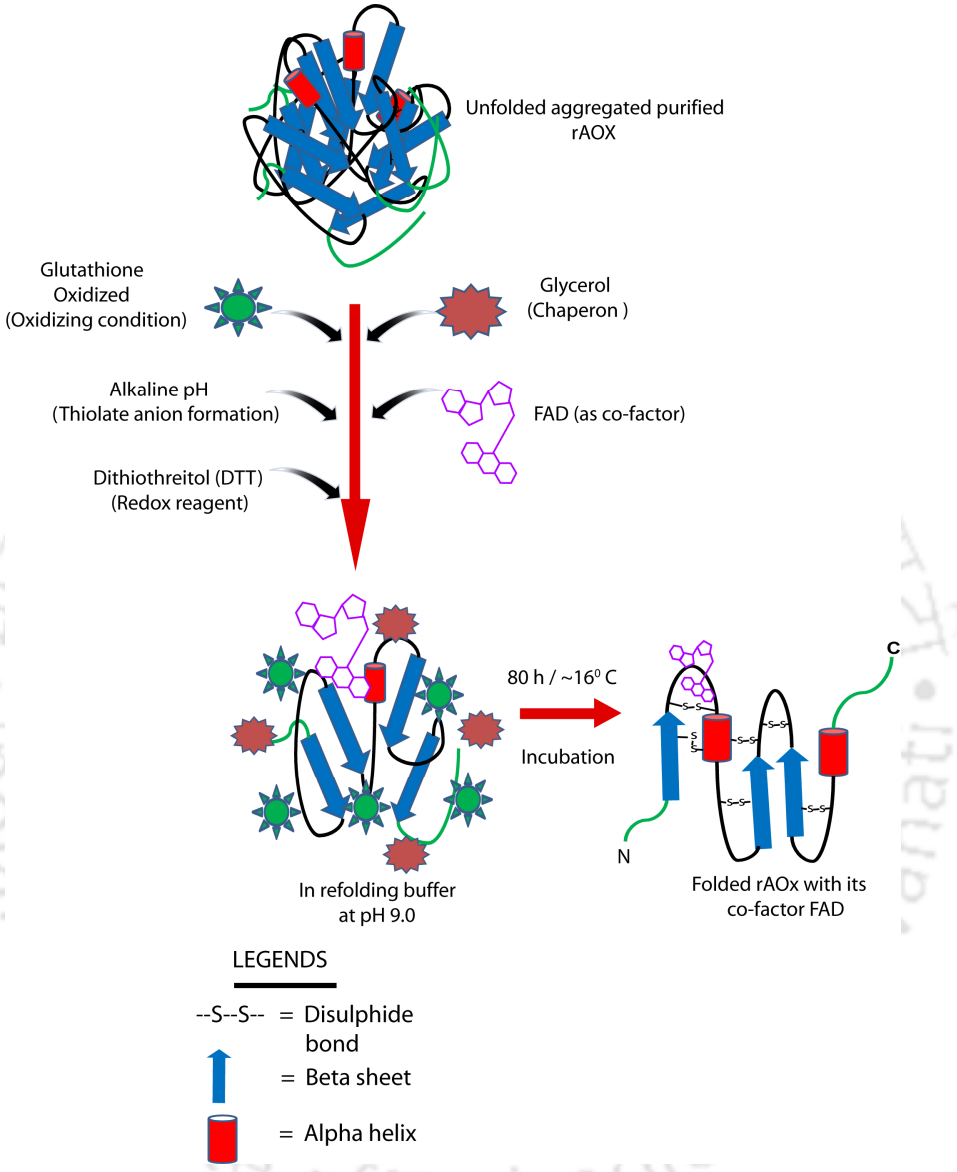

Figure 3.9. A schematic overview showing *in-vitro* refolding of apo-rAOx with its co-factor FAD in refolding buffer.

3.B.4 Biophysical characterizations of rAOx

3.B.4.1 MALDI-TOF/TOF mass spectrometry of apo-rAOX

A schematic overview of MALDI-TOF/TOF mass spectrometry protocol is shown in **Figure 3.10**. His-tag purified and concentrated apo-rAOx protein was loaded onto 12 % SDS-PAGE (**section 3.B.2.4**) in multiple wells and was electrophoresed until the bromophenol dye moves out of the gel. The gel was stained with mass spectrometry compatible coomasie G-250 dyeing protocol of Candiano *et al,* (2004) (**section 3.B.2.4**). Target protein bands were excised using a sterile scalpel and bands from multiple wells were pooled together following the procedure described previously (Shevchenko *et al.*, 2007) (**section 3.B.1.12**). In gel tryptic digestion of protein was performed following Trypsin profile in-gel digestion (IGD) Kit (Sigma Aldrich, USA) following manufacturer's protocol for coomasie stained gels (**Fig. 3.10 step 1**). Briefly, finely chopped target protein gel bands were placed in a siliconized polypropylene tube to reduce protein binding to the tube walls. The gel pieces were covered with required volume of destaining solution provided with the kit (200 mM ammonium bicarbonate in 40 % chromatography grade acetonitrile-water) and incubated at 37 °C for 30 min. After incubation, the solution was removed and the step was repeated one more time or until the gel pieces decolorizes. Gel pieces were dried in speed vac (Eppendorf-AG, Germany) for 15-30 min and the gel pieces were covered with trypsin solution (0.4 ug trypsin) in trypsin solubilization reagent(provided with the kit) (1 mM HCl) supplemented with trypsin reaction buffer (provided with the kit). The gel pieces were incubated overnight (16-20 h) at 37 °C. After incubation the liquid from the gel pieces was transferred to a fresh siliconized polypropylene tube. The solution contains the extracted peptides. 50 µl of peptide extraction solution was added to the gel pieces and after incubation at 37 °C for 30 min the solution was transferred and combined with the liquid from the previous step. The extracted peptide sample was subjected to purification and concentration by 10 µl capacity Zip-Tip having C18 resin at its nozzle (Supelco Tips C18, Supelco analytical, procured from Sigma Aldrich), following the manufacturer's instructions.

The processed sample from above steps was mixed with MALDI compatible α-Cyano-4-hydroxycinnamic acid matrix (CHCA, Sigma Aldrich, USA) in protein sample volume to matrix

ratio of 1:1 (v/v) (**Fig. 3.10 step 2**). Matrix was prepared according to the manufacturer's instruction at a concentration of 10 mg ml^{-1} in 50 % acetonitrile in 0.22 micron filtered water supplemented with 0.05 % trifluoroacetic acid (TFA) solution. Sample protein and matrix were mixed thoroughly by pulse vortexing and a brief spin thereafter. 1.2 µl of the mixture was spotted onto MALDI target plate (**Fig. 3.10 step 3**). The plate was aligned and calibrated with TOF/TOF Calibration mixture (Applied Biosystem, AB SCIEX, USA) prepared in accordance with the manufacturer's instruction prior to our sample analysis (**Fig. 3.10 step 4 & 5**). Reagents used for MALDI analysis were chromatography grade and proper care was under-taken to avoid keratin and direct skin contact while preparing the samples.

Sample parent ions generated in MS were selected for further MS/MS analysis for better sequence coverage. The MS/MS database search was performed by ProteinPilot software (AB SCIEX, USA) (**Fig. 3.10 step 5 & 6**).

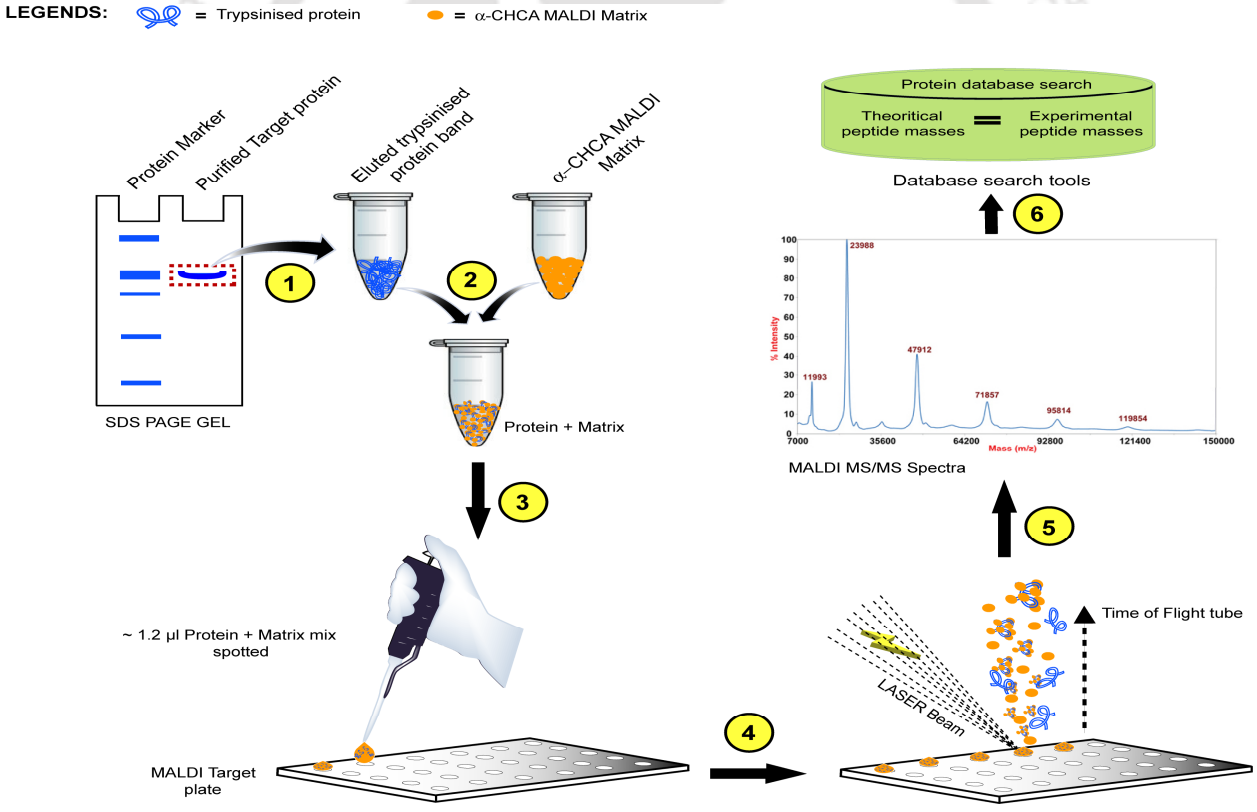

Figure 3.10. An overview of experimental steps involved in identification of mass and sequence coverage of rAOx by MALDI-TOF/TOF mass spectrometry.

3.B.4.2 Determining isoelectric point (p*I*) of rAOx by 2-D electrophoresis

The theoritical p*I* was computed using online Compute p*I*/M_w tool (ExPASY Bioinformatics Resource Portal, Switzerland) and confirmed experimentally through 2D electrophoresis following the protocol of Gőrg *et al*, (2000). Immobiline dry pH gradient strip (linear pH gradient 3-10, 7 cm, GE Healthcare, Sweden) was rehydrated overnight with rehydration solution/buffer (composition in **section 3.B.1.10**) supplemented with IPG buffer or Pharmalyte. Sample protein with rehydration buffer was reduced and alkylated. Sample was then actively rehydrated onto immobiline dry pH gradient strips by following the cup loading procedure described in manufacturer's instruction manual (GE Healthcare, Sweden). Focusing of IPG strip was done at 20 °C and 50 µA current per strip. Running condition was optimized at 500 V for 1 h (step and hold) followed by 1000 V for 30 min (gradient), 5000 V for 1 h 30 min (gradient), finally ending with 5000 V for 30 min (step and hold). Focused strip was equilibrated in two steps for reduction and alkylation following standard kit's procedure described previously (**section 3.B.1.10**). The IPG strip was run in second dimension in 12 % resolving gel along with standard protein molecular weight marker as reference. Gel was sealed with bromophenol-agarose sealing solution (**section 3.B.1.10**). Silver staining was performed as before following the protocol of Chevallet *et al*, (2006) (**section 3.B.1.11**) and the gel was scanned using ImageScanner III (GE Healthcare, Sweden). 2D gel spot was analyzed manually.

3.B.4.3 Determining isoelectric point (p*I*) of rAOx by Zeta potential

Zeta potential studies on recombinant AOx was determined taking the principal of electrophoretic mobility of the protein in different pH environment. The fundamental concept of identifying the Zeta potential of a protein is shown in **Figure 3.11** below. Zeta potential of purified alcohol oxidase was estimated in 20 mM sodium phosphate buffer with a pH ranging from 5.7 to 7.2. Isoelectric point of the purified protein was studied using Zetasizer Nano series (Malvern Instruments Limited, UK) to reconfirm and validate the isoelectric point determined using 2-d gel electrophoresis. Approximately, 5 ug ml^{-1} of purified AOX in different pH adjusted (pH 5.7 to pH 7.2 at a pH increment of 0.1) 20 mM sodium phosphate buffer was prepared and was filtered through 0.22 micron syringe filter to remove any foreign dust particles. The filtered protein in different pH buffer was charged into specially designed folded capillary cell with gold

plated beryllium/copper electrode (Malvern Instruments Limited, UK). Thus, a point where the plot of zeta potential versus pH gradient passes through zero zeta potential would re-confirm the isoelectric point of the protein.

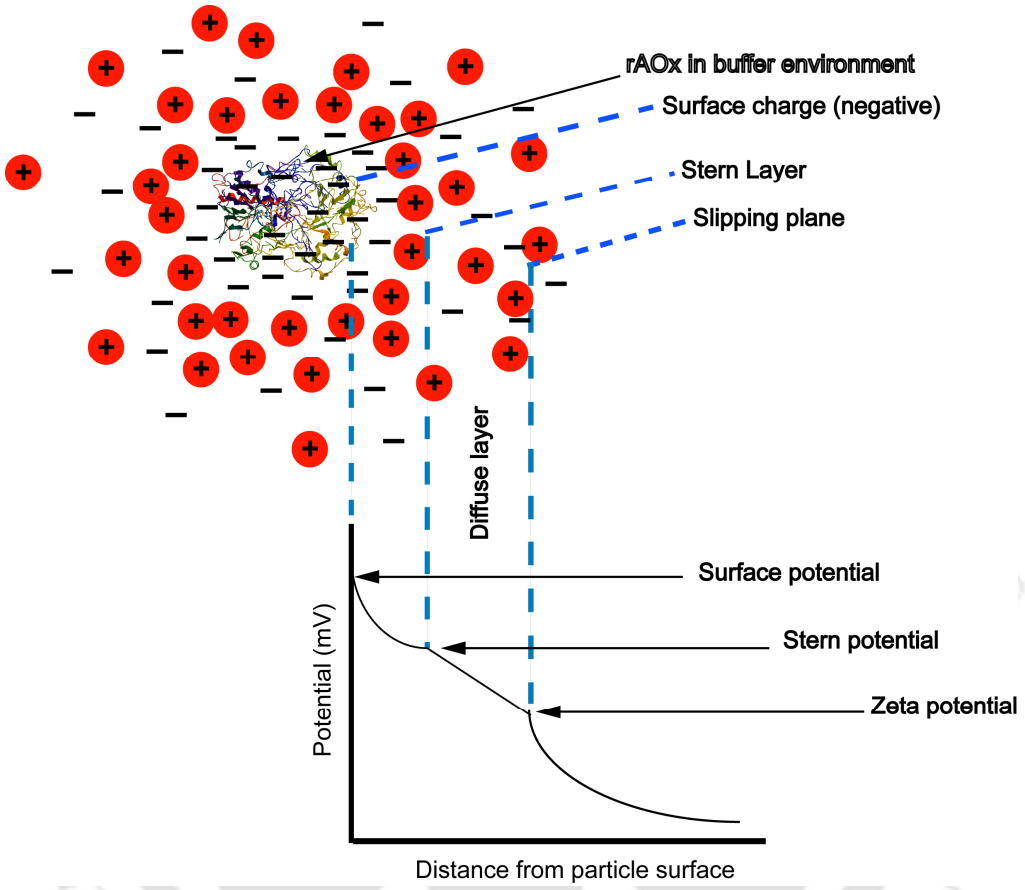

Figure 3.11. Diagram showing the ionic concentration and potential difference as a function of distance from the charged surface of a protein suspended in a dispersion medium

3.B.4.4 Fluorimetric identification of free FAD and rAOx-FAD holoenzyme in refolding buffer

Successful incorporation of cofactor FAD to apo-rAOx was studied through fluorescence spectroscopy of free FAD (control with unfolded rAOx and FAD but no GSSG and DTT) and rAOx-FAD holoenzyme (after ~80 h incubation and removing unbound free FAD) diluted in 20 mM sodium phosphate buffer pH 9.0 after excitation at $\lambda_{443\ nm}$ and monitoring the

decrease in emission maxima at $\lambda_{527\ nm}$ (FluoroMax 4, Horiba Scientific, Japan). A characteristic lowering of refolded rAOx-FAD holoenzyme spectra in comparison to free FAD suggests efficient incorporation of FAD into protein matrix.

3.B.4.5 Circular dichroism (CD) spectroscopy measurement

Conformational stability of rAOx was studied in different pH buffer environment ranging from pH 4.0 to pH 9.0. The stability of the protein secondary structure in both acidic and basic buffer conditions were evaluated through CD spectra acquired with JASCO-815 spectrometer (Jasco, Japan) equipped with circulating water bath at 25 °C. Different buffer compositions at 20 mM salt concentration were prepared on the basis of its buffering capacity. Buffer with pH 4.0 and pH 5.0 were sodium acetate; pH 6.0 and pH 7.0 were sodium phosphate; pH 8.0 and pH 9.0 were Tris/HCl. Spectra of FAD bound rAOx fraction were recorded after removal of unbound FAD by micro-centrifugal filtration and diluting the holoenzyme rAOx in 20 mM of the respective pH buffer at a range from 9.0 to 4.0. Sample protein at a concentration of 50 µg ml^{-1} was prepared in above buffers. Simultaneously, a control of unfolded rAOx in 20 mM Tris/HCl buffer devoid of GSSG and DTT were also studied. Samples were placed in 0.1 cm (optical path length) cell. Spectrums were recorded under constant nitrogen gas purging at a flow rate of 5.0 L min^{-1} from $\lambda_{190\ nm}$ to $\lambda_{260\ nm}$ with a resolution of 0.1 nm and a band width of 1.0 nm. Each spectrum was the average of two accumulations at a scanning speed of 20 nm min^{-1}. Background spectra of each corresponding pH buffer of same molar concentration as in the sample were recorded under identical experimental conditions. Background spectra were subtracted from its corresponding pH sample spectrum. To estimate the content of secondary structure, CD spectrums were analyzed using online CD spectra analysis program K2D (Andrade *et al.*, 1993) in the range from $\lambda_{200\ nm}$ to $\lambda_{240\ nm}$ available online in DichroWeb (Whitmore and Wallace, 2004; 2008).

3.B.4.6 Studying the aggregation potential through Dynamic Light Scattering (DLS) analysis of rAOx

The aggregation tendency and pattern of rAOx while refolding in its refolding buffer was monitored during its incubation at 16 °C for ~96 h, by sampling out the mixture at a regular interval of 24 h, to study the DLS pattern in Zetasizer Nano series (Malvern Instrument Limited, UK) (**Fig. 3.12**). For DLS analysis, purified and dialysed apo-rAOx eluted from nickel affinity chromatography column (**Fig 3.12 step 1 & 2**) was concentrated immediately using Vectaspin 20 centrifuge filters (Whatman, GE healthcare, UK) following manufacturer's instructions. A final protein concentration of ~10 µg ml^{-1} in refolding buffer with FAD (composition as mentioned in **section 3.B.3.4**) was maintained in the study (**Fig 3.12 step 3)**. Sample protein solution was incubated for ~96 h duration at 16 °C (**Fig 3.12 step 4)** and after every 24 h sample protein was monitored for particle size distribution (**Fig 3.12 step 5 & 6)** after filtering through 0.22 or 0.45 micron syringe filter and diluted in 20 mM Tris/HCl buffer pH 9.0 to a final volume of 2 ml. Commercial wild type AOx (cAOx) from *Pichia pastoris* (Sigma Aldrich, USA) and bovine serum albumin (Sigma Aldrich, USA) were studied as a positive and negative control in an identical experimental condition and concentration. All DLS studies were carried out at 16 °C (optimized refolding temperature), temperatures below 16 °C was found to frost the polypropylene cuvette walls, which significantly hampered our readings.

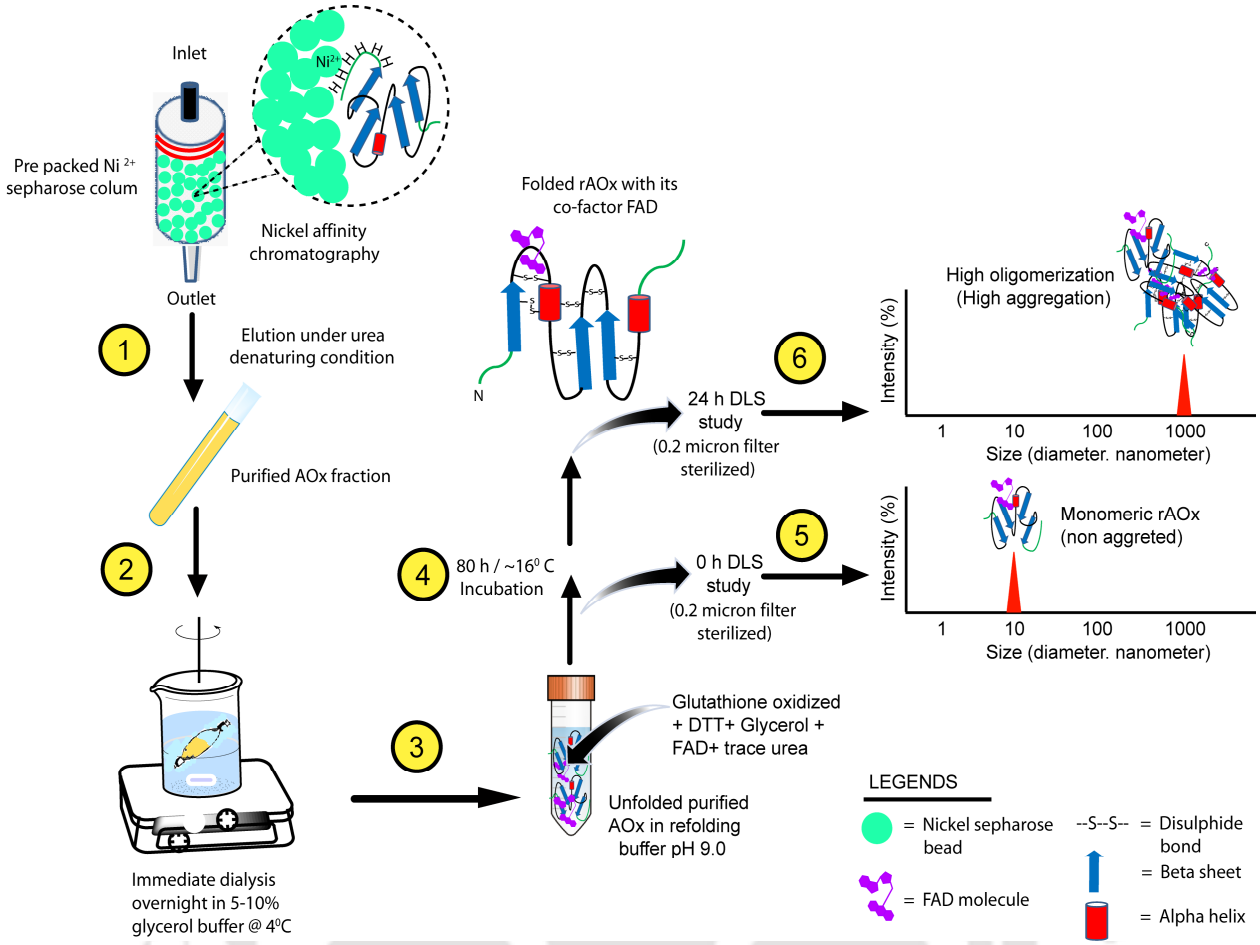

Figure 3.12. A schematic overview of studying the aggregation pattern of rAOx while it's refolding in refolding buffer after a regular interval of 24 h for 96 h duration.

3.B.5 *In-silico* studies of recombinant alcohol oxidase

3.B.5.1 *In-silico* sequence analysis of AOx from *A.terreus* MTCC6324

Contigs from primer walking data were aligned using DNA Baser sequence assembly software package (Heracle BioSoft SRL, Italy) which predicted the full length coding sequence of AOx (**section 3.B.1.26**). Nucleotide sequence translation and protein sequence back-translations was performed by Sixpack and Backtranseq application tools (European Molecular Biology Open Software Suite, EMBOSS), respectively. Sequence homology at protein and nucleotide level with sequence information of AOx from reported filamentous fungi and yeast species were analyzed using ClustalX version 2.1 and visualized by GeneDoc software (**section 3.B.1.14**). Conserve domain search was performed through NCBI Conserved Domains tool (Marchler-Bauer *et al*., 2011) to check for conserved N- and C-terminal Glucose-Methanol-Choline oxidoreductase domains in our deduced amino acid sequence. Phylogenetic relationships between 11 filamentous fungi and yeast species coding for AOXs were also evaluated using Molecular Evolutionary Genetics Analysis software (MEGA) version 6.05 (Tamura *et al*., 2013).

3.B.5.2 *Ab-initio* based rAOx protein structure prediction

Crystal structures of alcohol oxidases from filamentous fungi are limited and thus a composite approach combining threading, *ab initio* modeling and atomic level structural refinement approach was adopted using Iterative Threading Assembly Refinement (I-TASSER) Server (Roy *et al*., 2010). A schematic representation of I-TASSER algorithm adapted from Roy *et al*, (2010) is highlighted in **Figure 3.13**. Briefly, translated amino acid sequence was given as a query sequence and I-TASSER identified suitable templates from PDB using threading algorithms; secondly, structural assembly of threaded templates were achieved using *ab initio* modeling and structurally similar templates were clustered together as cluster centroids; thirdly, the energy minimized structures were selected after an iterative simulation to remove any steric hindrance and refines the overall structure; lastly, I-TASSER predicted five top 3D models for

the given input amino acid sequence. Models were ranked according to their confidence score (C-score), template modeling score (TM-score) and root mean square deviation (RMSD) values (Scoring parameters defined in appendix **Table A15**) The top ranking model with a C-score closer to 2 in range of -5 to 2, TM-score greater than 0.5 and a rationale RMSD value was selected for further structural validation. I-TASSER also predicted the function of the protein using an in build COFACTOR tool.

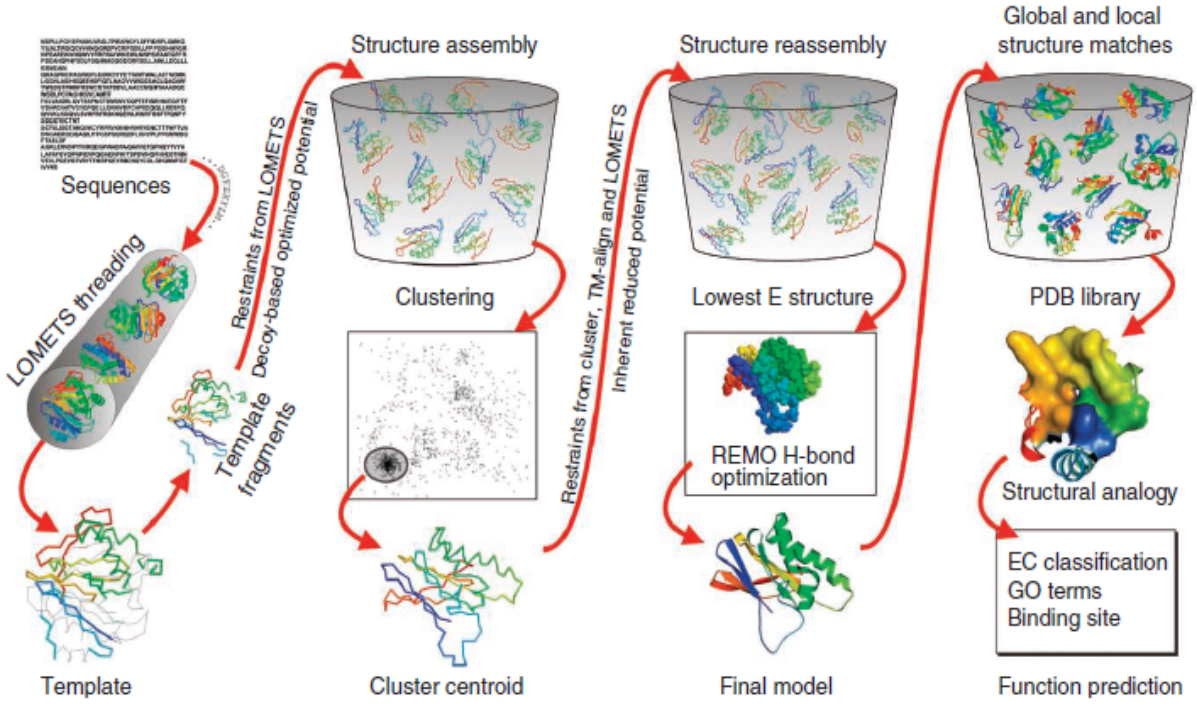

Figure 3.13. A schematic representation of I-TASSER algorithm for protein structure and function prediction (adapted from Roy *et al*, 2010)

3.B.5.3 Checking the stereo-chemical quality of predicted rAOx through Ramachandran plot

The best predicted model was analyzed for unusual amino acid content through Ramachandran plot in PROCHEK analysis (European Molecular Biology Laboratory-European

Bioinformatics Institute, UK) (Laskowski *et al.*, 1993). Templates used by I-TASSER to predict the model were also analyzed for the stereochemical quality of all protein chains in a given PDB structure, as a control study.

3.B.5.4 Molecular docking studies with predicted model of rAOx

To further validate and investigate the sequence to structure to function paradigm of the predicted AOx model, the apoenzyme was docked with its co-factor FAD to make a holoenzyme using Molegro virtual docker (MVD) (Molegro-a CLC bio company, Denmark) (Thomsen and Christensen, 2006). **Figure 3.14** shows the overall docking approach undertaken using MVD. For docking studies FAD molecule from crystal structure of aryl-alcohol oxidase from *P eryingii* (PDB id: 3FIM) was used as a ligand. Briefly, predicted AOx model and ligand FAD was imported in MVD workspace. Probable, binding sites or cavities were mapped on whole protein structure and were restricted to 5 cavities with a spherical binding pocket of radius 6 Å in which all residues considered were flexible. Due to stochastic nature of docking algorithm about 50 runs per cavity per pose were performed for each of the 10 FAD poses (torsions and orientation of the ligand). As a control study to validate our docking protocol and MVD's algorithm to predict the correct FAD binding site and conformation similar re-docking simulations were carried out using apoenzyme crystal structure of aryl alcohol oxidase (PDB id: 3FIM) with the FAD. Best conformation of FAD with its binding cavity was elucidated by manually investigating each cavity for its conserved interacting residues abiding the well established Rossmann fold architecture. The best pose of FAD was adjudged from the Moldock score of each of the 10 poses, evaluating the best energy minimized pose of interaction with the enzyme. 3D superimposition of the best pose of FAD from our docking studies was performed with that of the FAD bound with the crystal structure of 3FIM.

In-silico docking with alcohol substrates as ligand molecules were performed by long chain, short chain, secondary and aryl/aromatic alcohols to get an overall assessment of the function of the predicted rAOx holoenzyme model. Conserved residues in the active site known for catalytic reaction (Hernández-Ortega *et al.*, 2011a; 2011b) were also determined. Moldock score based binding energies was also evaluated which were further validated in our wet lab enzyme activity assays with alcohol substrates.

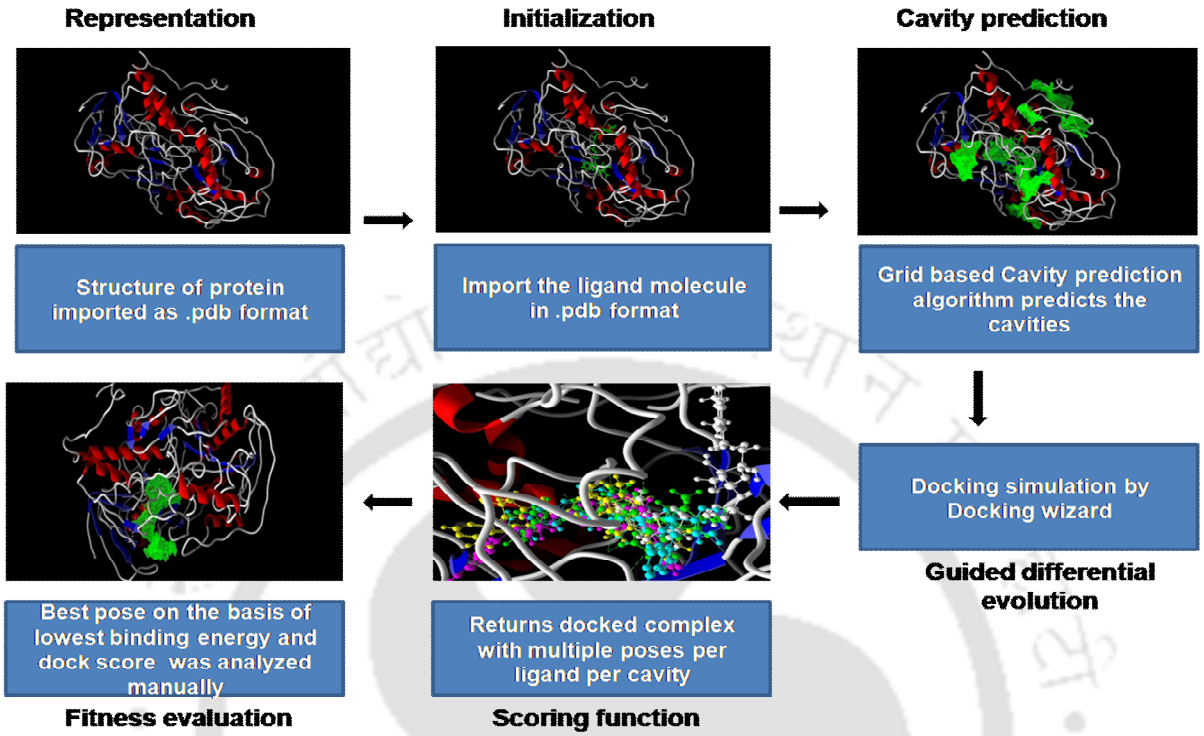

Figure 3.14. An overall schematic of the algorithm followed by Molegro Virtual Docker for our docking simulation studies

3.B.6 Functional characterization of recombinant alcohol oxidase

3.B.6.1 Determining enzyme activity and kinetics

A range of representative alcohol substrates from long chain, short chain, secondary and aryl/aromatic alcohols were assayed simultaneously for its activity with refolded rAOx. Activity of rAOx from inclusion bodies was assayed spectrophotometrically using stock solution of all the alcohol substrate at a concentration of 1 M in DMSO. Appropriate volume from the stock was pipetted out in assay mixture so as to form a final concentration of 5 mM of each alcohol in reaction mixture. Temperature and pH optima were evaluated in 0.1 M sodium phosphate buffer (Guillén *et al*., 1992; Ruiz-Dueñas *et al*., 2005). Enzyme activity was expressed in terms of units, where one unit is defined as that amount of enzyme that catalyzes the conversion one micromole (1µmol) of substrate into product in one minute under the conditions specified. Enzyme activities were calculated during the linear phase of oxidation of different representative alcohols to their corresponding aldehydes using their respective molar absorbance (ε) values. Apparent specific activity, K_m and k_{cat} values were estimated using Michaelis-menton equation through non-linear regression analysis and Lineweaver–Burk plots using the application package kinetic module in Sigmaplot version 11.0, as shown in the schematic overview below (**Fig. 3.15**).

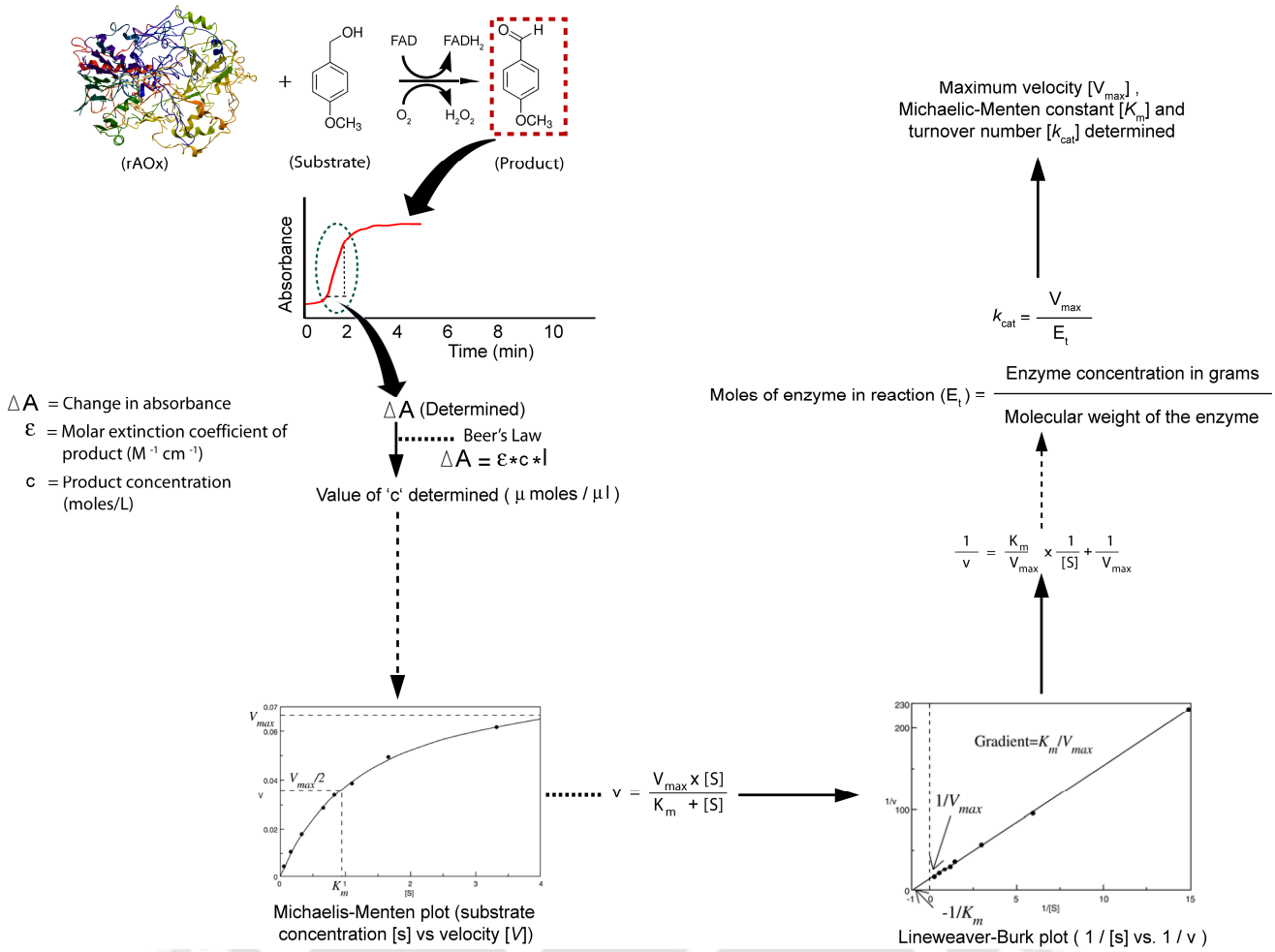

Figure 3.15. A schematic overview of determining the rAOX activity and kinetic parameters by monitoring the change in absorbance of the product with time.

3.B.6.2 Determining the Activation energy (E_a), enthalpy (ΔH), free energy (ΔG) and entropy (ΔS) of rAOx.

The classical activation energy plot of an enzyme is shown in **Figure 3.16**. The activation energy of the purified, reconstituted rAOx was calculated using Arrhenius plot by plotting the natural logarithm of enzyme activity in (U mg^{-1}) (ln V) versus the inverse of the absolute temperature (T^{-1}) in Kelvin scale (K^{-1}). The ΔH in kJ mol^{-1}, ΔG in kJ mol^{-1} and ΔS in J

mol $^{-1}$ K^{-1} were calculated from Arrhenius type equation (equation 1) by using the following derived equations 2, 3 and 4, respectively.

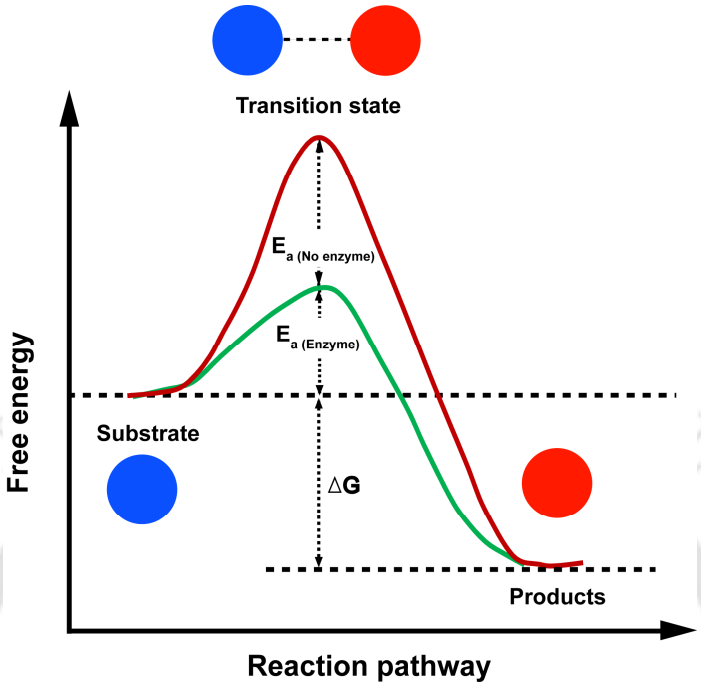

Figure 3.16. Activation energy plot of an enzyme

$$k = A\, e^{-Ea / RT} \quad \text{----------} \quad (1)$$

$$\Delta G = -RT \ln \left[\frac{k(a/d) * h}{kB * T} \right] \text{---} \quad (2)$$

$$\Delta H = Ea - RT \quad \text{----------} \quad (3)$$

$$\Delta S = \frac{\Delta H - \Delta G}{T} \quad \text{----------} \quad (4)$$

Where; E_a = The activation energy,

T (K) = Corresponding absolute temperature,

R = Universal gas constant (8.314 J mol^{-1} K^{-1}),

h = The Planck constant (11.04 x 10^{-36} J min),

k_B = The Boltzmann constant (1.38 x 10^{-23} JK^{-1}),

$k_{(a/d)}$ = 'a' for activation and 'd' for de-activation.

First order reaction constant is the slope of the regression line obtained by plotting (ln V) versus time at different temperatures expressed in kJ mol^{-1}.

3.B.6.3 Measuring the half life and decimal reduction values of rAOx.

The half life ($t_{1/2}$ min^{-1}) of the thermo inactivated rAOx enzyme was calculated according to the method of Cardoso and Emery, (1978) using equation no. 5. The decimal reduction value (*D* value) in h is defined as the time required to pre-incubate the enzyme at a given temperature to maintain 10 % residual activity and was calculated using the equation no. 6.

$$t_{1/2} = \frac{A-3.912}{kd} \text{ ---------- (5)}$$

$$D = \frac{A-2.3026}{kd} \text{ ---------- (6)}$$

Where; A= the y-intercept of the regression line

Values 3.912 and 2.3026 are the natural logarithm values of 50 (for $t_{1/2}$ min^{-1}) and 10 (for decimal reduction), respectively as given in equation (5) and (6).

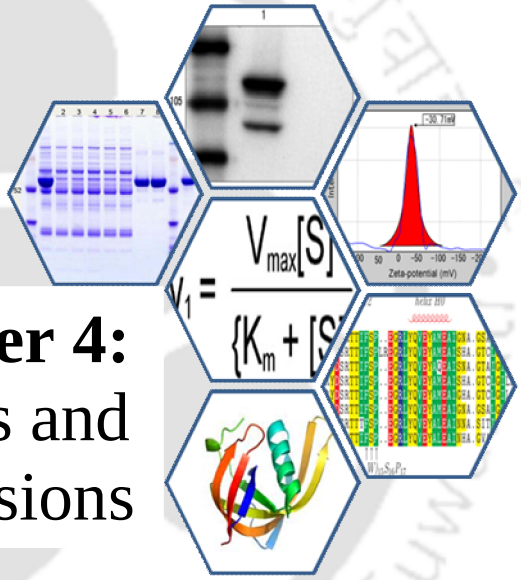

Chapter 4:
Results and Discussions

Chapter 4

Results and Discussions

4.A Results

4.A.1 Identification of AOx gene from *A.terreus* MTCC6324

In section **4.A.1.1** to **4.A.1.3** the identification of an AOx gene from *A.terreus* discerned by following combined proteomic and genomic approach has been described. The corresponding methods have been described under the **section 3A**. The elucidation of full length coding sequence of this massive AOx gene is the primary objective of this work. To achieve this goal focus has been laid on the construction of appropriate primers. Initially, a pair of internal PCR primers were designed from the peptide sequences obtained by the pmf of the 2D gel electrophoresed microsomal AOx protein. A second set of primers was designed from 3' and 5' end of the hypothetical nucleotide sequence of AOx from *A.terreus* NIH strain. As had been shown in **Fig 3.5** of **section 3.B.1** of the experimental methodologies part, the above two sets of primers were designed such that one set will amplify the AOx gene from the 5' end till the middle of the hypothetical AOx gene sequence (PCR 1) and the other will amplify from the middle of the AOx gene overlapping the PCR 1 to the 3' end (PCR 2). The two overlapping PCRs were cloned into T/A cloning vector and the DNA sequencing confirmed the two fragments to have significant match with the hypothetical AOx nucleotide sequence from *A.terreus* NIH2624. The two over lapping PCRs were re-ligated at a common restriction endonuclease site to form the full length AOx coding ORF, cloned in T/A vector. A final double stranded primer walking confirmed the coding region of AOx. The identified gene sequence has been successfully submitted to NCBI GenBank with a valid accession number.

4.A.1.1 mRNA isolation and preparation of cDNA

Alcohol oxidase cDNA was constructed from total RNA isolated from cells of *n*-hexadecane induced *A.terreus* MTCC6324 following the protocol as mentioned in experimental methodology **section 3.B.1.2**. The RNA concentration and corresponding ratio of absorbance at 260:280 nm for each of the protocol tested is described in **Table 4.1**. The data clearly shows that protocol (b) gave significantly good RNA yield of 1.012 µg μl^{-1} from ~100 mg of fungal cells when compared to the commercial kit based total RNA isolation protocol (protocol e) which gave an yield of 1.628 µg μl^{-1} from ~100 mg of fungal tissue. The integrity of the isolated RNA sample was determined by monitoring the intactness of the ribosomal RNA in the denaturing gel. About 5 µl of the total RNA isolate were resolved on 1.5 % agarose-formaldehyde denaturing gel (**Fig. 4.1**). Both 28S and 18S rRNA bands were visible in all the sample isolated by the different protocols, however the integrity and intactness of rRNA bands are more in case of total RNA isolated by protocol (b) in comparison to commercial kit isolated total RNA.

The RNA samples prepared by following protocol (b) served as a suitable template for the RT-PCR application to synthesize cDNA. The quality of the cDNA prepared from each of these isolated total RNA samples were verified with the amplification of GAPDH house-keeping gene corresponding to ~496 bp amplicon (**Fig. 4.2**). The quality of the cDNA produced from the total RNA samples isolated by following protocol (b) was similar to that produced from commercial kit as judged from their band intensities in the gel.

4.A.1.2 Designing primers from the peptide sequences of AOx protein

About 150 µg of *A.terreus* MTCC6324 microsomal protein extracts containing AOx activity were resolved in 2D gel (**Fig. 4.3A**). A total of seven abundant spots detected in the gel were subjected to pmf studies. The m/z peaks produced from the spots were manually uploaded on FindPept tool. Hypothetical un-reviewed AOx protein sequence from *A terreus* NIH2624 (GI: 115437438) available in National Center for Biotechnology Information (NCBI) was used as an input parameter to generate theoretical peptide masses for comparison with those obtained from the pmf peak list. Among the pmf spectra the one generated from the spot six produced m/z peak corresponding to the target protein. Two conserved internal peptide sequences (peptide 1 and

peptide 2) which were matched with the input AOx sequence (**Table 4.2**) were selected. The sequence information of the peptide fragments 1 and 2 were utilized to design forward primer (AOx-FP2) for second overlapping PCR and reverse primer (AOx-RP1) for first PCR, respectively (**Fig. 4.3B**).

4.A.1.3 Construction of full length AOx gene by overlapping PCR approach

The cDNA of AOx constructed from total RNA isolated from the *n*-hexadecane induced *A.terreus* MTCC6324 cells was utilized to obtain full length coding region of AOx by using gene specific overlapping PCR. The two PCR fragments, one (fragment 1) harboring the start codon till the end of reverse primer AOx-RP1 (PCR 1) and second (fragment 2), from the start of forward primer AOx-FP2 till the stop codon (PCR 2) proved successful in amplifying the full length coding region of AOx (**Fig. 4.4**). The DNA sequences of the individual PCR amplicons correspond to the nucleotide sequence read of ~1577 bp and ~1278 bp, respectively. The sequences bear 98 % sequence homology with NIH AOx sequence. Restriction digestion analysis with *Nde*I and *Bg1*II confirmed the orientation of individual PCR fragments in T/A cloning vector. The orientation of fragment 1 containing the AOx gene fragment from start codon was confirmed by the release of ~840 bp and ~3752 bp fragments, whereas the orientation of fragment 2 was confirmed by the release of ~1278 bp and ~3055 bp fragment (**Fig. 4.5**). The fragment 1 (~3752 bp) with the start codon (ATG…) was ligated with fragment 2 (~1278 bp) containing the stop codon (…TAA) to generate the full length coding sequence of AOx gene from *A. terreus* MTCC6324 to clone in T/A cloning vector. The insert in the clone was confirmed by digestion with *Eco*RI restriction enzyme, releasing an intact fragment at ~2001 bp (**Fig. 4.6**). Finally, a double stranded primer walking was performed to obtain the full length coding sequence information of AOx gene, confirming 2001 bp open reading frame. The sequence was analyzed for any probable mutations and its sequence similarity in NCBI database was adjudged with BLAST algorithm. The sequence analysis revealed few mismatches and a deletion of six contiguous stretches of nucleotides from position 685 to 690 corresponding to two serine residues when pair wise alignment was performed with un-reviewed conceptually translated sequence information of AOx from *A.terreus* NIH2624 strain available in NCBI GenBank (**Fig. 4.7**). The sequence analysis results infer novelty of the AOx gene from *A. terreus*

MTCC 6324. The sequence was then submitted to the NCBI GenBank database (**Fig. 4.8**) under the accession number JX139751.

Table 4.1. Quantification of total RNA isolated from *A.terreus* MTCC6324 by different protocols.

Protocols	OD_{260}	OD_{280}	A_{260}/A_{280}	RNA concentration (µg $µl^{-1}$)
a	0.0132	0.0088	1.5	0.528
b	0.0253	0.0135	1.87	1.012
c	0.0155	0.0091	1.70	0.62
d	0.0198	0.0111	1.78	0.79
e	0.0407	0.0205	1.99	1.628

Foot note of Table 4.2: The protocols followed for comparative study are (a) Extraction of total RNA by modified CTAB-based method (Zeng and Yang, 2002). (b) Extraction of total RNA by TRI reagent with an additional pretreatment with benzyl chloride. (c) A rapid isolation of total RNA by acid guanidinium thiocyanate-phenol-chloroform extraction (Chomczynski and Sacchi, 1987) (d) Extraction of total RNA by TRI reagent following manufacturer's protocol for plant tissue. (e) Extraction of total RNA by a commercial lipid tissue isolation kit following manufacturer's protocol. RNA samples were dissolved in RNase-free water and their concentration and purity were determined through spectroscopy.

Table 4.2. Identification of internal conserved amino acid sequence blocks by homology study between the pmf fragments and NCBI database of AOx hypothetical peptide sequences.

User mass	DB mass	Δmass (daltons)	Peptide	Position
855.074	855.493	0.419	Peptide 1: GVATVPSKP	239-247
1641.917	1641.788	-0.128	Peptide 2: NHITAGIQHGSWSHP	511-525

Foot note of Table 4.2: The pmf peak list (m/z values) generated from spot 6 of 2D gel was manually uploaded on FindPept online tool. Detectable m/z values were matched with the

theoretical peptide masses generated from the virtual tryptic digest of query amino acid sequence of AOx from *A.terreus* NIH2624 strain as input. The output result shows user mass (practical), DB mass (Database mass; theoretical mass), Δ mass (Delta mass; theoretical minus practical mass), peptide sequence and corresponding position in query sequence. The above table highlights only those two peptide fragments which corresponded to the conserved internal amino acid blocks from multiple sequence alignment of similar AOx from other filamentous fungi and yeast species.

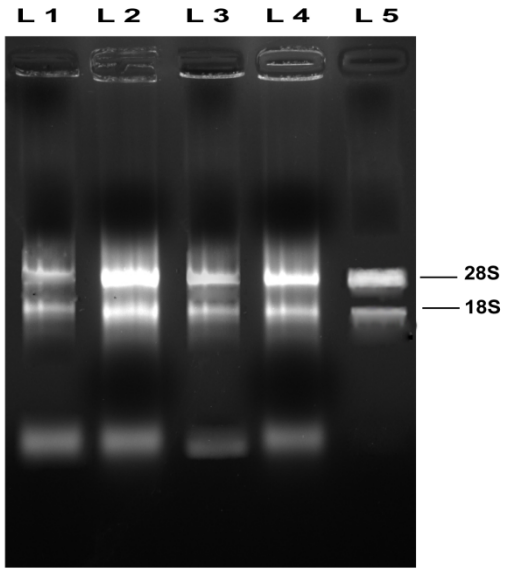

Figure 4.1. Formaldehyde agarose gel electrophoresis of total RNA isolated from *A.terreus* MTCC6324 following five isolation techniques. Lane L1—CTAB-based method (protocol a), L2—Benzyl chloride pretreatment and TRI reagent (protocol b), L3—Rapid isolation of total RNA (protocol c), L4—Extraction of total RNA by TRI Reagent only (protocol d), L5—Commercial kit (protocol e). The RNA was resolved in 1.5 % agarose concentration stained with ethidium bromide and the 28S and 18S ribosomal RNA bands were visible in all the preparations.

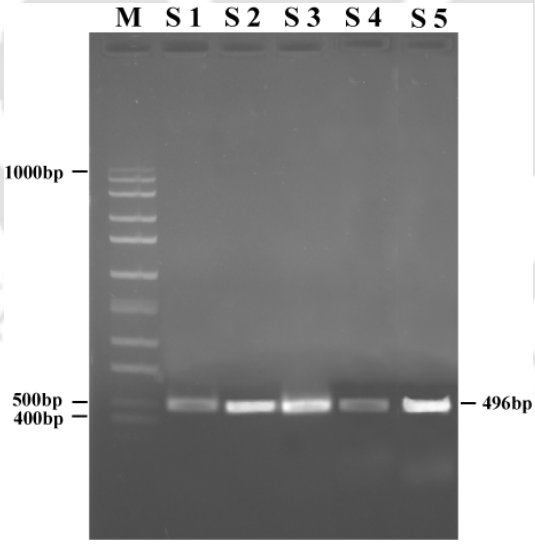

Figure 4.2. Agarose gel electrophoresis of GAPDH house-keeping gene amplicons by PCR amplification from the total RNA. Lane M-DNA molecular weight marker, Lane S1 to S5-corresponds to RNA samples isolated by following protocols (a) to (e).

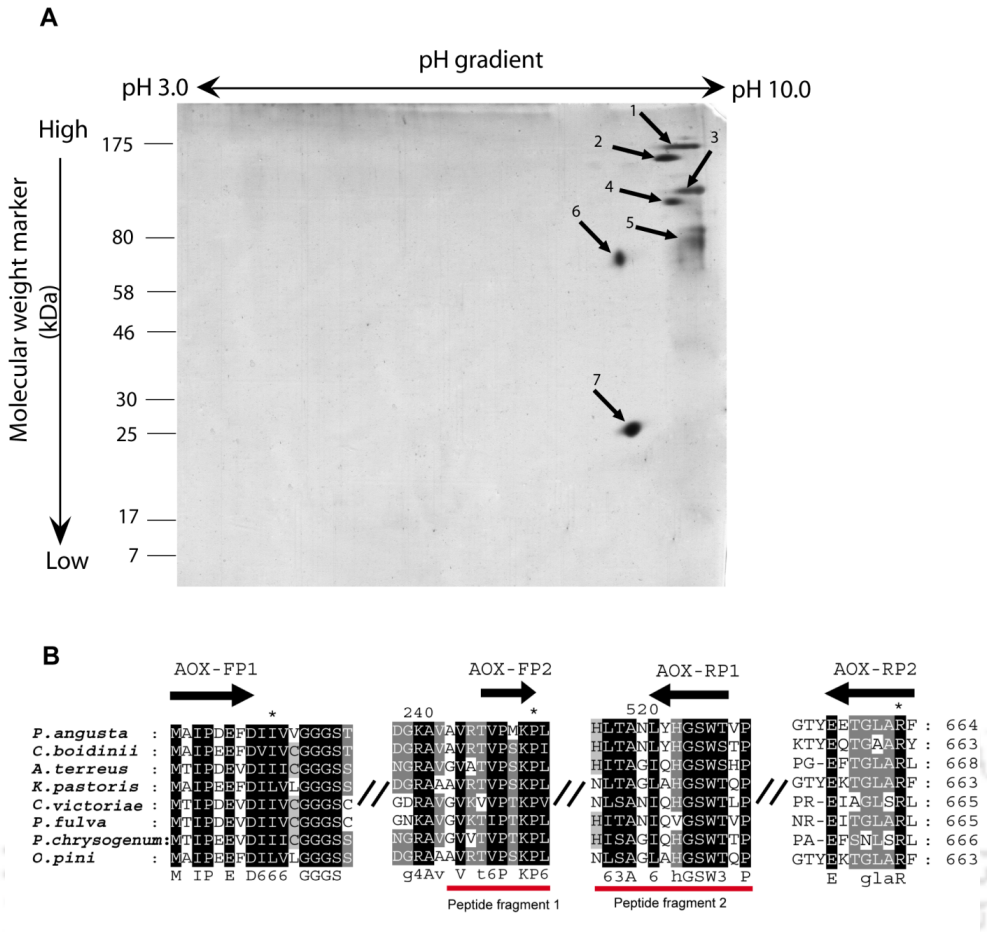

Figure 4.3. 2D electrophoresis of microsomal membrane bound proteins and multiple sequence alignment of AOx proteins from filamentous fungi and yeast species showing the primers for overlapping PCR based on internal peptide fragments identified from pmf data of spot 6. (**A**).Mass spectrometry compatible silver stained 2D gel image of *A.terreus* MTCC6324 microsomal proteome resolved in 12 % polyacrylamide resolving gel as second dimension. Seven spots (marked 1-7 along with black arrow heads) were analysed using MALDI-TOF-MS. (**B**). Internal peptide fragment 1 (GVATVPSKP) and fragment 2(NHITAGIQHGWSHP) shown in red bars, served as templates for designing overlapping PCR primers mapped as AOX-FP2 and AOX-RP1, respectively as an approach for characterizing full length AOx coding region. The gene identification numbers (GI) for the aligned amino acid sequences of AOxs are as follows: *P.angusta* (GI:113652); C.boidinii (GI:231528); *A.terreus* NIH2624 (GI:1 15437438); *K.pastoris* (GI: 2104963); *C. Victoriae* (GI: 13182929); *P.fulva* (GI: 9082281); *P.chrysogenum* (GI: 18028450). Sequences were aligned using CLUSTALW2 and viewed using GeneDock software. Forward and reverse primers are shown as black arrows with primer names mentioned above. Symbol (//) represents discontinuity in multiple sequence alignment. Highly conserved amino acid blocks are shaded in black color.

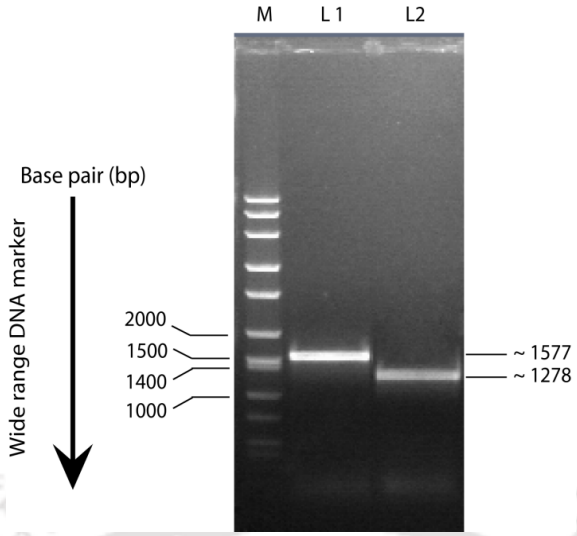

Figure 4.4. Agarose gel (0.8 %) electrophoresis of amplicons obtained by overlapping PCR using cDNA of *A. terreus* MTCC 6324 as a template. Lane M represents wide range DNA marker, lane L1 represents PCR 1, a ~ 1577 bp cDNA fragment of AOx from its start codon, lane L2 represents PCR 2, a ~ 1278 bp overlapping cDNA fragment of AOx till the stop codon. The gel was stained with ethidium bromide.

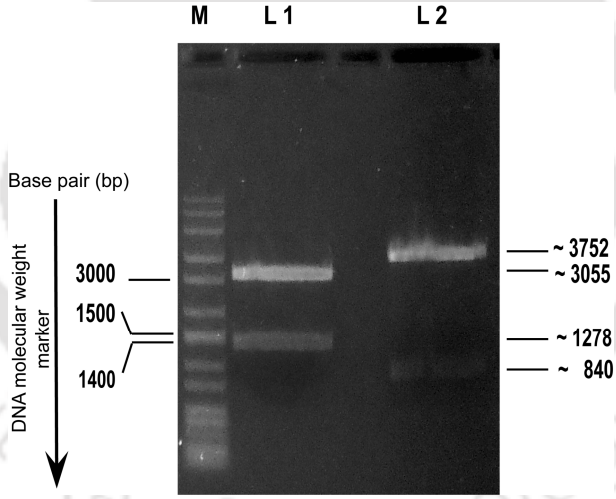

Figure 4.5. Agarose gel (0.8 %) electrophoresis for checking the orientation of the cloned PCR fragments (PCR 1 & 2) in T/A cloning vector through double restriction with *Nde*I and *Bgl*II, respectively. Lane M represents a wide range DNA molecular weight marker, lane L1 shows the double digested fragment pattern of PCR 2 releasing ~ 1278 bp (having the 3' stop codon of AOx gene), lane L2 showed the double digested fragment pattern of PCR 1 releasing ~ 3752 bp fragment (having the 5' start codon of AOx gene). The gel was stained with ethidium bromide

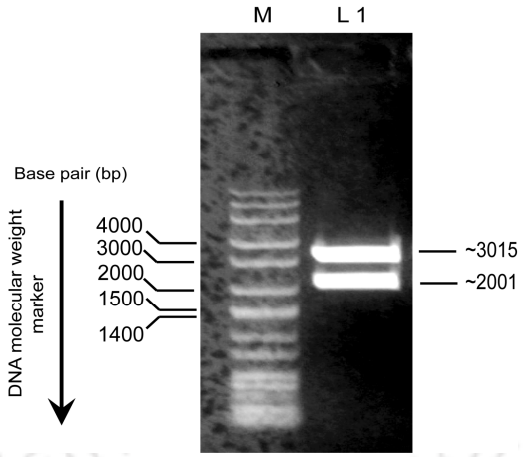

Figure 4.6. Agarose gel (0.8 %) electrophoresis for analysing the restriction digestion pattern of ligated overlapping PCR fragments in T/A vector with *Eco*RI restriction enzyme. The release of ~ 2001 bp full length AOx fragment from TA vector backbone of ~3015 bp was evident. The gel was stained with ethidium bromide.

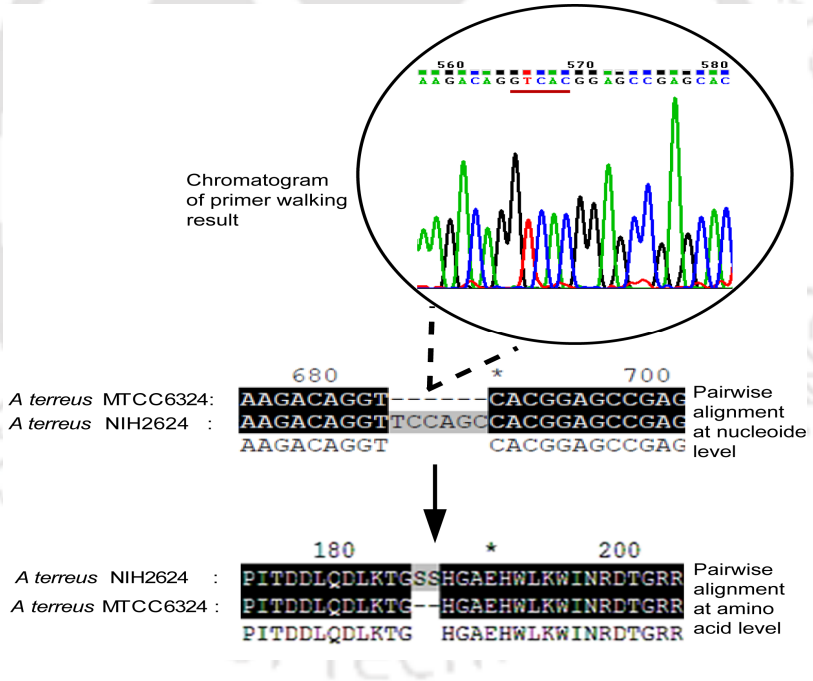

Figure 4.7. Pair-wise sequence alignment of primer walking DNA sequence with the hypothetical, un-reviewed AOx sequence information from *A. terreus* NIH strain at nucleotide and amino acid level shows a deletion of six contiguous nucleotide sequences (position 685-690) which codes for two serine residues at position 186 and 187. Corresponding sharp nucleotide chromatogram of the deleted region is highlighted, confirming the good quality of the sequencing data and ruling out any possible error in sequencing. Highly similar residues are highlighted in black.

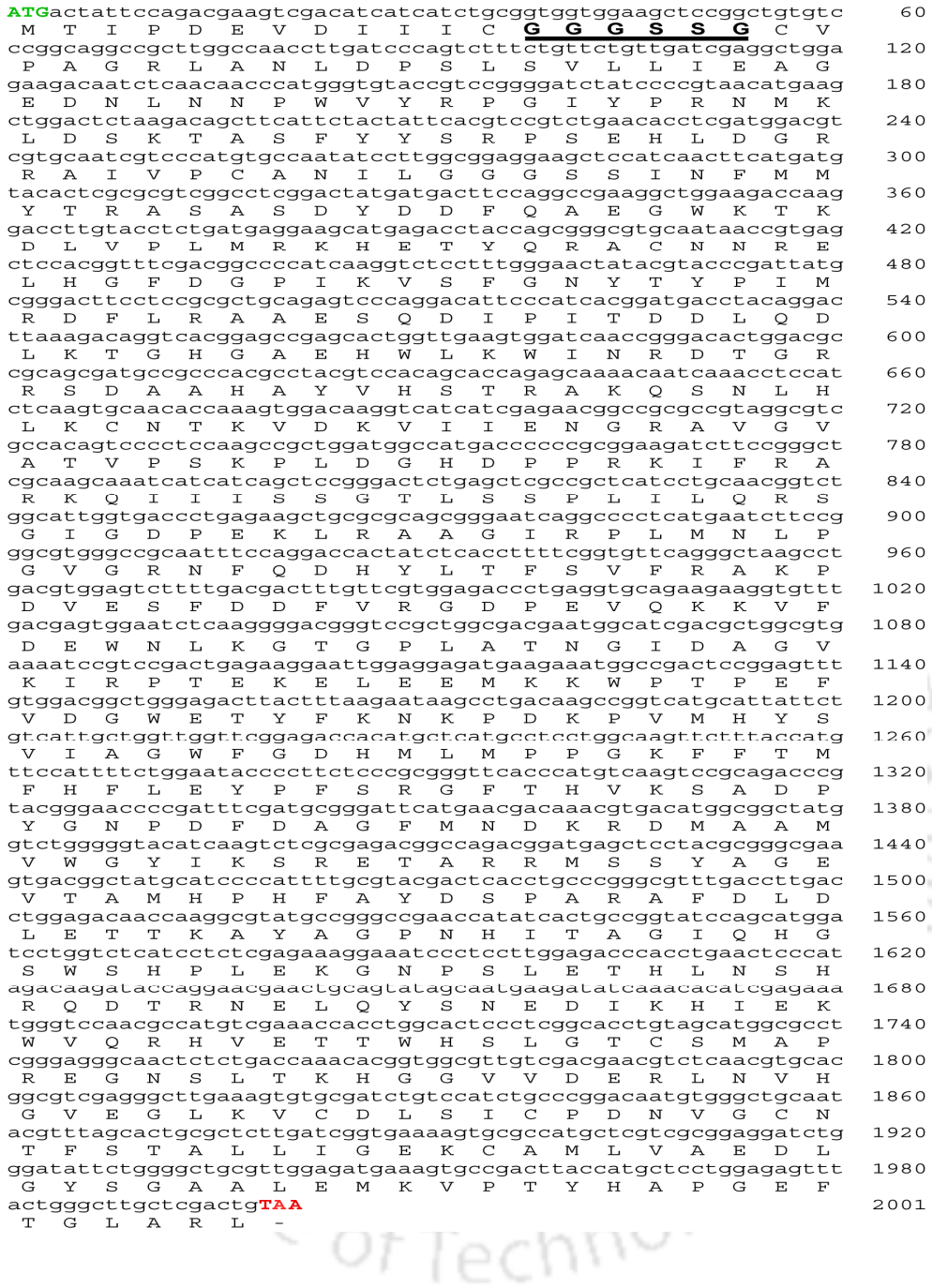

Figure 4.8. Nucleotide and deduced amino acid sequence of AOx from *A.terreus* MTCC6324. Double stranded primer walking confirmed an ORF of 2001 bp. The nucleotide sequences are shown as lower case with start and stop codon highlighted in green and red uppercase, respectively. Translated amino acid sequences are shown in uppercase where (-) denotes a stop codon. The N-terminal conserved amino acids taking part in Rossmann fold architecture (GXGXXG motif) are underlined in black with its residues in bold.

4.A.2 Over-expression of apo-rAOx in *E.coli* BL21(DE3) and subsequent *in-vitro* refolding of the purified apo-protein isolated from the inclusion bodies

Results pertaining to sub-cloning of the full length coding sequence of AOx gene from T/A cloning vector to bacterial expression vector and over-expression of recombinant AOx in bacterial expression host has been elaborated in the following two sections **4.A.2.1** and **4.A.2.2**. The sections will describe the PCR optimization for amplifying the target AOx gene from T/A cloning vector with specially designed PCR primer probes with flanking restriction site for proper ligation and integration at the desired multiple cloning site present on the bacterial expression system. The results on the optimization of parameters for efficient over-expression of the protein of interest in *E.coli* are also included. Expression of histidine tagged fusion protein was confirmed through western blot studies. The following sections will illustrate the isolation, solubilization and purification of rAOx from inclusion bodies by following a partial modification of an established protocol. A major challenge of purifying the inclusion body isolated, solubilized and highly aggregated histidine tagged fusion rAOx protein through affinity chromatography had been elaborately discussed. The section also described the significant experimental outcome of re-folding the purified rAOx with its co-factor FAD following a modification of an established protocol.

4.A.2.1 Sub-cloning AOx gene into bacterial expression system pET28a (+)

The AOx coding region was amplified using gene specific forward (AOX-pET28a-F) and reverse primers (AOX-pET28a-R) with *Eco*RI and *Hind*III restriction sites, respectively. A single PCR amplicon at ~2000 bp was observed on agarose gel (**Fig. 4.9**) and was subsequently ligated into *E.coli* expression vector pET28a (+) followed by transformation into expression host *E.coli* BL21 (DE3) for production of recombinant protein. The recombinant clones were selected and confirmed by double digestion with *Eco*RI and *Hind*III releasing a fragment of ~2001 bp AOx clone (**Fig. 4.10**).

4.A.2.2 Expression, purification and *in-vitro* activation of rAOx

A 2001 bp coding region of AOx was expressed in *E. coli* BL21 (DE3) strain by induction with 0.25 mM Isopropyl β-D-1-thiogalactopyranoside (IPTG) for 4 h (**Fig. 4.11A**) at 28 °C (**Fig. 4.11B**). The ~76 kDa apoenzyme rAOx (apo-rAOx) band appeared mainly in the insoluble fraction of the cell lysate. Approximately, 2.4 g wet cell of recombinant *E.coli* BL21 (DE3) was pelleted for isolation and purification of inclusion body after the cell lysis as described in experimental methodology section. Pure inclusion bodies were solubilized under basic pH environment to avoid any aggregation before purifying through single nickel affinity chromatography step. SDS-PAGE analysis of eluted fractions from HisTrap nickel sepharose 6 affinity column (**Fig. 4.12A**) showed that the purification protocol successfully yielded a solubilized homogenous apo-rAOx band at ~ 76 kDa. A homogenous apo-rAOx protein yield of ~10.2 mg of protein per 2.4 g wet cell weight per liter was achieved. Western blot analysis confirmed that the purified protein was expressed as a histidine tag at approximately the same molecular weight (~ 76 kDa) as in the SDS PAGE gel (**Fig. 4.12B**).

In-vitro re-folding of apo-rAOx with its co-factor FAD was performed after the purification. The refolding was performed by using ~10 µg ml^{-1} of purified apo-rAOx in the refolding buffer. Notably, the apo-rAOx protein concentration above the optimized value (~10 µg ml^{-1}) led to high aggregation and precipitation of the protein that hindered the refolding process. Thus, single step purification of rAOx with nickel affinity chromatography followed by *in-vitro* activation with co-factor FAD proved to be successful.

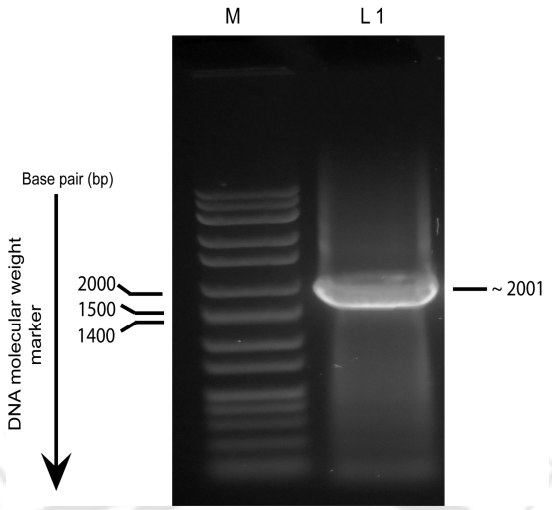

Figure 4.9. Qualitative agarose gel (0.8 %) electrophoresis of PCR amplified full length AOx gene from T/A vector. Lane M is a wide range DNA marker and lane L1 shows PCR amplicon of AOx at ~ 20001 bp using forward and reverse primers with *EcoR*I and *Hind*III restriction sites, respectively.

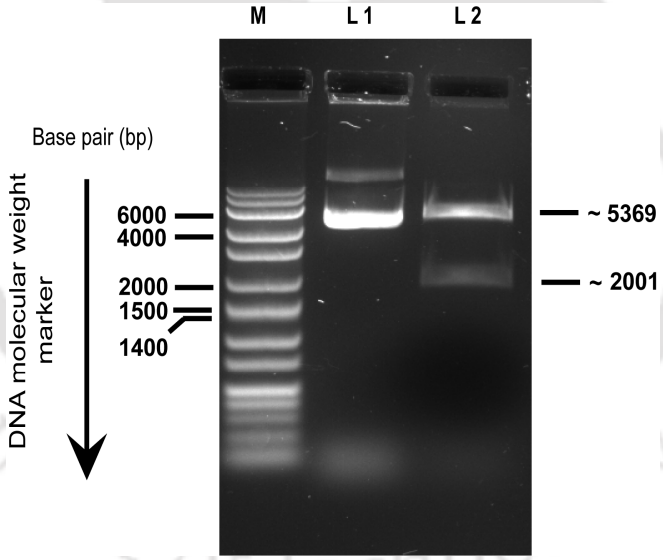

Figure 4.10. Confirmation of full length clone of AOx in pET28a (+) with double digestion. Lane M is a wide range DNA molecular weight marker, lane L1 shows an undigested cloned pET28a(+) plasmid, lane L2 shows the clone confirmation of pET28a(+) subcloned AOx gene with flanking *EcoR*I and *Hind*III restriction site at its 5' and 3' end, respectively by double digestion. Fragment release at ~ 2001 bp and vector backbone at ~ 5369 bp confirmed the clone. The agarose gel (0.8 %) was stained with ethidium bromide.

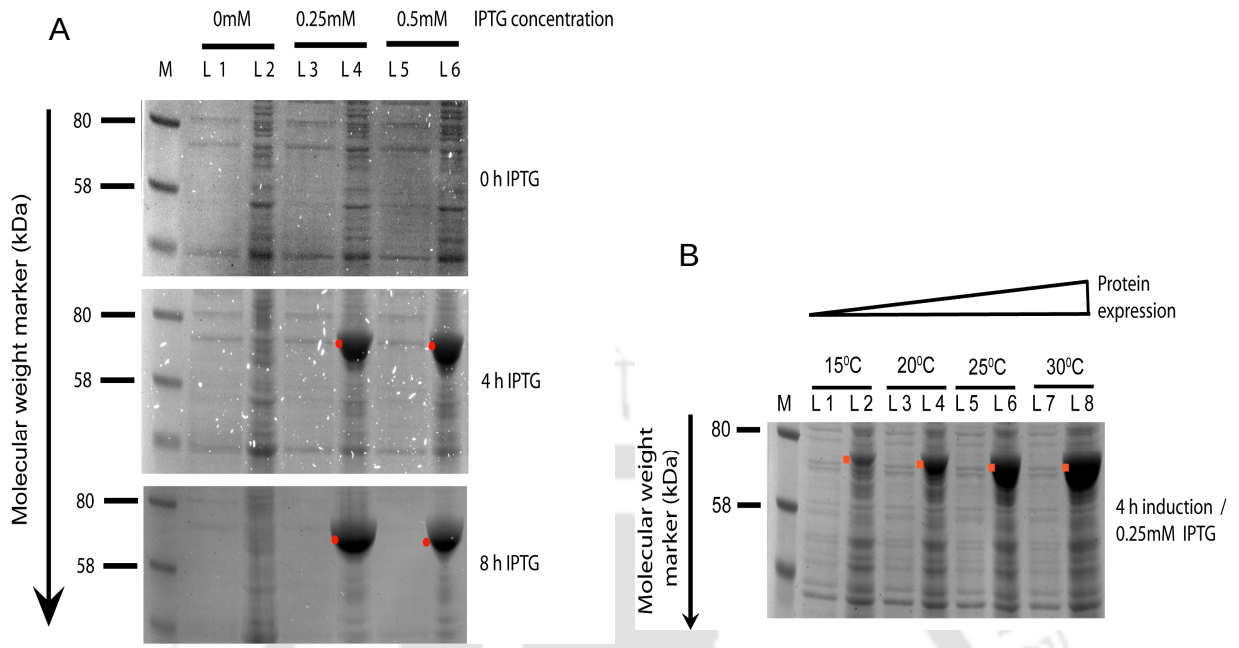

Figure 4.11. SDS-PAGE profile on expression of rAOx in *E.coli* BL21(DE3) under different IPTG concentration, time and temperature of induction. (**A**) Lane M is a protein molecular weight marker, Lane L1 – L2, L3 – L4 and L5 – L6 are the supernatant– pellet fractions loaded adjacent to each other for 0.00, 0. 25 and 0.50 mM IPTG induction, respectively. The expression was monitored for 0 h, 4 h and 8 h for its optimal time of induction corresponding to maximum over-expression. The over expressed rAOx protein of ~ 76 kDa(marked with a red dot) was observed in the pellet fraction of 4 h and 8 h IPTG induced cell lysate. (**B**) Lane M is a molecular weight marker, Lane L1- l8 are the supernatant and pellet fractions loaded alternatively for 15 °C, 20 °C, 25 °C and 30 °C induction temperature respectively at a constant shaking condition for 4 h and 0.25 mM IPTG concentration. Over-expressed protein bands are marked with red dots for easy identification.

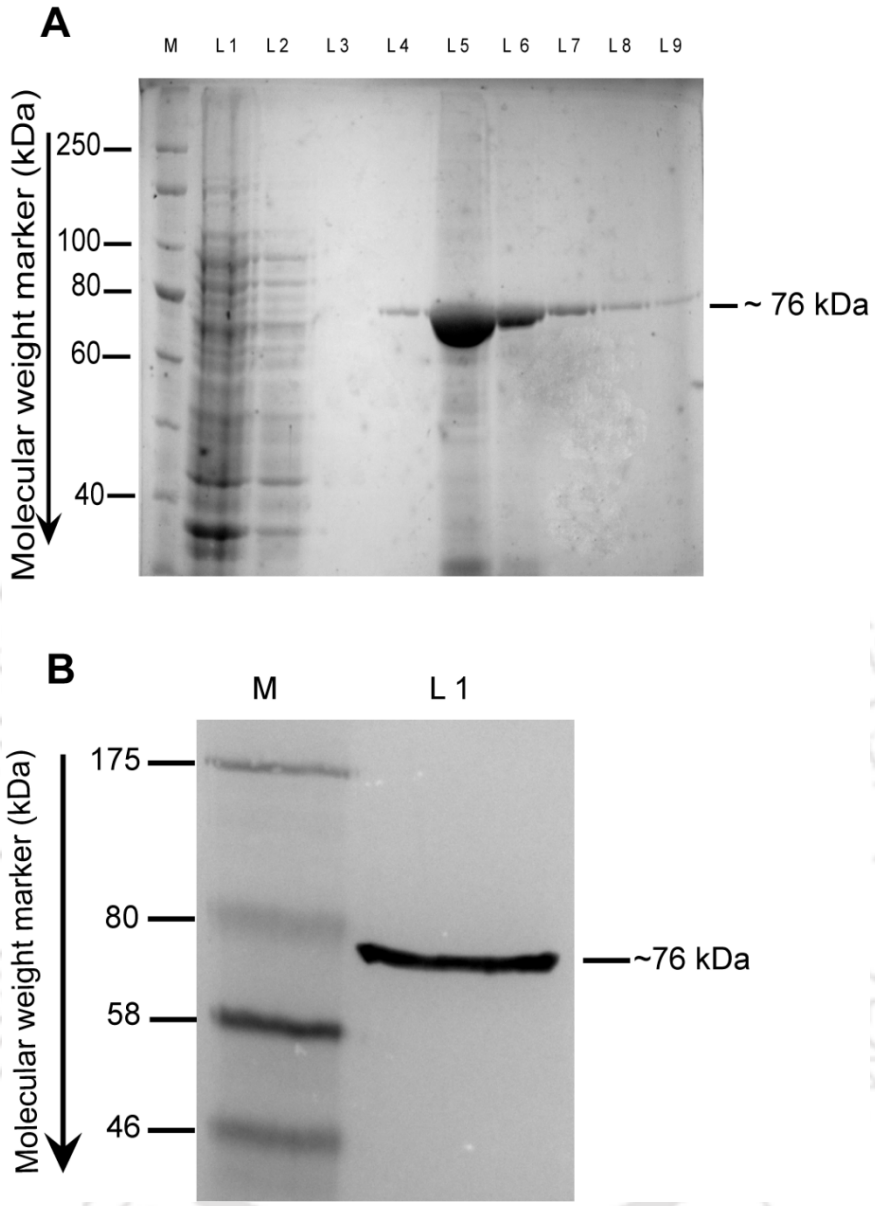

Figure 4.12. (A). SDS-PAGE of apo-rAOx purified by Ni-affinity chromatography. Lane M is protein molecular weight marker, lane L1 is crude solubilized supernatant, lane L2 is the unbound fraction from column, lane L3 is the washed flow through fraction, lane L4 –L9 are the elution fraction from column. Purified protein band at ~ 76 kDa is shown with a black bar. (**B**) Western blot of the purified rAOx with N- and C-terminal 6 x polyhistidine tags. Lane M is a protein molecular weight marker and lane L1 is the developed ~76 kDa rAOx blot on PVDF membrane.

4.A.3 Characterizations of physicochemical properties of rAOx

The results of biophysical characterization of rAOx related to its mass by MALDI-TOF/TOF, isoelectric point by 2D gel electrophoresis and Zeta potential, reconstitution of FAD with apo-AOx by fluorescence spectrophotometry, secondary structure information by CD spectrophotometer and aggregating nature by DLS studies have been discussed in the following section from **4.A.3.1** to **4.A.3.5.**

4.A.3.1 Characterization of apo-rAOx mass

Mass of apo-rAOX measured by MALDI-TOF/TOF was 74,614 Da, (**Fig. 4.13**) which was in good co-relation with the theoretical holoenzyme mass of 74475.26 Da calculated using our deduced amino acid sequence. Comparing the MALDI-TOF/TOF mass with SDS-PAGE revealed a loss of ~1.6 kDa contributed by N-terminal and C-terminal 6x His tag combined. The additional mass of ~ 1.6 kDa was not detected in MASCOT Protein pilot database search of MALDI-TOF/TOF data probably, due to the loss of N-terminal and C-terminal peptide ions or weak ionization of the tagged portion. Mascot database search of MS/MS data revealed a significant match with hypothetical AOx protein sequence from *A.terreus* NIH strain (gi|115437438) with a score of 165. Sequence coverage of 28 % was achieved with two matching peptide fragment having an ion score above 30 (peaks highlighted in green circle in **Fig. 4.13**).

4.A.3.2 Isoelectric point (p*I*) of rAOx

The p*I* of the apo-rAOx was studied by 2D electrophoresis and the generated datum was verified by zeta potential analysis (in pH range 5.7- 7.2). The p*I* of the protein was identified as pH 6.4 (**Fig. 4.14A**) and pH 6.52 (**Fig. 4.14B**) by electrophoresis and zeta potential studies, respectively; which were in good agreement with the theoretical p*I* of pH 6.62 (ExPASy Compute p*I*/M_w tool).

4.A.3.3 Reconstitution of apo-rAOx with co-factor FAD through fluorescence spectrophotometry

Fluorescence emission spectra of FAD reconstituted apo-rAOx and free FAD are shown in **Figure 4.15.** Excitation at λ_{443nm} gave similar emission spectra for both the samples with emission peak at ~ λ_{527nm}. A lower fluorescence intensity of the holoenzyme relative to that of free FAD inferred efficient incorporation of the cofactor FAD to the apo-rAOx matrix during its refolding process. At the same protein concentration, the FAD fluorescence intensity of rAOx was about 80 % to that of apo-AOx containing free FAD in presence of refolding buffer. This decrease in fluorescence of FAD upon coupling to apo-rAOx is likely to be caused by the surrounding protein shell.

4.A.3.4 Analysis of secondary structure of the rAOx

Circular Dichroic (CD) spectra of rAOx were assessed in different pH buffer environment from pH 9.0 to pH 4.0, after ~80 h incubation at 16 °C in refolding buffer. CD spectra recorded from $\lambda_{190\ nm}$-$\lambda_{260\ nm}$ (**Fig. 4.16)** revealed a stable conformation of folded rAOx in different pH environment and was found to be an ordered protein with α-helix, β-strand and random/non-regular structures as 28 ± 1%, 33 ± 2 % and 39 ± 2 %, respectively as predicted through CD spectra analysis program K2D (**Table 4.3**). CD spectra at pH 9.0 and pH 6.0 are overlapping which reflects similar stable secondary structure composition at both the pH conditions. A control study of an unfolded protein in identical folding buffer without glutathione oxidize and DTT were carried out where the α-helix, β-strand and random/non-regular structures were 8 ± 1 %, 44 ± 3 % and 48 ± 2 %, respectively, where a high β-strand and random/non-regular structures were predominant, a characteristic of an unfolded protein.

4.A.3.5 Studies on the aggregating nature of rAOX

Dynamic Light Scattering (DLS) studies with rAOx confirmed the highly aggregating tendency of the protein due to intermolecular interactions at high protein concentration. Purified apo-rAOx protein at a concentration of ~ 10 µg ml^{-1} (same concentration as in refolding studies) was monitored for 96 h duration in refolding condition with FAD. Simultaneously, we have

checked the aggregation profile of a commercial AOx (cAOx) from *pichia pastoris* and bovine serum albumin (BSA) as a positive and negative control, respectively. At 0 h, rAOx exhibited a major signal at ~10 nm diameter, (**Fig. 4.17A.1)**. After 24 h of incubation the major signal drastically shifted to ~1000 nm diameter, suggesting high aggregation pattern (**Fig. 4.17B.1**). Further incubation for 48 h, 72 h and 96 h showed a constant major peak at ~1000 nm diameter as shown in **Figure 4.17C.1**, **4.17D.1** and **4.17E.1**, respectively. In our positive control with the cAOx, the aggregation pattern at 0 h (**Fig. 4.17A.2**) was consistent over a period of 24 h (**Fig. 4.17B.2**). Further incubation for 48 h, 72 h and 96 h showed constant peak at ~1000 nm diameter indicating similar high aggregation pattern (**Figure 4.17C.2, 4.17D.2, 4.17E.2)**. Aggregation profile of BSA was similarly studied as a negative control to rule out the possibility of aggregation due to refolding buffer components. No significant aggregation pattern was observed with BSA (**Fig. 4.17A.3, 4.17B.3, 4.17C.3, 4.17D.3** and **4.17E.3**). The aggregation study clearly demonstrates the intrinsic tendency of apo-rAOx to form high molecular aggregates that pose a challenge in the efficient *in-vitro* refolding study of the protein with FAD.

Table 4.3. Secondary structural profile of rAOx under different pH environment

pH values	Type of rAOX	α – helix (%)	β – strand (%)	Random coil
9.0	folded	28	33	39
8.0	folded	28	33	39
7.0	folded	27	27	47
6.0	folded	28	33	39
5.0	folded	28	32	40
4.0	folded	28	32	40
9.0	unfolded	8	44	48

Foot note of Table 4.3: The raw CD spectrum was analyzed using online protein CD spectra analysis tool K2D available in DichroWeb. Each spectrum was uploaded as an ASCII file format after subtracting its corresponding blank data.

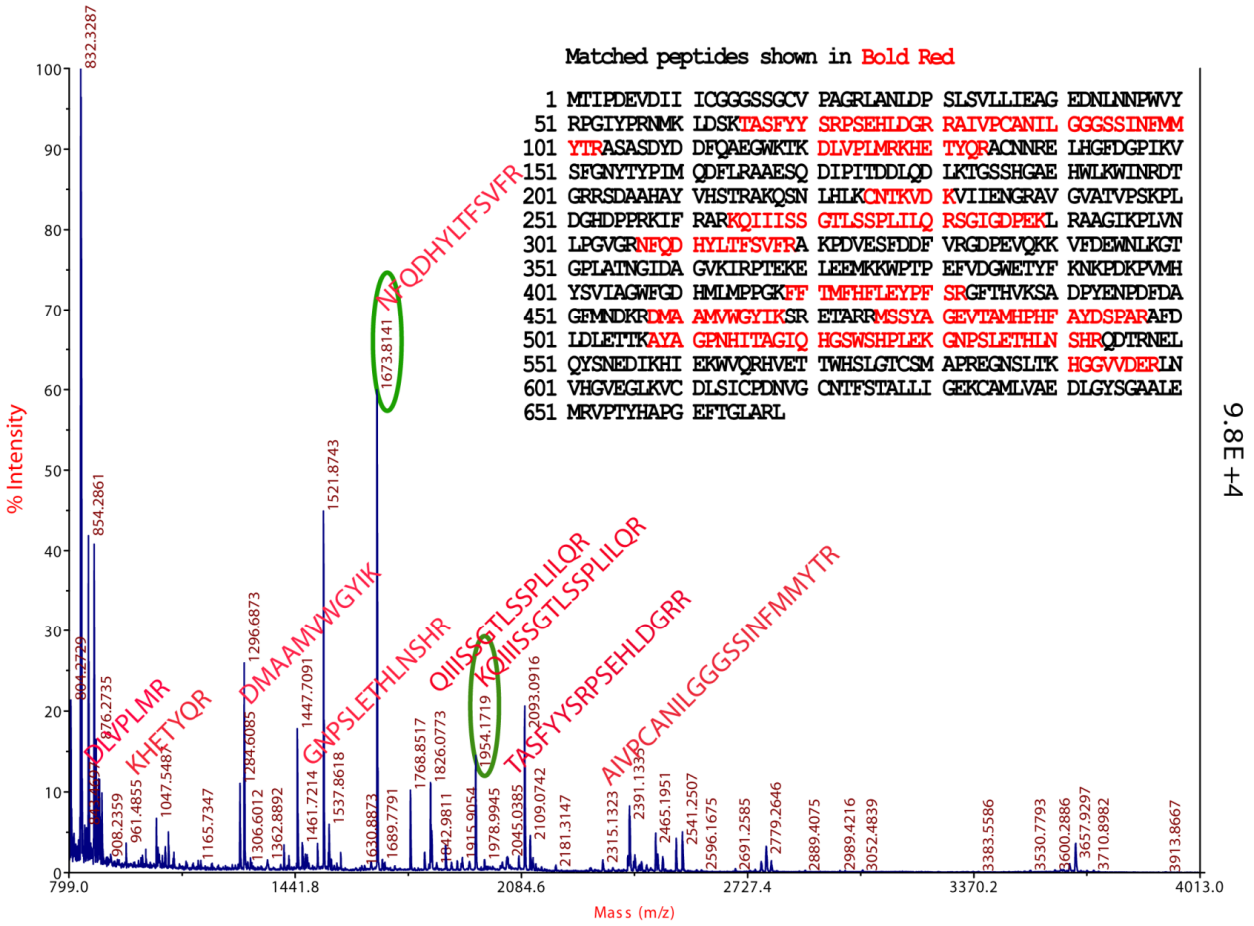

Figure 4.13. MALDI–TOF/TOF analysis of rAOx. Protein pilot database search of spot based MS data of trypsin digested purified rAOx is shown above. Matched peptides after MS/MS are highlighted in red uppercase single letter amino acid code having 28 % sequence coverage with un-reviewed amino acid sequence of AOx from *A.terreus* NIH2624. The mass of apo-rAOx was observed to be 74,614 Da. Two predominant parent peptides in MS having m/z values 1673.8141 and 1954.1697, circled in green had an ion match score of 33 and 32 respectively.

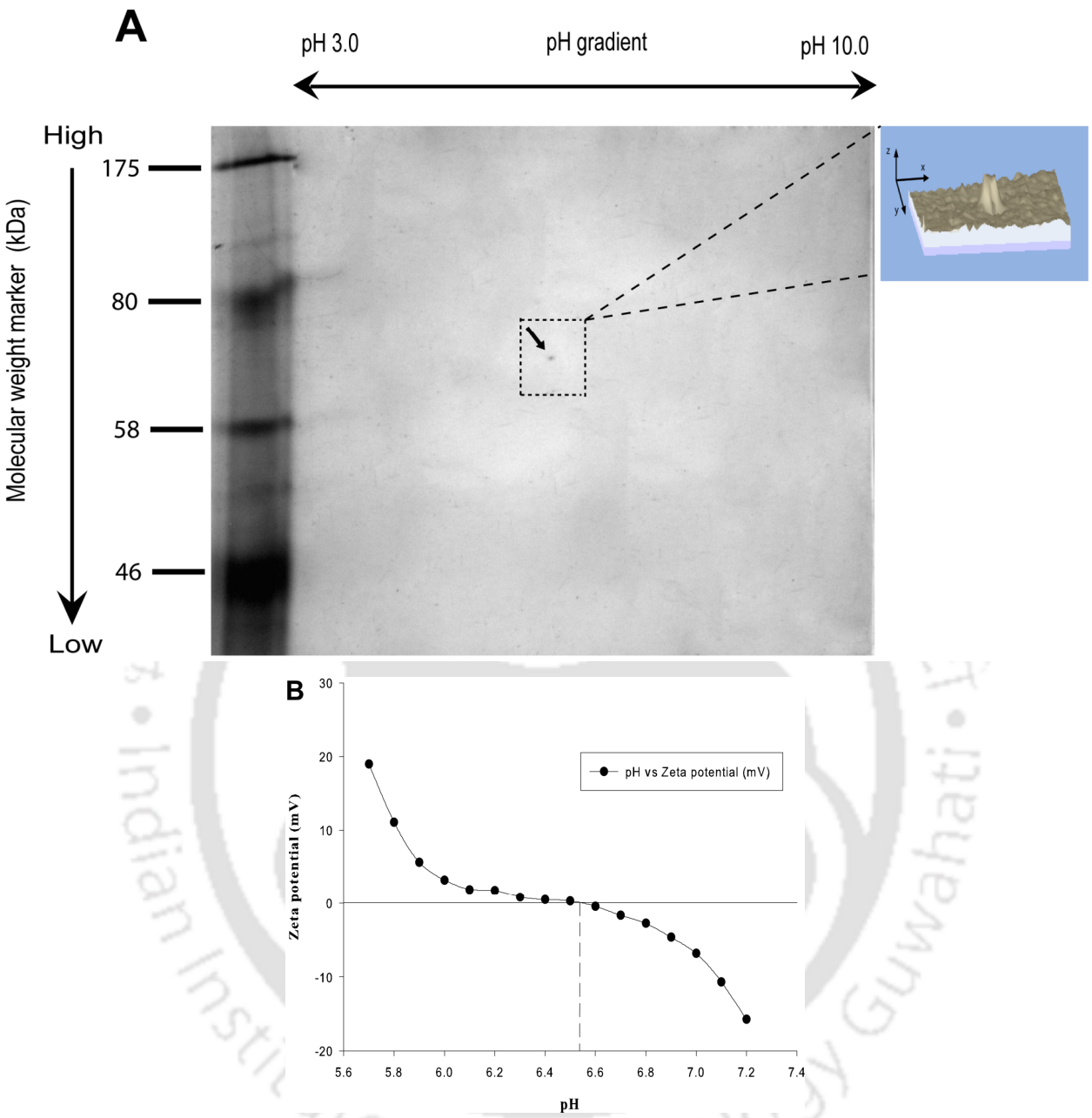

Figure 4.14. Determination of the isoelectric point (p*I*) of rAOx through 2D electrophoresis and Zeta potential studies. (**A**) Isoelectric point of rAOx as determined by 2D electrophoresis on immobiline dry strip pH 3.0 to 10.0 linear gradient. p*I* of rAOx is shown in black arrow. The protein spot is also shown as a sharp peak in 3D box of the zone marked on the gel (exploded figure in the side panel). (**B**) Zeta potential curve of rAOx with varying pH in range from pH 5.7 to 7.2. The point where the curve crosses the zero potential is shown as black dashed drop line on x-axis and was calculated to be 6.52.

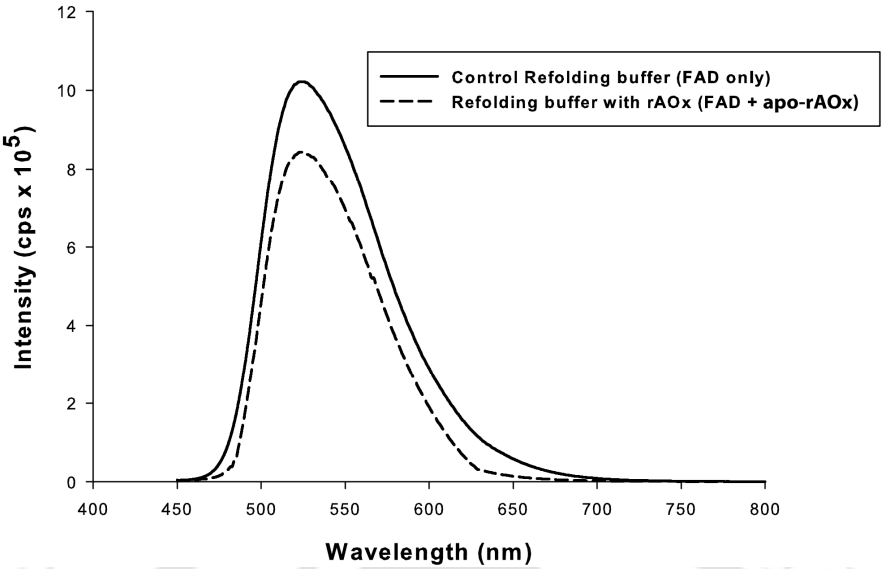

Figure 4.15. Fluorescence emission maxima ($\lambda_{\sim 527\ nm}$) of free FAD (solid black curve) and FAD reconstituted holoenzyme (rAOx) (black dashed curve) at an excitation of λ_{443nm}. The sample was diluted in 20 mM sodium phosphate buffer pH 9.0. The apo-rAOx was incubated with FAD for ~80 h at the condition specified in the experimental section (**section 3.B.3.4**).

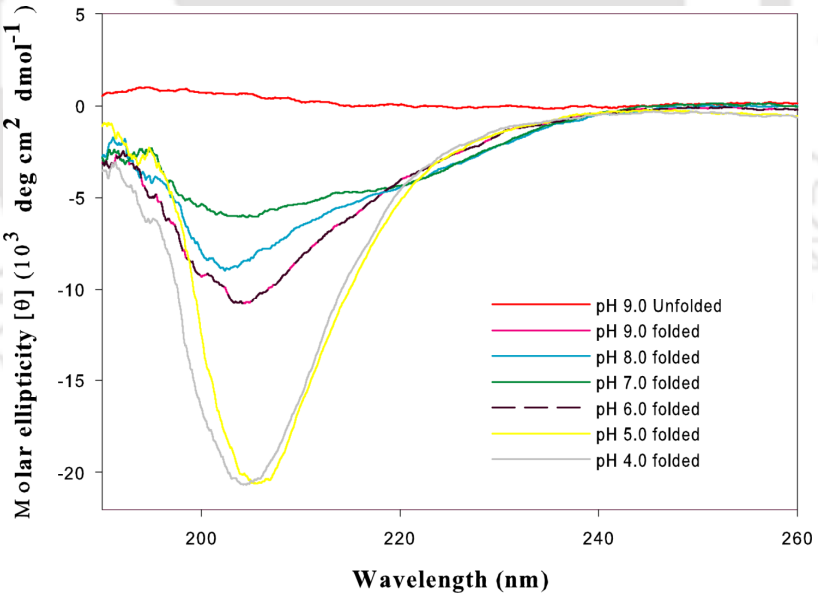

Figure 4.16. Dichroic spectra of rAOx in different pH environment after incubating the samples for ~80 h at 16 °C. Spectrum of purified apo-rAOx in identical folding buffer without glutathione and DTT was also studied as a control (red spectrum). Spectra of rAOx recorded in folding buffer at pH 9.0 (pink spectrum) and pH 6.0 (black dashed spectrum) are overlapping showing similar stable secondary structure conformation at both the pH values.

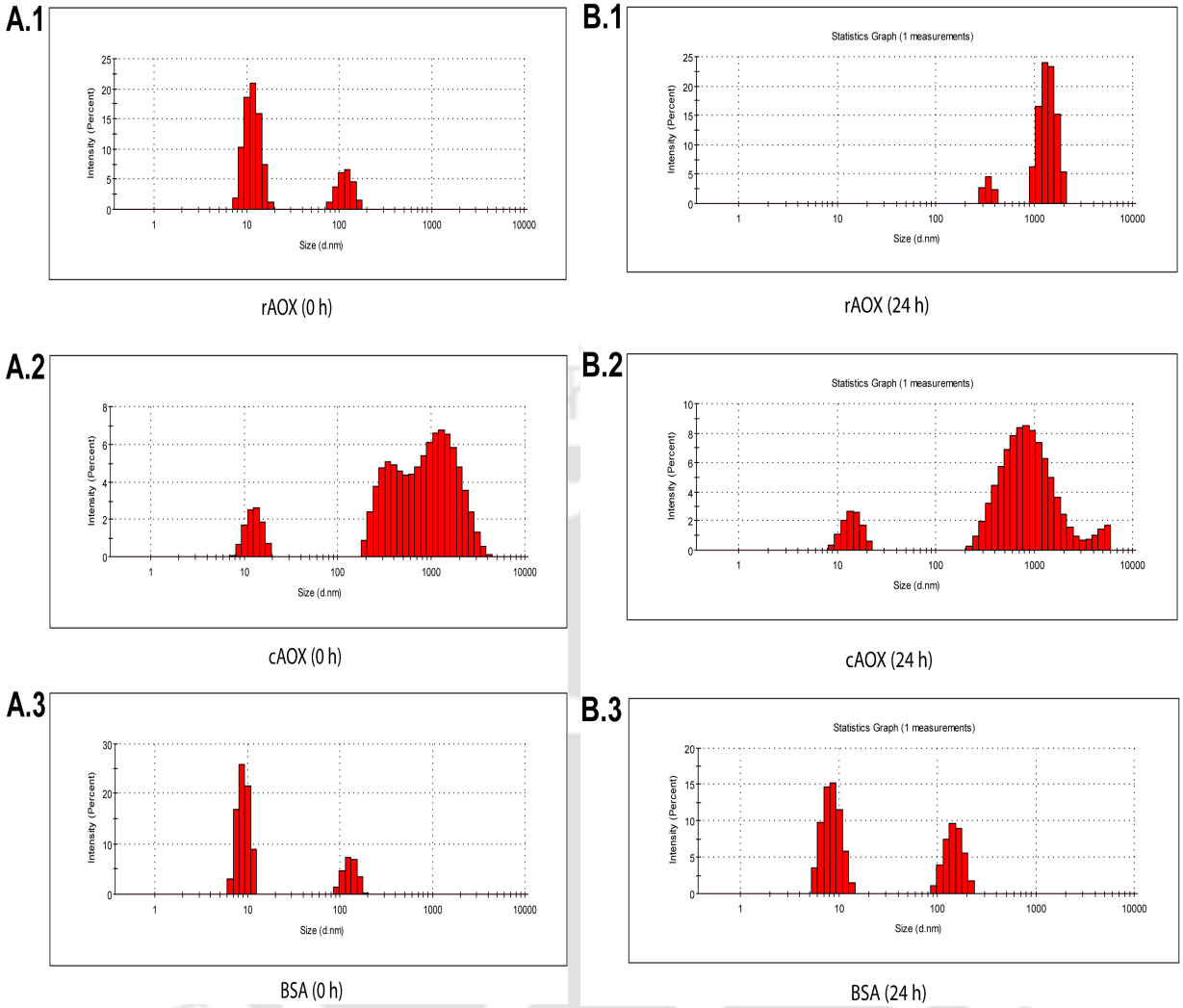

Figure 4.17. DLS analysis of rAOx, cAOx from *Pichia pastoris* and BSA for 0 h, 24 h, 48 h, 72 h and 96 h incubation, respectively at 16 °C. (**A**) Size of the purified rAOx in refolding buffer (0 h) shows the presence of peak at diameter (d) = ~ 10 nm (panel A.1). Panel A.2 shows the 0 h DLS signal of cAOx containing high aggregation reflected by a broad peak at diameter (d)= ~ 1000 nm. Panel A.3 represents the aggregation profile of BSA at 0 h. (**B**).Panel B.1, shows the highly aggregated complex formed after 24 h incubation of rAOx with major peak shift to diameter (d)= ~ 1000 nm. Panel B.2 shows the constant aggregation profile of cAOx with no major peak shift when compared to 0 h data. Panel B.3 represents the constant aggregation profile of BSA, no major peak shift suggests no higher aggregated complex formed after incubation for 24 h and acted as a positive control.

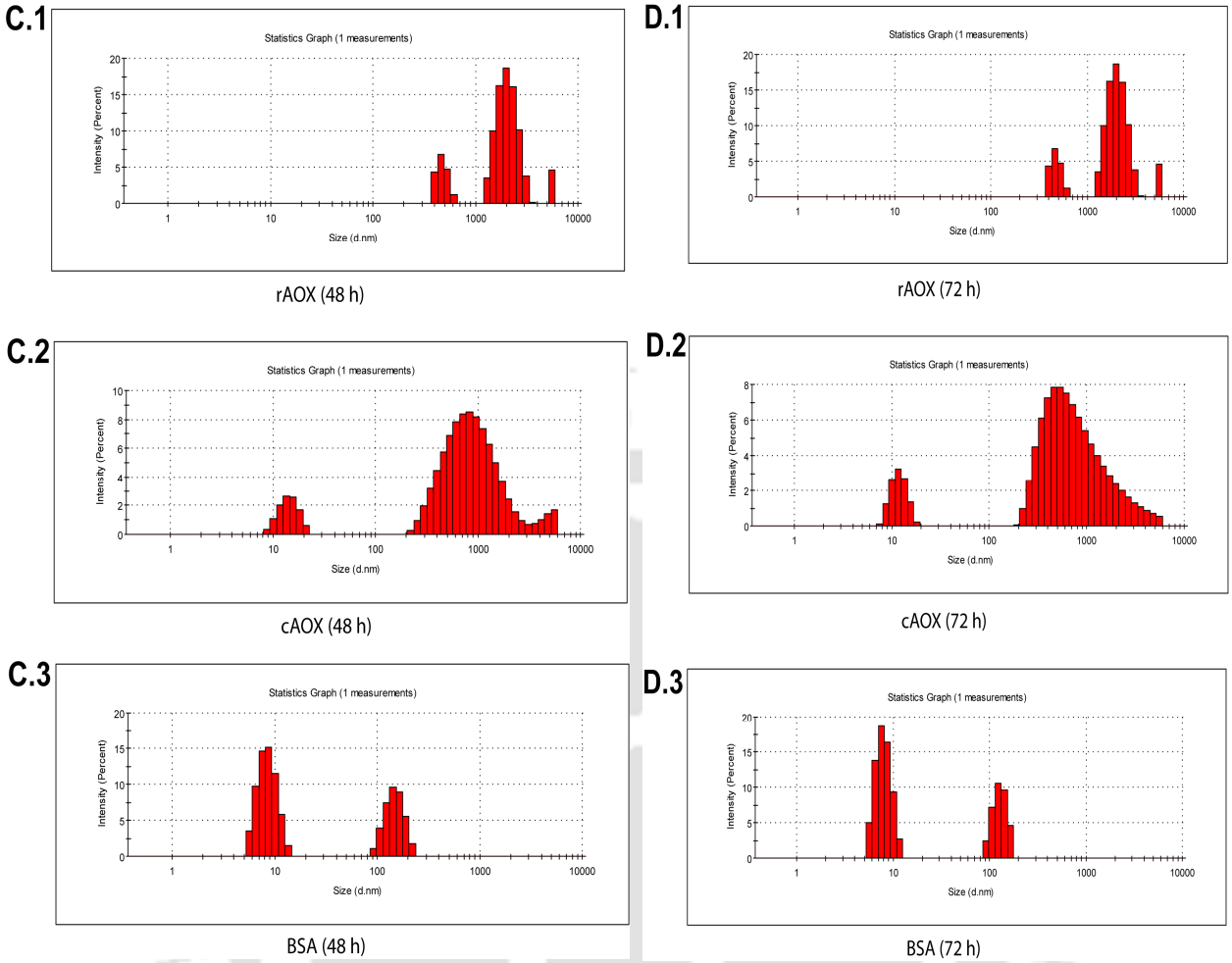

(**C**) rAOx aggregation profile at 48 h incubation is constant at a diameter (d) = ~ 1000 nm (panel C.1). Panel C2 shows the 48 h DLS signal of cAOx maintaining constant high aggregation profile at diameter (d)= ~ 1000 nm. Panel C.3 represents the aggregation profile of BSA at 48 h showing the constant non-aggregating nature of the protein. (**D**) Shows constant aggregation pattern after 72 h of incubation retained by rAOx (panel D.1), cAOx (panel D.2) and BSA (panel D.3).

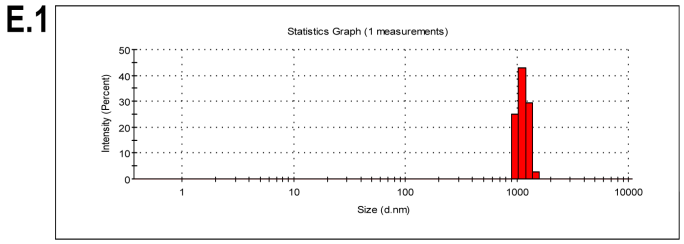

rAOX (96 h)

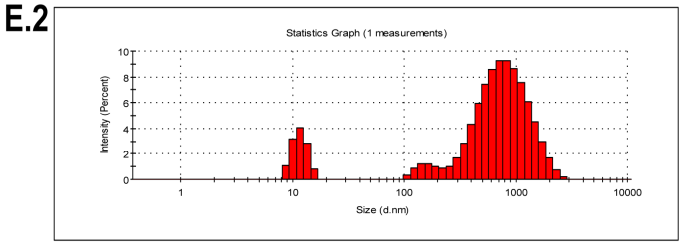

cAOX (96 h)

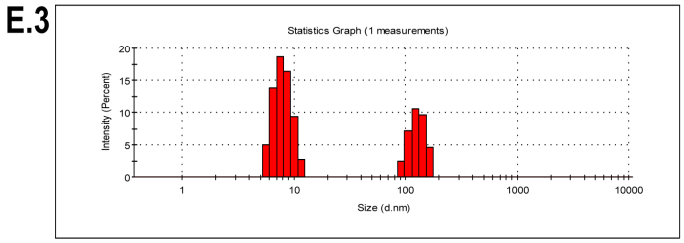

BSA (96 h)

(**E**) Shows constant aggregation pattern retained by rAOx (Panel E.1), cAOx (Panel E.2) and BSA (Panel E.3) during 24 h, 48 h and 72 h DLS studies.

4.A.4 *In-silico* studies on rAOx for sequence to structure and function paradigm

The current section describes the results obtained by *in-silico* studies on the rAOx. The work comprises the conserved domain analyses of the rAOx with other reported AOxs and phylogenetic analysis of our sequenced protein with that of the reported ones as described under the sub-section **4.A.4.1**. The results validated the novelty of the rAOx protein sequence deduced from the characterized rAOx gene. A successful 3D model of the characterized rAOx had been generated and results pertaining to its stereochemical validation are depicted through Ramachandran plot as described in the sub-section **4.A.4.2**. Function of the predicted model was also investigated through molecular docking studies with its co-factor FAD and substrate alcohol molecules and reported in the subsequent sections.

4.A.4.1 *In-silico* sequence analysis of rAOx

Conserve domain analysis showed N- and C-terminal domains conserved across Glucose-Methanol-Choline oxidoreductase family of proteins (**Fig. 4.18**). The flavoprotein nature of the protein was evident from the conserved Rossmann fold sequence motif (GXGXXG) present at the N-terminal end which facilitates FAD binding as a co-factor.

N-terminal multiple sequence alignment of *A. terreus* rAOx with the well studied aryl AOxs from lignin degrading strains (*P. simplicissimum* and *P. eryngii*) revealed significant sequence diversity (**Fig. 4.19A)**. Based on the phylogeny (**Fig. 4.19B)** it is evident that alcohol oxidase protein sequence characterized and reported in the present study shares similarity with the hypothetical un-reviewed AOx reported from *A.terreus* NIH2624 strain and thus shares a common ancestry in the evolutionary chain evident from the branching at node 1. The phylogenetic tree also highlights and validates that aryl-alcohol oxidases from *Pleurotus eryngii* (PDB id: 3FIM) and *Penicillium simplicissium* (PDB id: 1VAO) are not evolutionarily related to the AOx from *A.terreus*. The AOx gene reported from this study shares novel features among the alcohol oxidase group of enzymes based on amino acid sequence variability although sharing common conserved sequence motifs present in oxidoreductase family.

The full length coding sequence of AOx matched with genomic scaffold 14 of the draft whole genome sequence of *A.terreus* NIH6324 (gi|115438615|) and predicted 9 exons with intervening 8 introns joined through splicing to form 2001 bp mRNA coding for the full length monomeric AOx. The alignment of the plus strand of mRNA to the minus strand of the genomic sequence was performed using NCBI spidey online application tool with an overall percentage identity of 98.7 % (**Fig. 4.20**)

4.A.4.2 Molecular modeling and docking studies of rAOx

Ab-initio based modeling using I-TASSER server predicted model of rAOx with a confidence score (C-score) of -0.92 and estimated accuracy (TM-score) of 0.60 ± 0.14 (**Fig. 4.21**). The stereo chemical quality of the predicted model was evaluated through PROCHECK generating a number of postscript plots among which the Ramchadran plot predicting 79.5 % residues lying in the most favored region of the plot (**Fig. 4.22)**. The crystal structures namely 3Q9T, 3QVP and 3FIM reported for formate oxidase, glucose oxidase and aryl-alcohol oxidase, respectively, were used as the templates for assessing our predicted model and detected respective similarity of 86.6 %, 89 % and 88 % with our predicted model (**Table 4.4**). The selected model thus, was found to be reasonable for calculating the stereo-chemical parameters for predicting the functional activities. The model was predicted for its function as an aryl-alcohol oxidase with a highest TM-score of 0.785 as predicted by COFACTOR, an in-build application tool.

The modeled apo-rAOx was successfully docked with its co-factor FAD and was found to be in consistent with the conserved FAD binding amino acid residues, GXGXXG motif (where X being any residue) as Rossmann fold reported previously (**Fig. 4.23**). In our control study, aryl-AOx crystal structure (PDB id: 3FIM) in apoenzyme form was docked simultaneously with our FAD best pose (judged by using MolDock scoring matrix) and was superimposed with our FAD docked rAOx model from *A.terreus* (**Fig. 4.24A**). Superimposition of both the docked FAD molecules were analysed using Swiss PDB Viewer version 4.1 in ExPASy bioinformatics resource portal and a rationale root-mean-square distance signified a satisfactory evaluation of our docking performance. 3D superimposition of our predicted model with aryl AOx crystal structure (pdb id: 3FIM) revealed significant homology with chain B of

the structure (**Fig. 4.24B**), although at their amino acid sequence level non-homology is predominant.

Flexible docking simulation studies of our FAD bound modeled rAOx with some aryl alcohol substrates were performed and the best pose of each ligand was assessed by using MolDock score. The results clearly demonstrated the affinity of our predicted rAOx model for the aryl alcohol substrates in order of following preference with its total binding energy showing in the parenthesis as 4-methoxybenzyl alcohol (-82.87 kJ mol^{-1}) > 3-methoxybenzyl alcohol (-74.12 kJ mol^{-1})> 3, 4 dimethoxybenzyl alcohol (-71.75 kJ mol^{-1})> benzyl alcohol (-56.45 kJ mol^{-1}) (**Fig. 4.25A, B, C, D**). A funnel shaped cavity connecting the substrate binding site to the FAD isoalloxazine ring as conserved in other reported crystal structures of aryl-alcohol oxidases was also evident in the model. The amino acid residues Tyr 55, Pro 56, Phe 98 and Asn 354 were found to be conserved near the substrate binding site (**Fig. 4.26A, B, C and D)**. The role of Tyr 55 and Phe 98 has been proposed to contribute in π-π stacking interaction with the FAD isoalloxazine ring, an important signature pattern observed and reported for other aryl alcohol oxidase (Hernández-Ortega *et al.*, 2011a and 2011b).

Table 4.4. A Comparison of Ramachandran plots of the crystal structures used as templates in predicting the best 3D model structure of rAOx from *A.terreus* MTCC6324 using I-TASSER by PROCHECK. (**NA** denotes that it is not applicable)

Ramachandran Plot areas	**I-TASSER best model**		**PDB id: 3FIM**		**PDB id: 3Q9T**		**PDB id: 3QVP**	
	No. of residues	**Percentage (%)**	**No. of residues**	**Percentage (%)**	**No. of residues**	**Percentage (%)**	**No. of residues**	**Percentage (%)**
Most favored regions (A,B,L)	449	79.5	419	88.0	1262	86.6	443	89.0
Additionally allowed regions (a,b,l,p)	79	14.0	54	11.3	193	13.2	54	10.8
Generously allowed regions (~a,~b,~l,~p)	21	3.7	2	0.4	3	0.2	1	0.2
Disallowed regions (XX)	16	2.8	1	0.2	0	0	0	0
Non-glycine and non-proline residues	565	NA	476	NA	1458	NA	498	NA
End residues (excl. Gly and Pro)	2	NA	2	NA	6	NA	1	NA
Gly residues	57	NA	46	NA	153	NA	57	NA
Pro residues	42	NA	41	NA	114	NA	25	NA
Total no. of residues	666	NA	565	NA	1731	NA	581	NA

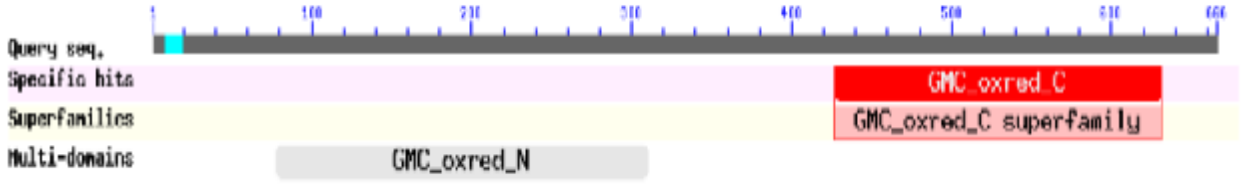

Figure 4.18. NCBI conserve domain search with rAOx amino acid sequence as a query input predicting conserved N-terminal (highlighted in ash color box) and C-terminal (highlighted in red color box) GMC oxidoreductase family of flavoprotein having the conserved N-terminal Rossmann fold motif (highlighted in sky blue color box)

A

```
                    *         20        *         40        *         60
P.angusta         : MAIPDEFDIIVVGGGSTGCCIAGRLANLDDQNLTVALIEGGENNINNPWVYLPGVYPRNMRLDSKT : 66
C.boidinii        : MAIPEEFDVIVCGGGSTGCVIAGRLANVDENLKVLLIENGENNLNNPWVYLPGIYPRNMRLDSKTA : 66
A.terreus NIH2624 : MTIPDEVDIIICGGGSSGCVPAGRLANLDPSLSVLLIEAGEDNLNNPWVYRPGIYPRNMKLDSKTA : 66
A.terreus MTCC6324: MTIPDEVDIIICGGGSSGCVPAGRLANLDPSLSVLLIEAGEDNLNNPWVYRPGIYPRNMKLDSKTA : 66
K.pastoris        : MAIPEEFDILVLGGGSSGSCIAGRLANLDHSLKVGLIEAGENNLNNPWVYLPGIYPRNMKLDSKTA : 66
C.victoria        : MTIPDEVDIIVCGGGSCGCVVAGRLANLDHNLQVLLIEAGENNLNNPWVFRPGIYPRNMKLDSKTA : 66
P.fulva           : MTIPDEVDIIVCGGGSCGCVVAGRLANLDHKLQVMLIEAGESNLNNPWVFRPGIYPRNMKLDSKTA : 66
P.chrysogenum     : MTIPEEVDIIICGGGSSGCVPAGRLANLDHNLSVLLIEAGEDNLNNQWVYRPGIYPNNMKLDSKTA : 66
O.pini            : MAIPEEFDILVLGGGSSGSCIAGRLANLDHSLKVGLIEAGENNLNNPWVYLPGIYPRNMKLDSKTA : 66
P.simplicissimum  : MSKTQEFRPLTLPPKLSLSDFNEFIQDIIRIVGSENVEVISSKDQIVDGSYMKPTHTHDPHHVMDQ : 66
P.eryngii         : MSFGALRQLLLIACLALPSLAATNLPTADFDYVVVGAGNAGNVVAARLTEDPDVSVLVLEAGVSDE : 66
                    M ip e d 6  gggs g   agr6a  d    v   e g  n  n    p
```

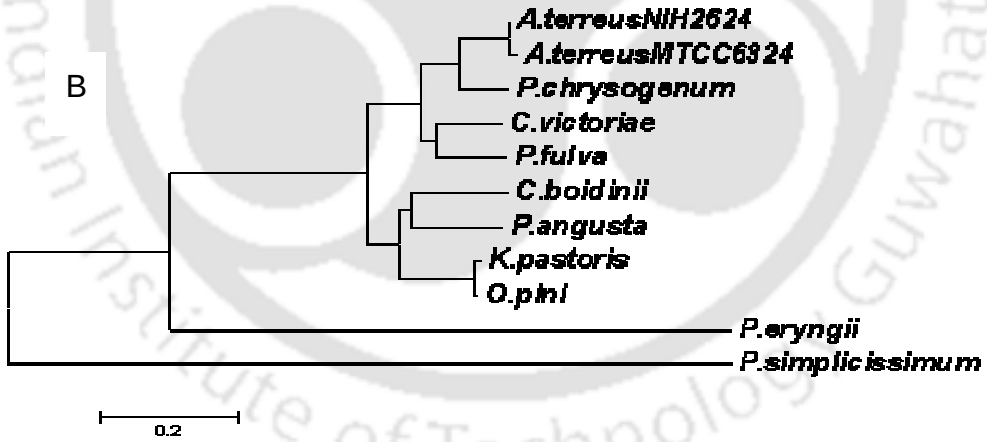

Figure. 4.19. (**A**) N-terminal multiple sequence alignment of AOx coding amino acid sequences from 11 species of filamentous fungi and yeast species. The amino acid sequence identity (using NCBI BLAST) of *A. terreus* AOx with other aryl AOxs from *P. eryngii* and *P. simplicissimum* showed 25 % and 37 %, respectively and poor homology was found in the N-terminal region of the protein. (**B**) Phylogenetic tree of the corresponding AOxs by Neighbour - Joining method using MEGA v 6.05 showed *A.terreus* MTCC and NIH strain sharing similar evolutionary lineage and significant branching out of AOx from *A .terreus* with that of well studied aryl AOxs from *P. eryngii* and *P. simplicissimum* predicted the novelty of our protein at the sequence level.

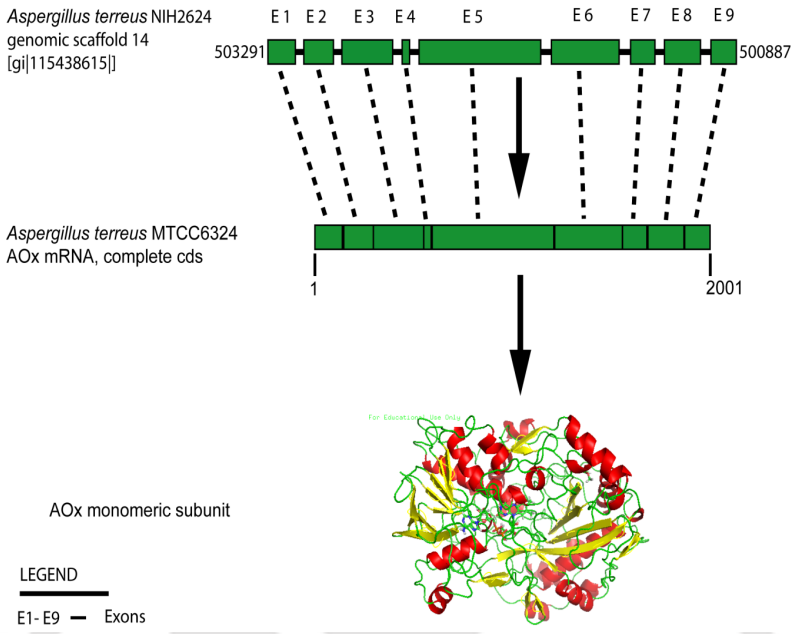

Fig. 4.20. mRNA to genomic alignment using NCBI spidey showing a match with the genomic scaffold 14 (gi|115438615|) with 9 coding exons and 8 intervening intronic sequences coding for full length 2001 bp AOx monomeric subunit.

Figure 4.21. The best 3D model of rAOx as predicted by I-TASSER online protein structure prediction software. The model was generated using Molsoft (Molsoft L.L.C, USA).

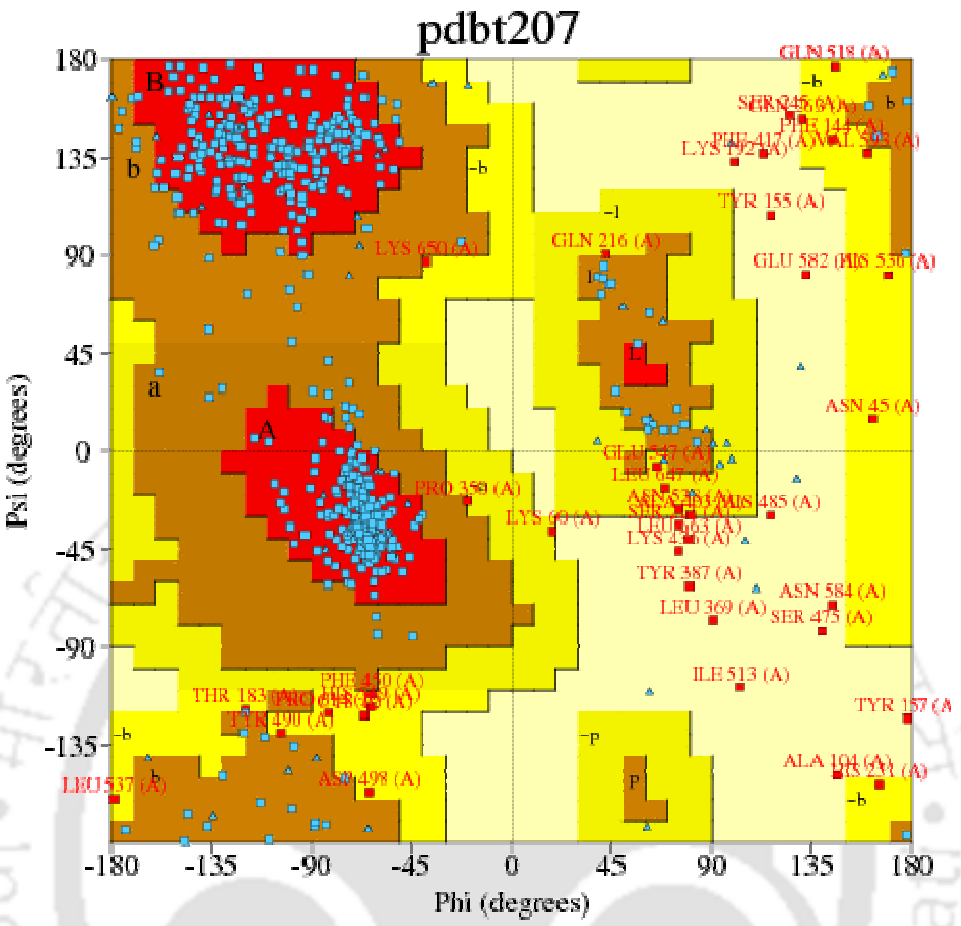

Figure 4.22. Ramachandran plot of predicted AOx model by PROCHECK showing 79.5 % residues lying in the most favored region of the plot. Residues lying in the additionally allowed, generously allowed and disallowed regions of the plot are 14 %, 3.7 % and 2.8 %, respectively.

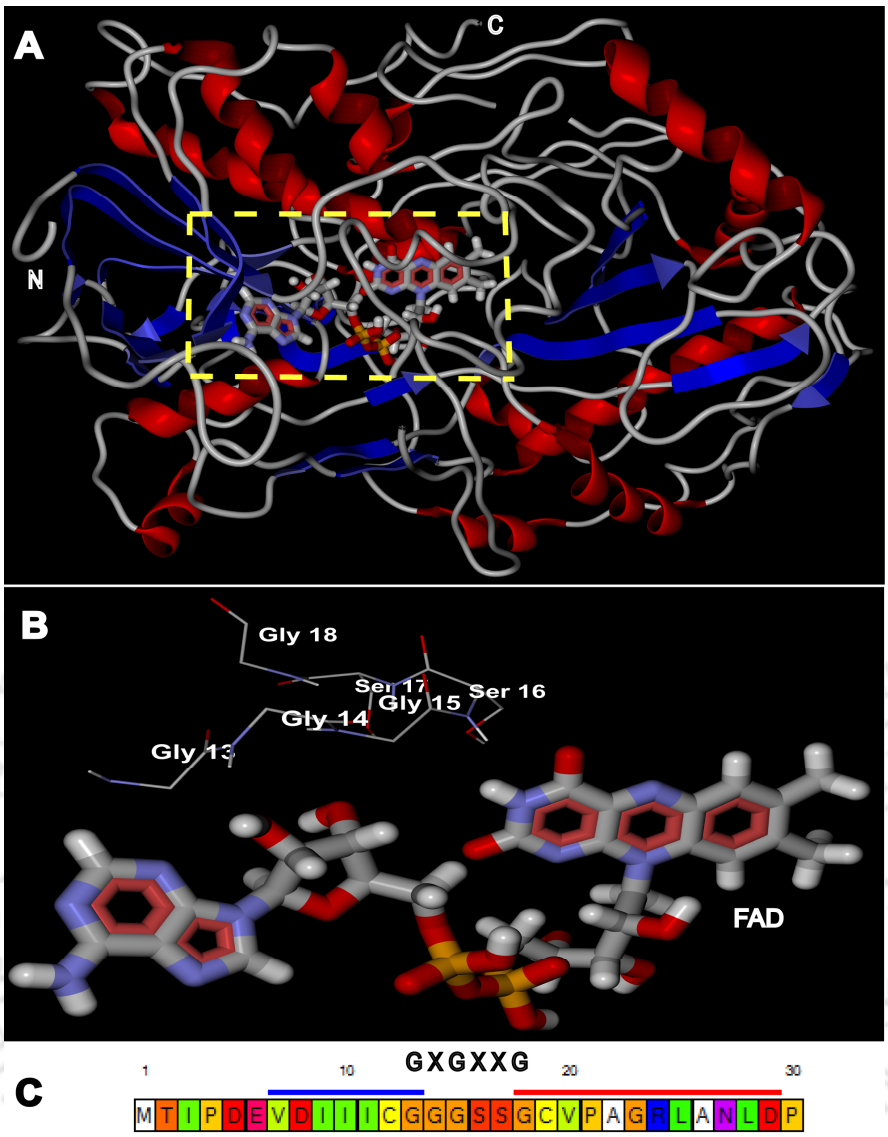

Figure 4.23. I-TASSER predicted *ab-initio* model of apo-rAOx docked with its co-factor FAD (**A**). The best model (predicted by I-TASSER) docked with FAD (using Molegro Virtual Docker version 4.0.2 (CLC bio-Qiagen Company). Red ribbon shows the α-helices, blue ribbon depicts β-sheets and loops are shown in grey tubular wire. FAD is represented as Corey-Pauling-Koltun (CPK) model bound at its conserved Rossmann fold motif (GXGXXG) highlighted by yellow dotted square as inset with its residue labeled as shown in a magnified panel (**B**) in the model. The same is also shown against the N-terminal loops region present between the first β-sheet (highlighted as blue bar) and first α-helix (highlighted as red bar) in the lower panel (**C**).

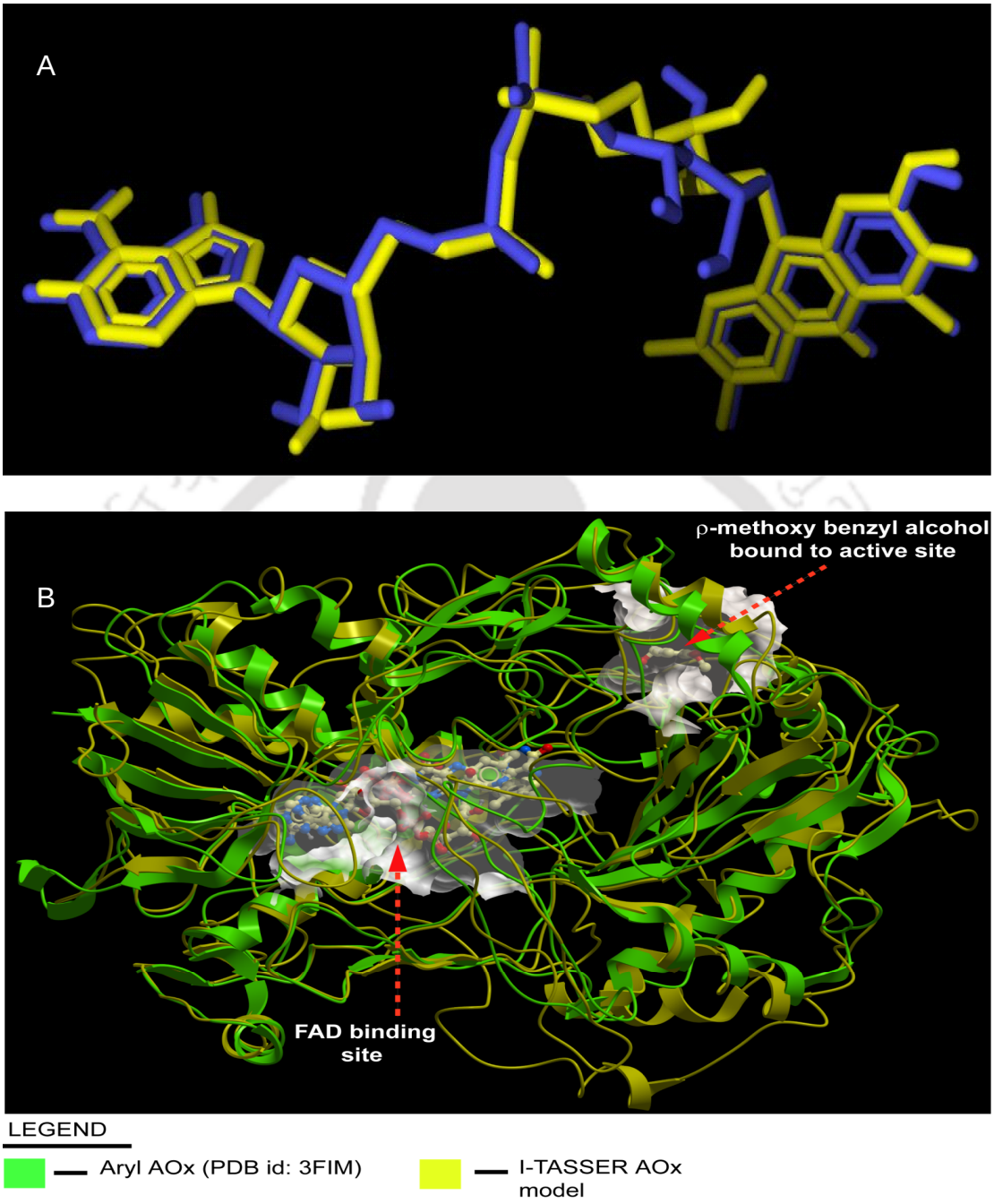

Figure 4.24. (**A**) 3D superimposition of best pose of FAD predicted in our docking simulation modeled AOx (yellow stick model) with 3FIM bound FAD (violet stick model). The RMSD of superimposition as predicted by Swiss PDB Viewer version 4.1 was 1.26 Å. (**B**) Protein 3D superimposition of FAD bound crystal structure of aryl AOx (PDB id: 3FIM) (yellow ribbon structure) with FAD docked modeled AOx (green ribbon structure). FAD and active substrate binding sites are shown as white highlighted cavity. FAD and substrate *ρ*-methoxybenzyl alcohol are shown as Corey-Pauling-Koltun model.

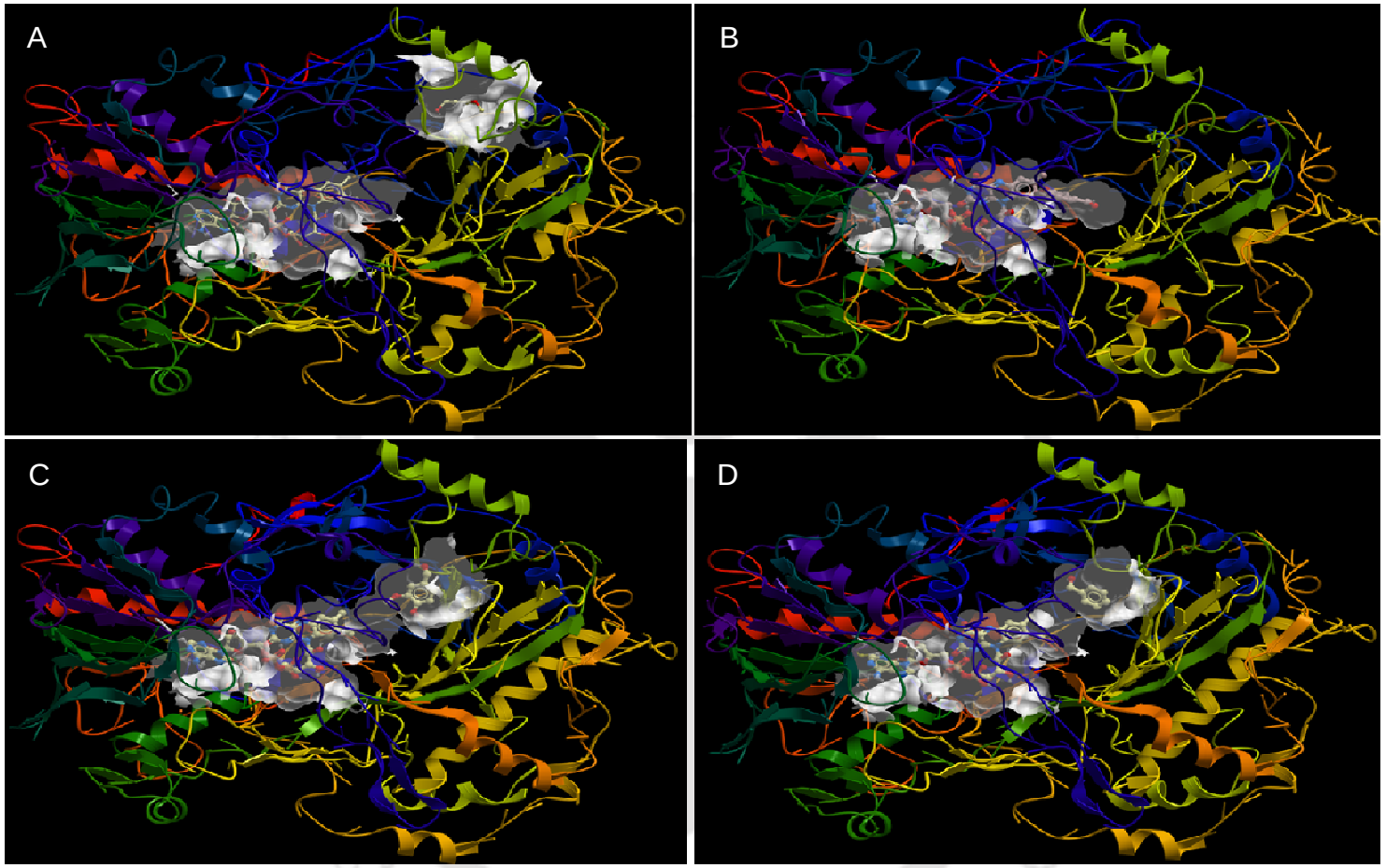

Figure 4.25. FAD bound apo-AOx docked with (**A**) ρ-methoxybenzyl alcohol (-82.87 kJ mol-1), (**B**) m-methoxybenzyl alcohol (-74.12 kJ mol-1) (**C**) 3,4 dimethoxybenzyl alcohol (-71.75 kJ mol-1) and (**D**) benzyl alcohol (-56.45 kJ mol-1) with binding energy in parenthesis .White cavities depicts the binding sites for FAD and alcohol ligands shown as CPK models. The close proximity of the two sites separated by narrow funnel shaped channel for better substrate sequestration and oxidation are evident in our docking results, which is a conserved motif well reviewed for other flavoproteins in the literature.

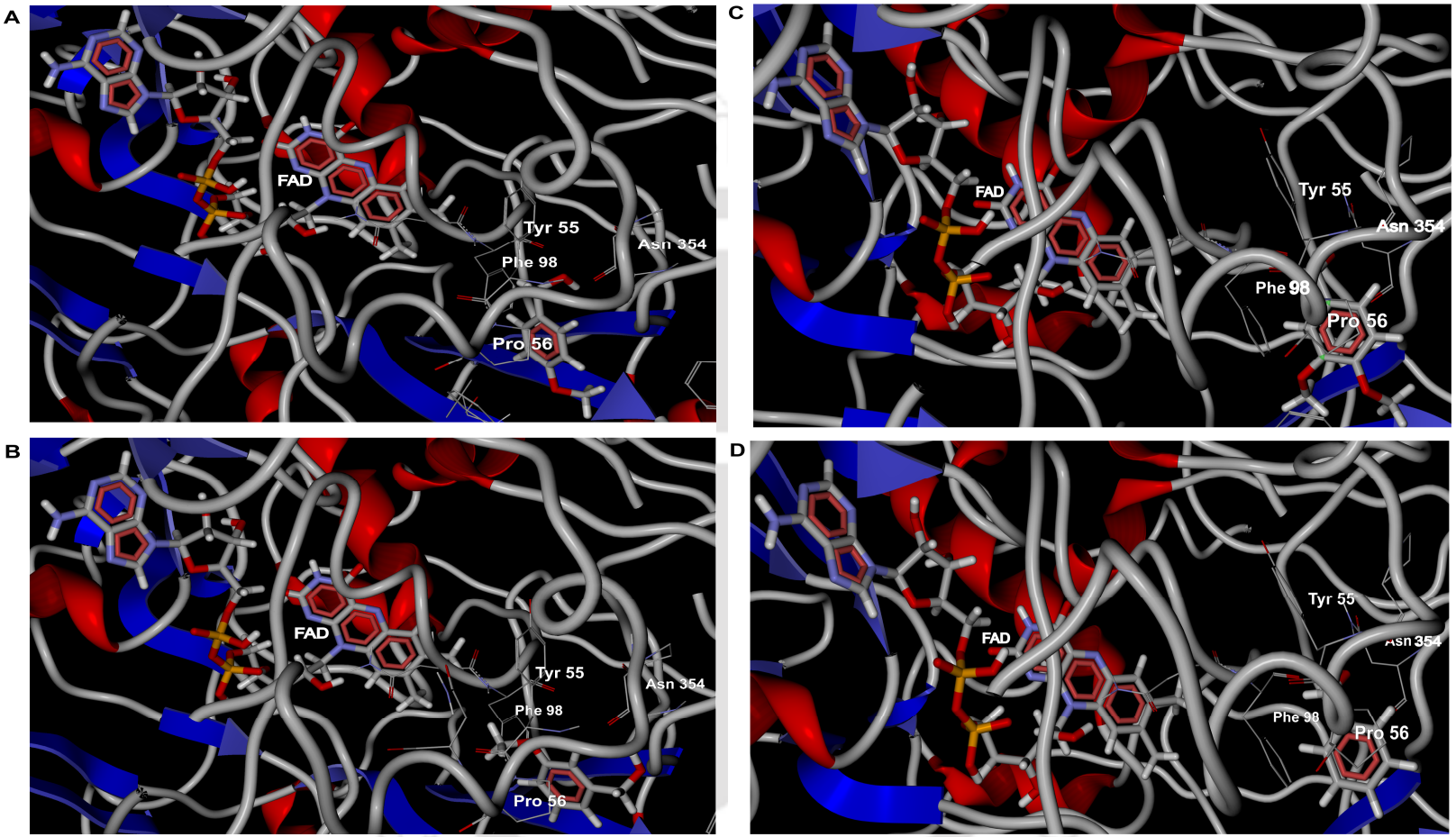

Figure 4.26. Docking view of aromatic alcohols (highlighted as thick stick Corey-Pauling-Koltun (CPK) model) as substrates with FAD docked (highlighted as thick stick CPK model) apo-rAOx holoenzyme complex. Conserved amino acid residues at a search radius of 6.0 Å (Tyr55, Pro56, Phe98 and Asn354) are highlighted as thin stick CPK model with its residues labeled. Panel (**A), (B), (C)** and (**D)** shows the close-up docking view generated by Molegro Virtual Docker version 4.0.2 (CLC bio-Qiagen Company) of *ρ*-methoxybenzyl alcohol (-82.87 kJ mol^{-1}); *m*-methoxybenzyl alcohol (-74.12 kJ mol^{-1}); 3,4 dimethoxybenzyl alcohol (-71.75 kJ mol^{-1}) and benzyl alcohol (-56.45 kJ mol^{-1}), respectively.

4.A.5 Steady state kinetics and thermo-inactivation studies of rAOx

This section describes the optimization of pH and temperature for the activity of rAOx, the stability of the recombinant enzyme under optimal conditions, and determination of thermo-activation and deactivation energies for the enzyme. This section also tries to validate the *in-silico* work reported in the preceding sections, particularly the function of the recombinantly expressed protein through experimental approach by analyzing the steady state kinetic parameters (Specific activity, K_m, K_{cat} and K_m/K_{cat}). The thermo activation and inactivation studies clearly demonstrates the stability of the refolded protein at temperatures higher than the optimal temperature for its activity and tries to establish the relationship between the denaturation kinetics and thermodynamic properties of rAOx through Arrhenius plot, predicting the activation and deactivation energies, half life ($t_{1/2}$) and decimal reduction value (*D*-value) of the rAOx. Deactivation kinetic parameters namely free energy change (ΔG), change in enthalpy (ΔH), and change in entropy (ΔS) were also calculated and analyzed in the following sections.

4.A.5.1 Enzyme activity and kinetic studies of AOx

In-vitro refolded rAOx showed an optimum temperature and pH of 30 °C and pH 6.0, respectively for its activity (**Fig. 4.27A** and **4.27B**). Thermal stability of rAOx showed that the enzyme was stable upto 30 °C and the stability was greatly reduced at 40 °C (50 % inactivation) and lead to 100 % inactivation after 5 min at 70 °C (**Fig. 4.27C**). Moreover the rAOx demonstrated partial pH stability in range from pH 6.0 to pH 9.0 after 1 h (**Fig. 4.27D**).

A range of alcohol substrates for activity of the rAOx was studied and found that only the aryl alcohol substrates showed detectable activity for the recombinant enzyme. Steady-state kinetic parameters of rAOx were evaluated based on its catalytic activity exhibited for the oxidation of four different aromatic alcohols. Kinetic constants pertaining to Specific activity, K_m, k_{cat} and k_{cat}/K_m for each of the substrates tested revealed that 4-methoxybenzyl alcohol (*ρ*-anisyl alcohol) is the best aromatic alcohol substrate followed by 3-methoxybenzyl alcohol (*m*-anisyl alcohol), 3, 4-dimethoxybenzyl alcohol (veratryl alcohol) and benzyl alcohol (**Table 4.5**). Catalytic efficiency as predicted by k_{cat}/K_m for 4-methoxybenzyl alcohol was 7829.5 min^{-1} mM^{-1}, which was the highest among the four aromatic alcohols tested.

4.A.5.2 Activation energy of rAOx

The Arrhenius plot of alcohol oxidase activity exhibited one "break point" at 25 °C (**Fig. 4.28 inset A**) with mean activation energies (E_a) of 704.34 and 41.47 kJ mol^{-1} in temperature range of 20-25 °C and 25-30 °C, respectively. Such high variation of activation energies indicates the conformational changes especially in the substrate binding site improving the affinity of rAOx for substrate (aromatic alcohols) binding. The greater slope of line (a) and lesser slope of line (b) indicates high and low activation energies associated in the respective temperature ranges and thus the rate constants associated were inferred to be high and less sensitive, respectively.

4.A.5.3 Thermoinactivation studies of rAOx

Alcohol oxidase activity decreased with increase in temperature of the reaction mixture beyond 30 °C and thus the thermal inactivation studies were performed in temperature range from 40 to 70 °C by plotting the residual activity of bioactive rAOx in natural logarithm (ln V) versus the pre-incubation time after fitting the data in linear regression (**Fig. 4.29 inset A**). The correlation co-efficient is high (0.98) which indicated a first order deactivation kinetics. Conformational deactivation energy (Ea_d) was calculated based on Arrhenius-type equation by plotting inactivation constants k_d (h^{-1}) obtained at 40, 50, 60 and 70 °C versus absolute temperature (**Fig. 4.29 inset B)** and was calculated to be 119 kJ, indicative of a covalent interaction between substrate and enzyme active site and agrees with a thermodynamically stable but catalytically inactive protein. Thus it predicts a stably refolded protein structure with no significant unfolding at denaturing temperatures.

Further deactivation properties of rAOx were studied by analyzing the decimal reduction values (*D*-values) and the temperature interval required for the thermal inactivation curve to traverse one log cycle (*z*-value) according to Lopez and Burgos, (1995). The observed z-value was calculated from the slope of the regression line by plotting log of *D* versus temperature (°C) and was found to be ~18 °C (**Fig. 4.30)** indicating a change of ~18 °C essential for a decimal reduction of enzyme activity per hour. A high decimal reduction values (*D*-values) at inactivating temperatures predicted instability of the enzyme at high temperature. Half life ($t_{1/2}$) of rAOx decreased significantly as temperature increased beyond 30 °C. No significant

variations in free energy (ΔG) enthalpy (ΔH) values were observed suggesting a stable enzyme structure due to constant heat capacity (**Table 4.6**).

Table 4.5. Steady-state kinetic parameters of *in-vitro* refolded rAOx

Alcohol substrates	**K_m (mM)**	**Specific activity (U mg^{-1})**	**k_{cat} (min^{-1})**	**k_{cat} / K_m (min^{-1}mM^{-1})**
Aromatic alcohols				
ρ-anisyl alcohol	1.08	111.11	8455.86	7829.5
m-anisyl alcohol	2.88	83.33	6341.70	2201.98
Veratryl alcohol	4.91	91.00	6925.42	1410.47
Benzyl alcohol	10.80	1.70	129.38	11.98
Vanillyl alcohol	ND	ND	ND	ND
Short chain alcohols				
Methanol	ND	ND	ND	ND
Ethanol	ND	ND	ND	ND
1-heptanol	ND	ND	ND	ND
Long chain alcohols				
1-Decanol	ND	ND	ND	ND
1-Dodecanol	ND	ND	ND	ND
1-Hexadecanol	ND	ND	ND	ND
Secondary alcohols				
Isopropanol	ND	ND	ND	ND
Isoamyl alcohol	ND	ND	ND	ND
3-Octanol	ND	ND	ND	ND

ND: Not Determined since no detectable activity was found with these substrates.

Mean K_m, k_{cat} and k_{cat}/K_m values were determined and all assays were performed in replicates of 3 (n=3)

Table 4.6. Elucidation of deactivation kinetic parameters at different incubation temperature in range from 30 °C to 70 °C of the purified rAOx.

Parameters	**Temperature range (°C)**				
	30	**40**	**50**	**60**	**70**
Δ*G* (kJ mol^{-1})	101.964	99.173	99.097	96.904	98.486
Δ*H* (kJ mol^{-1})	116.478	116.395	116.312	116.228	116.145
Δ*S* (J mol^{-1} K^{-1})	47.900	55.022	53.293	58.029	51.483
$t_{1/2}$ (min)	700.000	61.180	23.950	3.328	1.772

Foot note of Table 4.6: Free energy change (Δ*G*), change in enthalpy (Δ*H*), change in entropy (Δ*S*) and half life ($t_{1/2}$) are shown with its corresponding units defined in parenthesis.

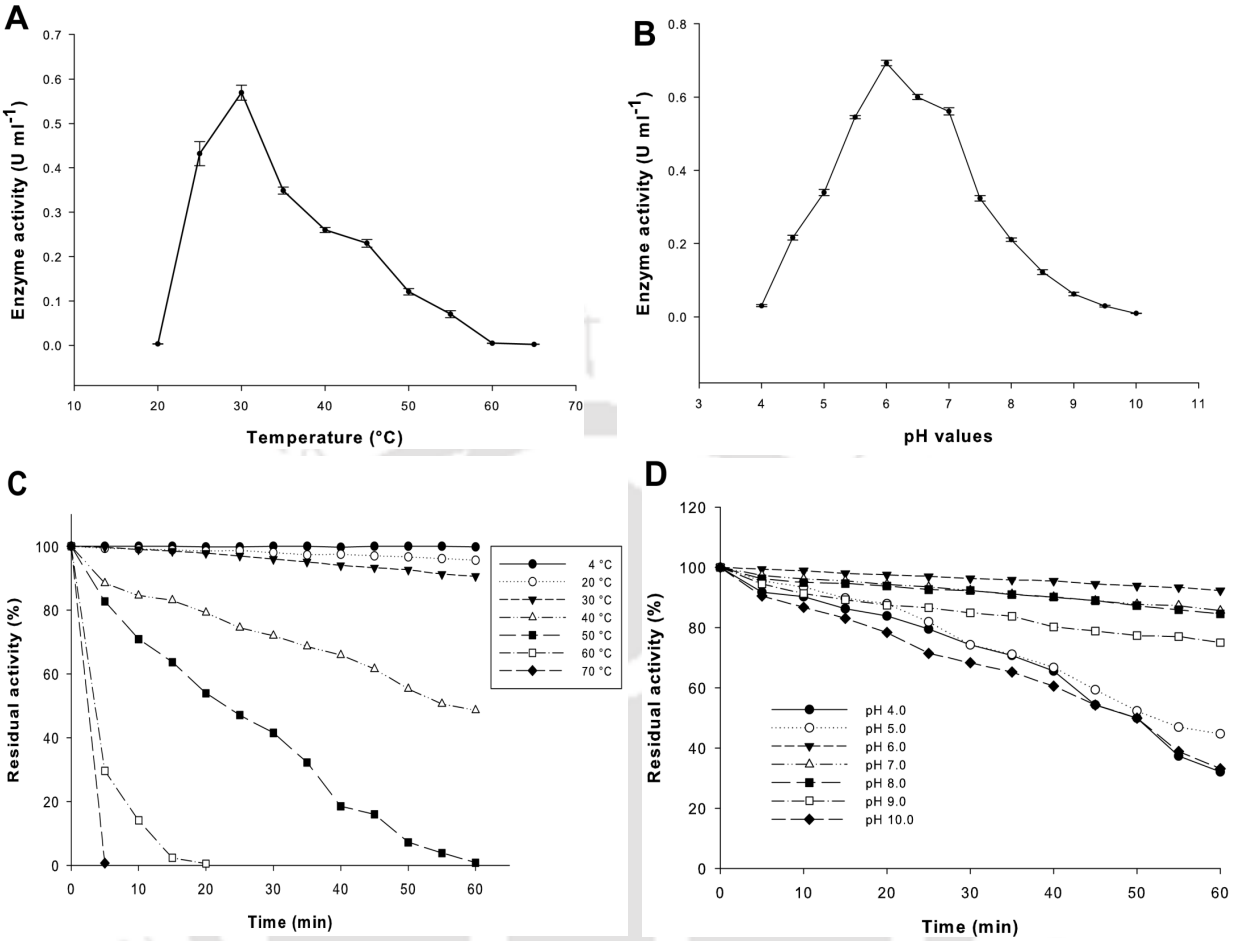

Figure 4.27. Studies on temperature and pH optima, thermal and pH stability of rAOx. Effect of temperature (**A**) and pH (**B**) on the activity of rAOx was studied using 5 mM *ρ*-anisyl alcohol in 100 mM sodium phosphate buffer. Data are the mean of three (n=3) independent experiments. (**C**) Thermal stability of rAOx when incubated for 1h at different termperature. Residual activity (%) was calculated taking enzyme activity value (in U mg^{-1}) with 5 mM *ρ*-anisyl alcohol as substrate in 100 mM sodium phosphate buffer, pH 6.0 as 100 %. (**D**) pH stability of rAOx at different pH buffer incubated for 1h. Residual activity was calculated as mentioned above. The pH 4.0 and 5.0 are 100 mM sodium acetate buffer, pH 6.0 to 8.0 are in 100 mM sodium phosphate buffer and pH 9.0 and 10.0 are in 100 mM Tris/HCl buffer.

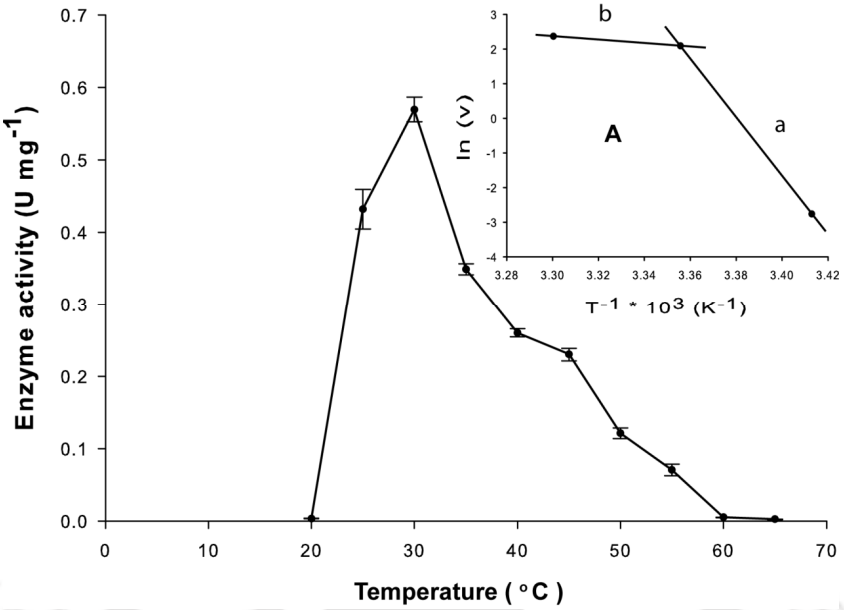

Figure 4.28. Effect of temperature on purified rAOx activity showing Arrhenius plot (A) as inset. Regression line (a) and (b) represents Arrhenius plot in temperature range of 20-25 °C and 25-30 °C, respectively.

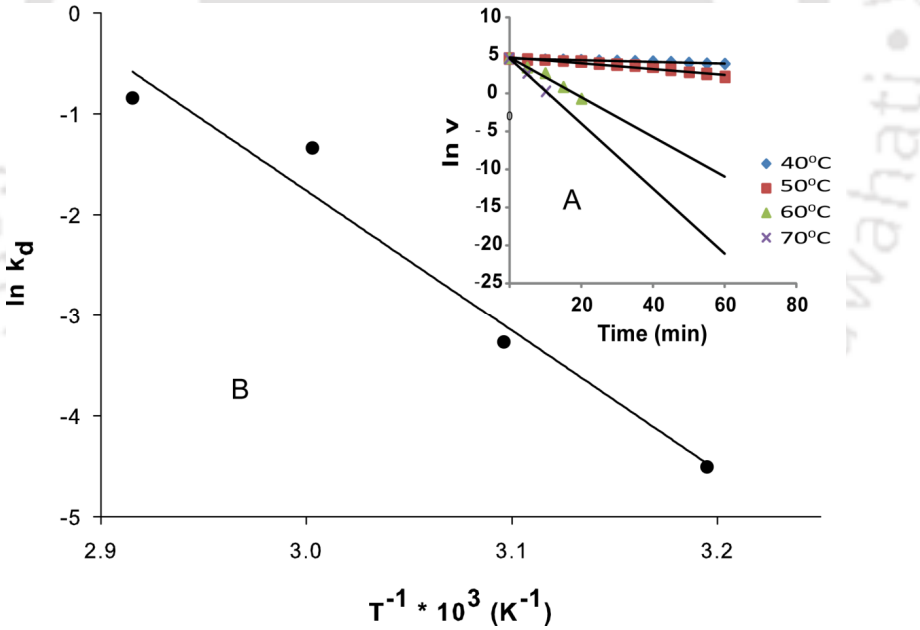

Figure 4.29. Temperature dependence of the thermo-inactivation constant of purified rAOx with an inset plot (A) showing the residual percentage activity in natural logarithm (ln v) versus the pre-incubation time after fitting the data in linear regression for calculation of k_d values. Slope of the plot of natural logarithm of k_d values versus T^{-1} (plot area B) predicted the conformational deactivation energy (Ea_d).

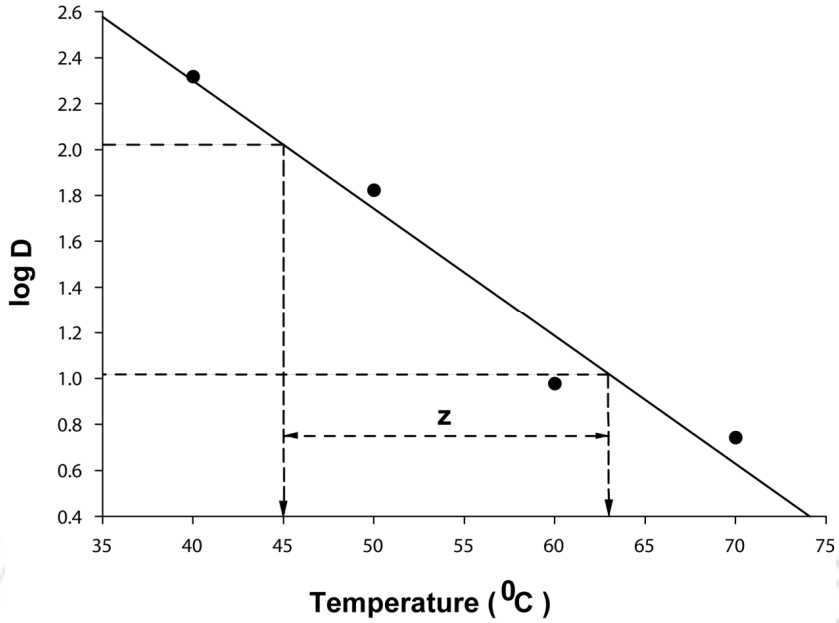

Figure 4.30. Temperature dependence of the decimal reduction value (*D*-value) of the purified rAOx. The value of the temperature interval required for traversing 1 log cycle is denoted by z in the above plot.

4.B Discussions

Characterization of AOx genes from methylotropic yeasts has been studied extensively, while the same is yet to be performed adequately in case of filamentous fungi (Goswami *et al*., 2013). Among the fungi, few basidiomycetes have been studied deeply on the function and molecular characteristics of the AOx produced by these strains. The function of the AOx from these sources is mostly ascribed to the oxidation of aryl alcohols to produce H_2O_2, which is involved in the peroxidative degradation of lignin (Ruiz-Dueñas and Martínez, 2009). Moreover, these aryl AOxs are produced extra cellularly by these lignin-degrading fungi and aryl alcohols are the known inducers for them. Conversely, *A.terreus* produces AOx intracellularly along with cytochrome P450 (CYP450) in the microsomes of the cell and the enzyme is well induced by the non-alcoholic substrates such as, hydrocarbons (Kumar and Goswami, 2006). The functional role of the AOxs from *A. terreus* is thus recognized as catalyst for the oxidation of the intermediate alcohol substrates formed during the CYP450 catalyzed degradation of various hydrocarbon substrates (Vatsyayan *et al*., 2008).

The future objective of the current work is to elucidate the active side residues through x-ray crystallographic study. Notably, recombinant AOx isolated from fungal expression system are difficult to crystallize due to the microheterogeniety of carbohydrate moieties and other contaminants which are also co-purified with the target protein (Ruiz-Dueñas *et al*., 2005). Moreover, fungal expression leads to glycosylation of the protein, which significantly increases the x-ray diffraction (Varela *et al*., 200a) leading to poor resolution of the crystal structure. Considering the above facts, *E.coli* has been considered for cloning and expression of the AOx gene from *A.terreus*. Moreover, in bacterial system the cloning strategy is straightforward and less time consuming as the protocol on heterologous expression in bacterial system and associated purification steps of the expressed protein has been substantially improved since last decade.

The reconstitution of the co-factor FAD with the apo-protein is a critical step in achieving functionally active protein. The refolding of the apo-AOx was achieved under alkaline and moderately low temperature conditions (Ruiz-Dueñas *et al*., 2005). However, to achieve high recovery of the reconstituted enzyme and to avoid the technical difficulty paused by the refolding

buffer in purifying the histidine tagged refolded protein through affinity column, the method was partially modified. Accordingly, the refolding step was performed after purifying the apo-AOx from the inclusion bodies through Ni^{2+}- affinity column. A significant recovery of the functionally active rAOx from inclusion bodies was achieved and the fluorescence data confirmed the successful incorporation of cofactor FAD with the protein matrix. CD study of the rAOx was carried out in presence of glycerol (a critical component of the refolding buffer), which prevented off-pathway aggregation and acted as an osmolyte thus conferred structural stability to our native refolded protein.

Comparing MALDI-TOF/TOF mass of apo-AOx with SDS-PAGE revealed a loss of ~1.6 kDa (mass of N-terminal and C-terminal 6x Histidine tag combined) possibly due to the poor ionization of trypsinized N- and C- terminal peptide fragments and poor detection at detector surface. The *p*I (6.5±0.1) of the apo-AOx was found to be more basic compared to the *p*I of other reported aryl rAOx expressed in *E.coli* (Ruiz-Dueñas *et al*., 2005). The reason is attributed to the presence of higher basic amino acid residues that constituted ~17% of the total amino acids present in the AOx protein.

The CD spectra are strongly dependent on pH as observed. The protein might have experienced conformational transition to a disordered state at pH below 6.0, which is evident from the increase in magnitude of the negative ellipticity (θ) at around 200 nm (Corrêa and Ramos, 2009). The pH dependent aggregation was apparent due to partial unfolding of the protein, evident from the light scattering observed at acidic pH. However, the aggregation is compensated to some extent by the presence of glycerol as a chaotropic agent. The primary aim of the present CD study with rAOx was to investigate the secondary structure of the protein which was successfully predicted as the ordered structure by comparing the results with the reports available for other similar protein. The time dependent CD analysis and detail light scattering studies were thus not considered in this investigation. We analyzed the effect of pH on the secondary structure conformation and found that the CD profile with a strong negative bands in the range from 200 to 260 nm and signal intensity at ~ 208 nm greater than at 222 nm which is a typical of α+β protein well studied for other proteins as reported by Yang *et al*, (1996).

Reports on the crystal structures of AOx enzymes from fungal sources are limited with PDB id 1VAO and 3FIM from *P. simplicissimum* (Mattevi *et al*., 1997) and *P. eryngii* (Varela *et*

al., 2000a), respectively are the most prominent submissions. Both these crystal structures revealed significant dissimilarities between their 3D structures as well as in their amino acid sequence content. Multiple sequence alignment of *A. terreus* rAOx with the above aryl AOxs from these lignin degrading strains revealed significant sequence diversity. The cDNA sequence of the aryl AOx from *A.terreus* deduced by us consisted of 666 amino acids, whereas, the widely studied aryl AOxs from *P. pulmonarius*, *P. eryngii* and *P. simplicissimum* consisted of 594, 593 and 560 amino acid residues, respectively (Varela *et al*., 1999; 2000a; Benen *et al*., 1998). The amino acid sequence identity (using NCBI BLAST) of *A. terreus* AOx with other aryl AOxs from *P. pulmonarius*, *P. eryngii* and *P. simplicissimum* showed 27 %, 25 % and 37 %, respectively. Even with the prevailing sequence variation, the predicted model of *A.terreus* rAOx showed significant structural homology with chain B of aryl AOx from *P. eryngii* (PDB id: 3FIM) (Fernández *et al*., 2009) and its function was that of an aromatic AOx. The Ramachandran plot predicted our modeled protein to be stereo-chemically significant, thus increasing the authenticity of the *ab-initio* based 3D model. Further validations of our modeled 3D structure were proven through docking simulation studies with its co-factor FAD, which precisely predicted the conserved N-terminal binding region (Rossmann fold; GXGXXG motif, X=any amino acid residue) in our model. The docking also confirmed the β-α-β fold essential for non-covalent interaction with FAD. Function as predicted by I-TASSER was further validated through docking simulations carried out with our modeled rAOx along with four aromatic alcohols used in our kinetic studies. Based on MolDock scoring function the substrates were evaluated on the basis of its binding energies and was found to be consistent with the kinetics studies. The docking studies clearly demonstrated the close proximity of the active substrate binding site and the co-factor FAD binding site separated by a narrow funnel shaped cavity connecting the both. It also confirmed that the active site lies in close vicinity of the FAD isoalloxazine ring. This kind of topology is conserved across all members of Glucose-Methanol-Choline (GMC) oxidoreductase family of proteins and is well reported (Ferreira *et al*., 2009; Hernández-Ortega *et al*., 2011a). Presence of few conserved aromatic amino acid residues (Phe 98 and Tyr 55) near the FAD isoalloxazine ring and substrate binding site could be involved in π-π stacking interaction with FAD isoalloxazine ring, thus stabilizing the co-factor. Molecular

modeling and docking results gave a visual insight into better understanding on the function and catalytic mechanism of this novel AOx enzyme.

In-vitro refolded rAOx showed an optimum temperature and pH of 30 °C and pH 6.0, respectively for its activity. A range of alcohol substrates for activity of the rAOx was studied and found that only the aryl alcohol substrates showed detectable activity for the recombinant enzyme. Steady-state kinetic parameters of rAOx were evaluated based on its catalytic activity exhibited for the oxidation of four different aromatic alcohols. Kinetic constants pertaining to V_{max}, K_m, k_{cat} and k_{cat} /K_m for each of the substrates tested revealed benzyl alcohol as a poor substrate while 4-methoxybenzyl alcohol (*ρ*-anisyl alcohol) being the best aromatic alcohol substrate followed by 3-methoxybenzyl alcohol (*m*-anisyl alcohol) and 3, 4-dimethoxybenzyl alcohol (veratryl alcohol). Variation in activation energies (Ea) observed in temperature range from 20-25°C (704.34 kJ mol-1) and 25-30°C (41.47 kJ mol-1) associated with conformational change in the catalytic site improving affinity.

Conformational deactivation energy (E_{ad} =119 kJ mol^{-1}) predicts a covalent interaction between substrate and enzyme active site leading to thermodynamically stable but catalytically inactive enzyme. A high decimal reduction value (*D* value) of thermoinactive rAOx predicted enzyme being unstable at higher temperatures. Enzyme half life ($t_{1/2}$) decreased significantly as temperature exceeds beyond the optimal temperature of 30°C for rAOx. Δ*H* and Δ*G* values were found to be constant predicting no change in enzyme heat capacity thus maintaining a stable structure. However, this is the first investigation on the thermoinactivation of recombinant AOx from filamentous fungi and no data exists pertaining to similar studies on the other reported and well studied AOxs for comparative analysis.

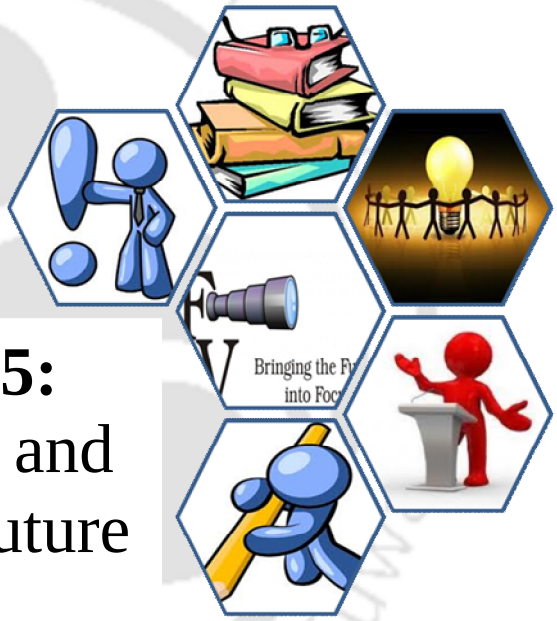

Chapter 5:
Conclusion and Scope for Future Work

Chapter 5

Conclusion and Future Direction of Research

5.A Conclusion

Characterization of an alcohol oxidase gene from a hydrocarbon degrading filamentous fungus, *Aspergillus terreus* MTCC 6324, has been successfully accomplished. This is the first report on the characterization of a full length coding nucleotide sequence of AOx from filamentous fungi following a combined proteomics and genomics approach. The characterized gene of 2001 bp has been successfully expressed as apo-AOx protein in an *E. coli* expression system. The significant sequence variation of the characterized *A.terreus* rAOx protein from the prevailing AOxs demonstrated the novelty of the protein. The apo-AOx was assembled with its co-factor FAD to a functionally active form following an established method with partial modification. Functionally, the rAOx was found to be closer to the aryl AOxs reported from few lignin degrading fungi. With the help of docking studies conserved topology and amino acid residues at FAD and substrate binding site were predicted. The docking studies predicted 4-methoxybenzyl alcohol as the best substrate for the rAOx which was later validated experimentally. Biophysical studies confirmed that the recombinant AOx protein folds in an ordered secondary structure after reconstitution with FAD. A very high aggregating tendency of the rAOx was also demonstrated. Thermo-inactivation studies confirmed that the recombinant AOx is thermodynamically stable but catalytically inactive and it retained a stable structure without any significant unfolding at denaturing temperatures. Recalling the previous work from this lab on the presence of different AOx activities in the cells of *A. terreus* MTCC 6324, the present findings on the identification aryl AOx coded by single gene hinted the existence of isozymes of different AOx activities in the native strain of this filamentous fungi.

The present work has advanced our knowledge on the characteristics of aryl AOx from the filamentous fungi, *A. terreus* and will open the scope for production of the functionally active enzyme through recombinant DNA technology.

5.B Future Direction of Research

The potential industrial applications of aryl AOx for the biocatalytic production of various flavor and aroma compounds, such as vanillin, benzaldehyde, *ρ*-anisaldehyde, has been well documented. The success of the present investigation on the heterologous expression of the functionally active aryl AOx has opened the scope of utilizing this novel enzyme in the said industrial venture. However, to use this recombinant enzyme for viable industrial applications further refinement on the molecular protocols for its improved preparation is essential. The striking gaps on the field which need to be addressed appropriately to full-fill the objectives are outlined below.

The expression protocol needs further tuning to harvest the recombinant apo-protein directly to the soluble fraction of the cell homogenate to obviate the additional steps of isolating the enzyme from inclusion bodies. The heterologous expression of AOx in eukaryotic host, although believe to create hindrance in crystallographic study, such expression route conversely promote the secretion of the apo-protein directly in to the soluble fraction thus, likely to facilitate the industrial production of this redox protein. The higher K_m value detected by us for the recombinant AOx may be attributed to the improper reconstitution of the co-factor FAD with the apo-AOx. Further improvement of the parameters involved in the reconstitution process may be necessary to realize the maximum functional activity of the construct. Additionally, systematic investigation on this enzyme through crystallization and site directed mutagenesis studies may help in understanding the mechanism of AOx catalyzed oxidation of aryl alcohol substrates and its tailored applications in the field of organic synthesis and industrial biotechnology.

Bibliography

Bibliography

Alberts AW, Chen J, Kuron G, Hunt V, Huff J, Hoffman C *et al* (1980) Mevinolin: A highly potent competitive inhibitor of hydroxymethylglutaryl-coenzyme A reductase and a cholesterol-lowering agent *Proc. Natl. Acad. Sci.*77:3957-3961.

Alvarado-Caudillo Y, Bravo Torres JC, Novoa VZ, Silva JH, Torres-Guzman JC, Gutierrez-Corona JF, Zazueta-Sandoval R (2002) Presence and physiologic regulation of alcohol oxidase activity in an indigenous fungus isolated from petroleum-contaminated soils. *Appl Biochem Biotech* 98:243-256.

Andrade MA, Chacón P, Merelo JJ, Morán F. (1993) Evaluation of secondary structure of proteins from UV circular dichroism using an unsupervised learning neural network. *Prot Engineering* 6: 383-390.

Azevedo AM, Vojinovic V, Cabral JMS, Gibson TD, Fonseca LP (2004) Operational stability of immobilized horseradishperoxidase in mini-packed bed bioreactors. *J. Mol. Catal B: Enzymatic* 28:12112-12118.

Banthorpe DV, Cardemil E, Del C, Contraras M (1976) Purification and properties of alcohol oxidase from *Tanacetum vulgare*. *Phytochem* 15:391-394.

Blasig R, Mauersberger S, Reige P, Schunck WH, Jockisch W, Franke P, Muller HG (1988) Degradation of long chain *n*-alkanes by the yeast *Candida maltosa*.Oxidation of *n*-alkanes and intermediates using microsomal membrane fractions. *Appl. Microbiol. Biotechnol.* 28:589-597.

Boteva R, Visser A, Filippi B, Vriend G, Veenhuis M. van der Klei IJ (1999) Conformational transitions accompanying oligomerization of yeast alcohol oxidase, a peroxisomal flavo-enzyme. *Biochemistry* 38:5034-5044.

Bourbonnais R, Paice MG (1988) Veratryl alcohol oxidases from the lignin degrading basidiomycete *Pleurotus sajorcaju*. *Biochem J* 255:445-450.

Bradford MM. (1976) Rapid and sensitive method for the quantization of microgram quantities of protein utilizing the principle of protein-dye binding. *Anal Biochem* 72: 248–254.

Bruckmann M, Termonia A, Pasteels JM, Hartmann T (2002) Characterization of an extracellular salicyl alcohol oxidase from larval defensive secretions of *Chrysomela populi* and *Phratora vitellinae* (*Chrysomelina*). *Insect Biochem Molec* 32:1517-1523.

Calam CT, Oxford AE, Raistrick H (1939) Studies in the biochemistry of micro-organisms: Itaconic acid, a metabolic product of a strain of *Aspergillus terreus* Thom. *Biochem J.* 33:1488–1495

Candiano G, Bruschi M, Musante L, Santucci L, Ghiggeri GM, et al. (2004) Blue silver: a very sensitive colloidal Coomassie G-250 staining for proteome analysis. *Electrophoresis.* 25: 1327-33.

Cardoso JP and Emery AN (1978) A new model to describe enzyme inactivation. *Biotechnol Bioeng*. 20, 1471-1477.

Chenchik A, Diachenko L, Moqadam F, Tarabyki V, Lukyano S, Sieber PD (1996) Full-length cDNA cloning and determination of mRNA 5′ and 3′ ends by amplification of adaptor-ligated cDNA. *BioTechniques* 21:526-534.

Cheng Q, Liu HT, Bombelli P, Smith A, Slabas AR (2004) Functional identification of AtFao3, a membrane bound long chain alcohol oxidase in *Arabidopsis thaliana*. *FEBS Lett* 574:62-68.

Chevallet M, Luche S, Rabilloud T. (2006) Silver staining of proteins in polyacrylamide gels. *Nat Protoc* 4: 1852–1858.

Chomczynski P, Sacchi N (1987) Single-step method of RNA isolation by acid guanidinium thiocyanate-phenol-chloroform extraction. *Anal Biochem.*162:156-9.\

Chung CT, Niemela SL, Miller RH (1989) One-step preparation of competent Escherichia coli: Transformation and storage of bacterial cells in the same solution. *Proc Natl Acad Sci* 86: 2172-2175.

Costanzo G, Di Mauro E, Negri R, Pereira G, Hollenberg C (1995) Multiple overlapping positions of nucleosomes with single in vivo rotational setting in the *Hansenula polymorpha* RNA polymerase II MOX promoter. *J Biol Chem* 270:11091-11097.

Dalbøge H, Lange L (1998) Using molecular techniques to identify new microbial biocatalysts. *TIBTECH*. 16:265-272.

Daniel G, Volc J, Filonova L, Plihal O, Kubátová E, Halada P (2007) Characteristics of *Gloeophyllum trabeum* alcohol oxidase, an extracellular source of H_2O_2 in brown rot decay of wood. *Appl Environ Microbiol* 73:6241-6253.

Dickinson FM, Wadforth C (1992) Purification and some properties of alcohol oxidase from alkane-grown *Candida tropicalis. Biochem J* 282:325-331.

Fan F, Germann MW, Gadda G (2006) Mechanistic studies of choline oxidase with betaine aldehyde and its isosteric analogue 3,3-dimethylbutyraldehyde. *Biochemistry* 45:1979–1986.

Farmer VC, Henderson ME, Russell JD (1960) Aromatic alcohol oxidase activity in the growth medium of *Polystictus versicolor*. *Biochem. J.* 74:257-262.

Fernández IS, Ruiz-Dueñas FJ, Santillana E, Ferreira P, Martínez MJ, et al. (2009) Novel structural features in the GMC family of oxidoreductases revealed by the crystal structure of fungal aryl-alcohol oxidase. *Acta Crystallogr D: Biol Crystallogr* 65: 1196 – 1205.

Ferreira P, Hernández-Ortega A, Herguedas B, Martínez AT, Medina M (2009) Aryl-alcohol oxidase involved in lignin degradation: a mechanistic study based on steady and pre-steady state kinetics and primary and solvent isotope effects with two different alcohol substrates. *J Biol Chem* 284:24840-4847.

Ferreira P, Hernández-Ortega A, Herguedas B, Rencoret J, Gutiérrez A, Martínez MJ, Jiménez-Barbero J, Medina M, Martínez AT (2010) Kinetic and chemical characterization of aldehyde oxidation by fungal aryl-alcohol oxidase. *Biochem J* 425:585-593.

Ferreira P, Medina M, Guillén F, Martínez MJ, van Berkel WJH, Martínez AT (2005) Spectral and catalytic properties of aryl-alcohol oxidase, a fungal flavoenzyme acting on polyunsaturated alcohols. *Biochem J* 389:731-738.

Fiser A, Sali A (2003) Modeller: generation and refinement of homology-based protein structure models. *Methods Enzymol*. 374:461-491.

Fraaije MW, R HH, van den Heuvel A, Mattevi WJH van Berkel Covalent (2003) Flavinylation enhances the oxidative power of vanillyl-alcohol oxidase. *J Mol Catal B: Enzym* 21:43-46.

Fraaije MW, Veeger C, van Berkel WJH (1995) Substrate specificity of flavin-dependent vanillyl alcohol oxidase from *Penicillium simplicissimum*. *Eur J Biochem* 234:271-277.

Fujii I, Ono Y, Tada H, Gomi K, Ebizuka Y, Sankawa U (1996) Cloning of the polyketide synthase gene atX from *Aspergillus terreus* and its identification as the 6-Methylsalicylic acid synthase gene by heterologous expression. *Mol Gen Genet* 253:1–10.

Gattiker A, Bienvenut WV, Bairoch A, Gasteiger E (2002) FindPept, a tool to identify unmatched masses in peptide mass fingerprinting protein identification. *Proteomics* 2:1435-1444.

Ghanem M, Gadda G (2005) On the catalytic role of the conserved active site residue His466 of choline oxidase. *Biochemistry* 44:893–904.

González JB, Baños JG, Covarrubias AA, Arroyo AG (2008) Lovastatin biosynthetic genes of Aspergillus terreus are expressed differentially in solid-state and in liquid submerged fermentation. *Appl. Microbiol. Biotechnol* 79: 179-186.

Görg A, Obermaier C, Boguth G, Harder A, Scheibe B, *et al*. (2000) The current state of two-dimensional electrophoresis with immobilized pH gradients. *Electrophoresis*. 6: 1037-53.

Goswami P, Chinnadayyala SSR, Chakraborty M, Kumar AK, Kakoti A. (2013) An overview on alcohol oxidases and their potential applications. *Appl Microbiol Biotechnol.* 97:4259–4275.

Goswami P, Cooney JJ (1999) Sub-cellular localization of enzymes involved in oxidation of n-alkane by *Cladosporium resinae*. *Appl Microbiol Biotechnol* 51:860-864.

Green MR, Sambrook J (2012) Molecular Cloning: a laboratory manual-4th ed. *Cold Spring Harbour Laboratory Press*, Cold Spring Harbour, New York, USA.

Greenspan MD, Yudkovitz JB (1995) Mevinolinic acid biosynthesis by *Aspergillus terreus* and its relationship to fatty acid biosynthesis. *J Bacteriol*.162:704–707.

Grewal N, Parveen Z, Large A, Perry C, Connock M (2000) Gastropod mollusk aliphatic alcohol oxidase: subcellular localization and properties. *Comp. Biochem. Phys. B.* 125: 543-554.

Gruzman MB, Titorenko VI, Ashin VV, Lusta KA, Trotsenko YA (1996) Multiple molecular forms of alcohol oxidase from the methylotrophic yeast *Pichia methanolica. Biochemistry (Moscow)* 61:1537-1544.

Guillen F, Martinez AT, Martinez MJ (1990) Production of hydrogen peroxide by aryl-alcohol oxidase from the ligninolytic fungus *Pleurotus eryngii*. *Appl Microbiol Biotechnol* 32:465-469.

Guillen F, Martinez AT, Martinez MJ (1992) Substrate specificity and properties of the aryl-alcohol oxidase from the ligninolytic fungus *Pleurotus eryngii*. *Eur J Biochem* 209:603-611.

Gurkan C, Symeonides SN, Ellar DJ (2004) High-level production in *Pichia pastoris* of an anti-p185HER-2 scFv using an alternative secretion expression vector. *Biotechnol Appl Biochem* 39:115-122.

Gvozdev AR, Tukhvatullin IA, Gvozdev RI (2010) Purification and properties of alcohol oxidase from *Pichia putida*. *Biochemistry (Moscow)* 75:242-248.

Gvozdev AR, Tukhvatullin IA, Gvozdev RI (2010) Purification and properties of alcohol oxidase from *Pichia putida*. *Biochemistry (Moscow)* 75:242-248.

Hartner FS, Glieder A (2006) Regulation of methanol utilisation pathway genes in yeasts. *Microb Cell Fact* 5:39. doi:10.1186/1475-2859-5-39.

Hernández-Ortega A, Borrelli K, Ferreira P, Medina M, Martínez AT, Guallar V (2011a) Substrate diffusion and oxidation in GMC oxidoreductases: an experimental and computational study on fungal aryl-alcohol oxidase. *Biochem J* 436:341–350.

Hernández-Ortega A, Ferreira P, Martínez AT (2012a) Fungal aryl-alcohol oxidase: a peroxide-producing flavoenzyme involved in lignin degradation. *Appl Microbiol Biotechnol* 93:1395–1410.

Hernández-Ortega A, Lucas F, Ferreira P, Medina M, Guallar V, et al. (2011b) Modulating O2 reactivity in a fungal flavoenzyme: involvement of aryl-alcohol oxidase Phe-501 contiguous to catalytic histidine. *J. Biol. Chem* 286: 41105–41114.

Holzmann K, Schreiner E, Schwab H (2002) A *Penicillium chrysogenum* gene (AOX) identified by specific induction upon shifting pH encodes for a protein which shows high homology to fungal alcohol oxidases. *Curr Genet* 40:339-344

Hommel R, Ratledge C (1990) Evidence for two fatty alcohol oxidases in the biosurfactant-producing yeast *Candida* (Torulopsis) *bombicola*. *FEMS Microbiol Lett* 70:183-186.

Hommel RK, Lassner D, Weiss J, Kleber HP (1994) The inducible microsomal fatty alcohol oxidase of *Candida (Torulopsis) apicola*. *Appl Microbiol Biotechnol* 40:729-734.

Huang K, Fujii I, Ebizuka Y, Gomi K, Sankawa U (1995) Molecular Cloning and Heterologous Expression of the Gene Encoding Dihydrogeodin Oxidase, a Multicopper Blue Enzyme from *Aspergillus terreus*. *J Biol Chem* 270:21495-21502.

Ilchenko AP (1984) Oxidase of higher alcohols in the yeast *Torulopsis candida* grown on hexadecane. *Mikrobiologiya* 53:903-906.

Isobe K, Kato A, Ogawa J, Kataoka M, Iwasaki A, Hasegawa J, Shimizu S (2007) Characterization of alcohol oxidase from *Aspergillus ochraceus AIU 031*. *J Gen Appl Microbiol* 53:177-183.

Isobe K, Kawakami Y (2007) Preparation of convection interaction media isobutyl disc monolithic column and its application to purification of secondary alcohol dehydrogenase and alcohol oxidase. *J Chromatography:A* 1144:85-89.

Janssen FW, Kerwin RM, Ruelius HW (1965) Alcohol oxidase, a novel enzyme from a basidiomycete. *Biochem Biophys Res Commun*. 20:630-634.

Janssen FW, Ruelius HW (1968) Alcohol oxidase, a flavoprotein from several basidiomycetes species: Crystallization by fractional precipitation with polyethylene glycol. *Biochim Biophy Acta.* 151:330-342.

Jeanmougin F, Thompson JD, Gouy M, Higgins DG, Gibson TJ. (1998) Multiple sequence alignment with Clustal X. *Trends Biochem Sci* 23: 403-405.

Kanamasa S, Dwiarti L, Okabe M, Park EY (2008) Cloning and functional characterization of the cis-aconitic acid decarboxylase (CAD) gene from *Aspergillus terreus*. *Appl. Microbiol. Biotechnol* 80:223–229.

Karp H, Jarviste A, Kriegel TM, Alamäe T (2003) Cloning and biochemical characterization of hexokinase from the methylotrophic yeast *Hansenula polymorpha*. *Curr Gent* 44: 268-276.

Kawagoshi Y, Fujita M (1997) Purification and properties of polyvinyl alcohol oxidase with broad substrate range obtained from *Pseudomonas vesicularis var. povalolyticus* PH. *World J Microbiol Biotechnol* 13:273-277.

Kawai F, Hu X (2009) Biochemistry of microbial polyvinyl alcohol degradation *Appl Microbiol Biotechnol* 84:227–237.

Keilin D, Hartree EF (1945) Properties of catalase catalysis of coupled oxidation of alcohols. *Biochem. J.* 39:293-300.

Kellogg RM, Kruizinga W, Bystrykh LV, Dijkhuizen L, Harder W (1992) Structural analysis of a stereochemical modification of flavin adenine dinucleotide in alcohol oxidase from methylotrophic yeast. *Tetrahedron* 48*:*4147-4162

Kemp GD, Dickinson FM, Ratledge C (1988) Inducible long chain alcohol oxidase from alkane-grown *Candida tropicalis*. *Appl. Microbiol. Biotechnol.* 29:370-374.

Kemp GD, Dickinson FM, Ratledge C (1990) Light sensitivity of the n-alkane-induced fatty alcohol oxidase from *Candida tropicalis* and *Yarrowia lipolytica*. *Appl Microbiol Biotechnol* 32:461-464.

Khan F, He M, Taussig MJ (2006) Double-hexahistidine tag with high-affinity binding for protein immobilization, purification, and detection on Ni-nitrilotriacetic acid surfaces. *Anal. Chem*. 78: 3072–3079.

Kimura M, Takatsuki, Yamaguchi I. (1994) Blasticidin S deaminase gene from Aspergillus terreus (BSD): a new drug resistance gene for transfection of mammalian cells. *Biochimica et Biophysica Acta* 1219: 653-659.

Ko HS, Fujiwara H, Yokoyama Y, Ohno N, Amachi S, Shinoyama H, Fujii T (2005) Inducible production of alcohol oxidase and catalase in a pectin medium by *Thermoascus aurantiacus* IFO 31693. *J Biosci Bioeng* 99:290-292.

Koutz P, Davis GR, Stillman C, Barringer K, Cregg J, Thill G (1989) Structural comparison of the *Pichia pastoris* alcohol oxidase genes. *Yeast* 5:167-177.

Kramarenko T, Karp H, Jarviste A, Alamäe T (2004) Sugar repression in the methylotrophic yeast *Hansenula polymorpha* studied by using hexokinase-negative, glucokinase-negative and double kinase-negative mutants. *Folia Microbiol* 5:521-529.

Krauzova VI, II chenko AP, Sharyshev AA, Lozinov AB (1985) Possible pathways of the oxidation of higher alcohols by membrane fractions of yeast culture on hexadecane and hexadecanol. *Biochimie* 50:726-732.

Krauzova VI, Komarova GN, Il'chenko AP, Gulevskaia SA (1984) Alcohol oxidation by *Candida guilliermondii* yeasts grown on hexadecanol. *Mikrobiologiya* 53:621-627.

Kumar AK, Goswami P (2009) Dissociation and reconstitution studies of a broad substrate specific multimeric alcohol oxidase protein produced by *A. terreus. J Biochem* 145:259-265.

Kumar AK, Goswami P. (2006) Functional characterization of alcohol oxidases from *Aspergillus terreus* MTCC 6324. *Appl. Microbiol. Biotechnol.* 72: 906–911.

Kumar AK, Goswami P. (2008) Purification and properties of a novel broad substrate specific alcohol oxidase from *Aspergillus terreus* MTCC 6324. *BBA-Protein. Proteom.* 1784:1552–1559.

Kumar V. and Rapheal V (2010) Induction and purification by three phase partitioning of aryl alcohol oxidase (AAO) from *Pleurotus ostreatus*. *Appl Biochem Biotechnol* 163:423-443.

Laemmli UK. (1970) Cleavage of structural proteins during the assembly of the head of bacteriophage T4, *Nature* 227: 680–685.

Laht S, Karp H, Kotka P, Jarviste A, Alamäe T (2002) Cloning and characterization of glucokinase from a methylotrophic yeast *Hansenula polymorpha*: different effects on glucose repression in *H. polymorpha* and *Saccharomyces cerevisiae. Gene* 296:195-203

Lario PI, Sampson N, Vrielink A (2003) Sub-atomic resolution crystal structure of cholesterol oxidase: what atomic resolution crystallography reveals about enzyme mechanism and the role of the FAD cofactor in redox activity. *J Mol Biol* 326:1635–1650.

Laskowski RA, MacArthur MW, Moss DS, Thornton JM. (1993) *PROCHECK*: a program to check the stereochemical quality of protein structures. *J. Appl. Cryst* 26: 283-291.

Lee JD, Komagata K (1983) Further taxonomic study of methanol-assimilating yeasts with special references to electrophoretic comparison of enzymes. *J Gen Appl Microbiol* 29:395-416.

Li Y, Wang W, Du X, Yuan Q. (2010) An improved RNA isolation method for filamentous fungus *Blakeslea trispora* rich in polysaccharides. *Appl Biochem Biotechnol* 160: 322–327.

Lomsadze A, Ter-Hovhannisyan V, Chernoff YO, Borodovsky M (2005) Gene identification in novel eukaryotic genomes by self-training algorithm. *Nucleic Acids Research* 33: 6494–6506.

Marchler-Bauer A, Lu S, Anderson JB, Chitsaz F, Derbyshire MK, et al. (2011) CDD: a Conserved Domain Database for the functional annotation of proteins. *Nucleic Acids Res, Database issue* 39: D225–D229.

Matsunaga T, Kishi N, Tanaka H, Watanabe K, Yoshimura H and Yamamoto I (1998) Major cytochrome P450 enzyme responsible for oxidation of secondary alcohols to the corresponding ketones in mouse hepatic microsomes: Oxidation of 7-hydroxy-D8-tetrahydrocannabinol to 7-oxo-D8-tetrahydrocannabinol. *Drug Metab. Dispos.* 26:1045-1047.

Mattevi A, Fraaije MW, Coda A, van Berkel WJH (1997) Crystallization and preliminary X-ray analysis of the flavoenzyme Vanillyl alcohol oxidase from *Penicillium simplicissimum*. *Proteins* 27:601-603.

Mauersberger S, Kargel E, Matyashova RN, Muller HG (1987) Subcellular organization of alkane oxidation in the yeast *Candica maltosa*. *J Basic Microbiol* 27:565-582.

Moreau RA, Huang AHC (1979) Oxidation of fatty alcohol in the cotyledons of jojoba seedlings. *Arch Biochem Biophys* 194:422-430.

Moreau RA, Huang AHC (1981) Enzymes of wax ester catabolism in jojoba. *Methods Enzymol* 71:804-813.

Morita M, Hamada N, Sakai K, Watanabe Y (1979) Purification and properties of secondary alcohol oxidase from a strain of *Pesudomonas*. **Agric Biol Chem** 43:1225-1235.

Morita M, Watanabe Y (1977) A secondary alcohol oxidase: a component of a polyvinyl alcohol degrading enzyme preparation. *Agric Biol Chem* 41:1535-1537.

Nakagawa T, Uchimura T, Komagata K (1996) Isozymes of methanol oxidase in a methanol utilizing yeast, *Pichia methanolica IAM 12901*. J Ferment Bioeng 81:498-503.

Ng IS, Zheng X, Chen BY, Chi X, Lu Y, Chang CS (2013) Proteomics approach to decipher novel genes and enzymes characterization of a bioelectricity-generating and dye-decolorizing bacterium *Proteus hauseri* ZMd44. *Biotechnol Biopro Engineer* 18: 8-17.

Nicholas KB, Nicholas HB Jr, Deerfield DW II. (1997) GeneDoc: Analysis and Visualization of Genetic Variation. *EMBNEW.NEWS* 4: 14.

Ozimek P, Veenhuis M, Van der Klei IJ (2005) Alcohol oxidase: A complex peroxisomal, oligomeric flavoprotein. *FEMS Yeast Res* 5:975-983

Qian D, Du G, Chen J (2004) Isolation and culture characterization of a new poly vinyl alcohol degra ding strain : *Penicillium sp. WSH02–21*. *World J Microbiol Biotechnol* 20:587-591.

Quaye O, Lountos GT, Fan F, Orville AM, Gadda G (2008) Role of Glu312 in binding and positioning of the substrate for the hydride transfer reaction in choline oxidase. *Biochemistry* 47:243–256.

Rao S, Rossmann M. (1973) Comparison of super-secondary structures in proteins. *J. Mol. Biol.* 76: 241–56.

Robelo CR, Novoa VZ, Sandoval RZ (2004) Effects of Carbon Source on Expression of Alcohol Oxidase Activity and on Morphologic Pattern of YR-1 Strain, a Filamentous Fungus Isolated from Petroleum-Contaminated Soils. *Appl Biochem Biotechnol* 113-116.

Romero E, Martínez AT, Martínez MJ (2010) Molecular characterization of a new flavooxidase from a *Bjerkandera adusta* anamorph. *Proc OESIB, Santiago de Compostela*, 14–15 September.

Roy A, Kucukural A, Zhang Y. (2010) I-TASSER: a unified platform for automated protein structure and function prediction. *Nature Protocols* 5: 725–738.

Ruiz-Dueñas FJ, Ferreira P, Martínez MJ, Martínez AT (2005) In vitro activation, purification, and characterization of *Escherichia coli* expressed aryl alcohol oxidase, a unique H_2O_2 producing en-zyme. *Protein Expr Purif* 45:191-199.

Ruiz-Dueñas FJ, Martínez AT (2009) Microbial degradation of lignin: how a bulky recalcitrant polymer is efficiently recycled in nature and how we can take advantage of this. *Microbial Biotechnol* 2:164-177.

Sahm H (1977) Metabolism of methanol by yeasts. *Adv Biochem Eng* 6:77-103.

Sakai K, Hamada N, Watanabe Y (1985) Purification and properties of secondary alcohol oxidase with an acidic isoelectric point. *Agric Biol Chem* 49:817-825.

Sakai K, Hamada N, Watanabe Y (1986) Degradation mechanism of poly(vinyl alcohol) by successive reactions of secondary alcohol oxidase and β-diketone hydrolase from Pseudomonas sp. *Agric Biol Chem* 50:989–996.

Sakai Y, Tani Y (1992) Cloning and sequencing of the alcohol oxidase-encoding gene (AOD1) from the formaldehyde-producing asporogeneous methylotrophic yeast, *Candida boidinii* S2. *Gene* 114:67-63.

Savitha J, Ratledge C (1991) Alcohol oxidase of *Aspergillus flavipes* grown on hexadecanol. *FEMS Microbiol Lett* 80:221-224.

Schierová M, Linka M, Pazoutová S (2000). Sulfate assimilation in *Aspergillus terreus*: analysis of genes encoding ATP-sulfurylase and PAPS-reductase. *Curr. Genet*. 38: 126-31.

Schwanke RC, Renard G, Chies JM, Campos MM, Batista Junior EL, *et al*. (2009) Molecular cloning, expression in *Escherichia coli* and production of bioactive homogeneous recombinant human granulocyte and macrophage colony stimulating factor. *International Journal of Biological Macromolecules* 45: 97–102.

Segers G, Bradshaw N, Archer D, Blissett K, Oliver RP (2001) Alcohol oxidase is a novel pathogenic factor for *Cladosporium fulvum*, but aldehyde dehyrogenase is dispensible. *Mol Plant Microbe In* 13:367-377.

Shevchenko A, Tomas H, Havliš J, Olsen JV, Mann M. (2007) In-gel digestion for mass spectrometric characterization of proteins and proteomes. *Nat Protoc 1*: 2856 – 2860.

Shevchenko A, Tomas H, Havliš J, Olsen JV, Mann M. (2007) In-gel digestion for mass spectrometric characterization of proteins and proteomes. *Nat Protoc* 1: 2856 – 2860.

Shimao M, Nishimura Y, Kato N, Sakazawa C (1985) Location of polyvinyl alcohol oxidase produced by a bacterial symbiont, *Pseudomonas sp. strain VM15C. Appl Environ Microbiol* 49:8-10.

Shimao M, Tsuda T, Takahashi M, Kato N, Sakazawa C (1983) Purification of membrane-bound polyvinyl alcohol oxidase in *Pseudomonas sp VM15C. FEMS Microbiol Lett* 20:429-433.

Silva-Jiménez H, Zazueta-Novoa V, Durón-Castellanos A, Rodríguez-Robelo C, Leal-Morales CA, Zazueta-Sandoval R (2009) Intracellular distribution of fatty alcohol oxidase activity

in *Mucor circinelloides YR-1* isolated from petroleum contaminated soils. *Antonie Van Leeuwenhoek* 96:527-535.

Silva-Jiménez H, Zazueta-Sandoval R (2005) Intracellular fate of hydrocarbons: possible existence of specific compartments for their biodegradation. *Appl Microbiol Biotechnol* 121-124:205-217.

Slabas AR, Elborough K, Vanhanen S, West M, Cheng Q, Lindner N, Casey J, Sanglard D (1999) *International patent application* WO 99/47685.

Smidt OD, Preez JCD, Albertyn J (2008) The alcohol dehydrogenases of *Saccharomyces cerevisiae*: a comprehensive review. *FEMS Yeast Research* 8:967-978.

Soldevila AI, and Ghabrial SA (2001) A novel alcohol oxidase/ RNA-binding protein with affinity for mycovirus double-stranded RNA from the filamentous fungus Helminthosporium (Cochliobolus) victoriae: molecular and functional characterization *J Biol Chem* 276:4652–4661

Srisuk N, Limtong S, Yurimoto H, Sakai Y, Kato N (2006) Physiological Study and Alcohol Oxidase Gene(s) of Thermotolerant Methylotrophic Yeasts Isolated in Thailand. *Kasetsart J (Nat. Sci.)* 40:121-135.

Stasyk OV, Stasyk OG, Komduur J, Veenhuis M, Cregg JM, Sibirny AA (2004) A hexose transporter homologue controls glucose repression in the methylotrophic yeast *Hansenula polymorpha*. *J Biol Chem* 279:8116-8125.

Suye SS (1997) Purification and properties of alcohol oxidase from *Candida methanosorbosa* M-2003. *Curr Microbiol* 34:374-377.

Suzuki T (1976) Purification and some properties of polyvinyl alcohol degrading enzyme produced by *Pseudomonas*. *Agric Biol Chem* 40:497-504.

Tamboli DP, Telke AA, Dawkar VV, Jadhav SB, Govindwar SP. (2011) Purification and characterization of bacterial Aryl Alcohol Oxidase from *Sphingobacterium* sp. ATM and its uses in textile dye decolorization. *Biotechnol Biopro Engineer* 16:661-668.

Tamura K, Stecher G, Peterson D, Filipski A, Kumar S (2013) MEGA6: Molecular Evolutionary Genetics Analysis version 6.0. *Mol Biol Evol* doi: 10.1093/molbev/mst197.

Tani Y, Miya T, Ogata K (1972) The microbial metabolism of methanol. *Agric. Biol. Chem* 36: 68-75.

Thomsen R, Christensen MH. (2006) MolDock: a new technique for high-accuracy molecular docking. *J. Med. Chem*. 49: 3315–3321.

Unden G, Bongaerts J (1997) Alternative respiratory pathways of *Escherichia coli*: energetics and transcriptional regulation in response to electron acceptors. *Biochimica et Biophysica Acta* 1320:217-234.

van den Heuvel RHH, Fraaije MW, Laane C, van Berkel WJ (2001a) Enzymatic synthesis of vanillin. *J Agric Food Chem* 49:2954–2958.

Van Der Klei IJ, Harder W, & Veenhuis M. (1991) Biosynthesis and assembly of alcohol oxidase, a peroxisomal matrix protein in methylotrophic yeasts: A review. *Yeast.* 7: 195-209.

Vanhanen S, West M, Kroon JTM, Lindner N, Casey J, Cheng Q, Elborough KM, Slabas AR (2000) A consensus sequence for long-chain fatty-acid alcohol oxidases from *Candida* identifies a family of genes involved in lipid.omega-oxidation in yeast with homologues in plants and bacteria. *J Biol Chem* 275:4445-4452.

Varela E, Bockle B, Romero A, Martinez AT, Martinez MJ (2000a) Biochemical characterization, cDNA cloning and protein crystallization of aryl-alcohol oxidase from *Pleurotus pulmonarius*. *Biochim Biophys Acta* 1476:129–138

Varela E, Guillen A, Martinez AT, Martinez MJ (2001) Expression of *Pleurotus eryngii* aryl alcohol oxidase in *Aspergillus nidulans*: purification and characterization of the recombinant enzyme. *Biochim Biophys Acta* 1546:107–113.

Varela E, Jesús Martínez M, Martínez AT (2000b) Aryl-alcohol oxidase protein sequence: a comparison with glucose oxidase and other FAD oxidoreductases. *Biochim Biophys Acta* 1481:202–208.

Varela E, Martinez AT, Martinez MJ (1999) Molecular cloning of aryl-alcohol oxidase from the fungus *Pleurotus eryngii*, an enzyme involved in lignin degradation. *Biochem. J.* 341: 113-117.

Vatsyayan P, Kumar AK, Goswami P, Goswami P. (2008) Broad substrate Cytochrome-P450-monooxygenase activity in the cells of *Aspergillus terreus* MTCC 6324. Biores. Technol. 99: 68–75.

Ventura L, Antonio J, Gonzalez P, Ramon D (1997) Cloning and molecular analysis of the *Aspergillus terreus* arg1 gene coding for an ornithine carbamoyltransferase. *FEMS Microbiol Letters* 149: 207-212.

Vojinovic V, Azevedo AM, Martins VCB, Cabral JMS, Gibson TD, Fonseca LP (2004) Assay of H_2O_2 by HRP catalysed co-oxidation of phenol-4-sulphonic acid and 4-aminoantipyrine: characterisation and optimisation. *J. Mol. Catal B: Enzym* 28:129-135.

Walker JD, Cooney JJ. (1973) Aliphatic hydrocarbons of Cladosporium resinae cultured on glucose, glutamic acid and hydrocarbons. *Appl. Microbiol. Biotechnol.* 26:705-708.

Watanabe Y, Hamada N, Morita M, Tsujisaka Y (1976) Purification and properties of a polyvinyl alcohol-degrading enzyme produced by a strain of Pseudomonas. *Arch Biochem Biophys* 174:575–581.

Weblink 1: http://mycota-crcc.mnhn.fr

Weblink 2: http://www.broadinstitute.org

Weblink 3: http://www.doctorfungus.org/thefungi/Aspergillus_terreus.php

Werner W, Rey HG, Weilenger H. (1970) Uber die eigenschaften eine neuen chromogens fur die blutzuckerbestimmung nach der GOD/POD methode, *Z. Anal. Chem*. 254: 224–228

Whitmore L, Wallace BA. (2004) DICHROWEB, an online server for protein secondary structure analyses from circular dichroism spectroscopic data. *Nucleic Acids Research* 32:668-673.

Whitmore L, Wallace BA. (2008) Protein secondary structure analyses from circular dichroism spectroscopy: methods and reference databases. *Biopolymers* 89: 392-400.

Wilm M, Shevchenko A, Houthaeve T, Breit S, Schweigerer L, Fotsis T, Mann M (1996) Femtomole sequencing of proteins from polyacrylamide gels by nano-electrospray mass spectrometry. *Nature* 379: 466-469.

Woodward JR (1990) Biochemistry and applications of alcohol oxidase from methylotrophic yeasts. In: Codd GA, Dijkhuizen L, Tabita FR, Hoff DMN (eds) *Advances in Autotrophic Microbiology and One-Carbon Metabolism. Leeds, UK*, pp 205-238.

Yamatsu A, Matsumi R, Atomi H, Imanaka T (2006) Isolation and characterization of a novel poly(vinyl alcohol)-degrading bacterium, Sphingopyxis sp. PVA3. *Appl Microbiol Biotechnol* 72:804–811.

Zeng Y, Yang T (2002) RNA isolation from high viscous samples rich in polyphenols and polysaccharides. *Plant Molecular Reporter* 20: 417a-417e.

Zhang Y, Li Y, Shen W, Liu D, Chen J (2006) A new strain, *Streptomyces venezuelae* GY1, producing a poly(vinyl alcohol)- degrading enzyme. *World J Microbiol Biotechnol* 22:625–628.

Zhao S, Lin Z, Ma W, Luo D, Cheng Q (2008) Cloning and characterization of long-chain fatty alcohol oxidase LjFAO1 in *lotus japonicas*. *Biotechnol Prog*. 24:773-779.

Zlateva T, Boteva R, Filippi B, Veenhuis M, van der Klei IJ (2001) Deflavination of flavo-oxidases by nucleophilic reagents. *Biochim Biophys Acta* 1548:213-219.\

Appendix

Appendix

Table A1. Culture medium for bacteria

Media	Constituents	Concentration (g l^{-1})	pH
Luria Bertani broth (LB)	Casein enzymic hydrolysate	10.0	7.5±0.2
	Yeast extract	5.0	
	NaCl	10.0	
Luria Bertani agar (LB)	Casein enzymic hydrolysate	10.0	7.5±0.2
	Yeast extract	5.0	
	NaCl	10.0	
	Agar	15.0	

Note: Both the above bacterial media were procured as a readymade powdered media from HIMEDIA Laboratories (India). LB broth and LB agar were prepared by mixing 25.0 g l^{-1} and 40.0 g l^{-1}, respectively and autoclaved at 15 lb (121^0C) for 15 min before inoculating with bacterial culture.

Table A2. Composition of *n*-hexadecane basal medium

Components	Concentration (g l^{-1})
$MgSO_4.7H_2O$	0.2
NH_4NO_3	1.0
$CaCl_2$	0.02
KH_2PO_4	1.0
K_2HPO_4	1.0
$FeCl_3$	0.002
Yeast extract	1.0

Note: The components were mixed and the pH of the medium was adjusted to 5.8. 50 ml of basal medium was transferred to 500 ml Erlenmeyer flasks and 2% (v/v) *n*-hexadecane was added to the medium for AOx induction. The media containing the substrate was sterilized at 15 lb (121^0C) for 15 min before inoculating with fungal mycelium.

Table A3. Composition of *A.terreus* lysis buffer

Components	Concentration
EDTA	10 mM
MgCl2	1 mM
PMSF	1 mM

Note: The above components were added to 50 mM Tris/HCl buffer, pH 8.0 and after disrupting the cells, the cell homogenate was immediately mixed with 1 mM DTT. Do not autoclave the lysis buffer.

Table A4. List of buffers

Buffers/solutions	Concentration	Composition	pH
Tris/HCl buffer	50 mM	Tris base (6.057 g l^{-1})	8.0 with 1N HCl
MOPS electrophoresis buffer	10X stock	MOPS (200 mM, pH 7.0) Sodium acetate (80 mM) EDTA (10 mM, pH 8.0)	8.0
TAE-Tris Acetate EDTA buffer	50X , 100 ml stock	Tris base (24.2 g) Glacial acetic acid (5.71 ml) 0.5M EDTA, pH 8.0 (10 ml)	8.0
Tris-glycine SDS gel running buffer	10X, 1 l stock	Tris base (30.0 g) Glycine (144.0 g) SDS (10.0 g)	8.3
Sodium phosphate buffer	100 ml, 0.2 M (stock)	19 ml 0.2 M NaH_2PO_4 (solution A) 81 ml 0.2 M Na_2HPO_4 (solution B)	7.4
Binding buffer for Ni^{2+} affinity chromatography	NA	20 mM sodium phosphate buffer pH 7.4, 500 mM NaCl, 4 M urea and 20 mM immidazole	7.4
Elution buffer for Ni^{2+} affinity chromatography	NA	20 mM sodium phosphate buffer pH 7.4, 500 mM NaCl, 4M urea and 500 mM immidazole	7.4

Note: Binding buffer and elution buffer used for Ni2+ affinity chromatography were filter sterilized with 0.22 or 0.45 micron filter. NA stands for not applicable.

Table A5. Transformation and storage solution for bacterial competent cell preparation

Components	Concentration
LB broth (pH 6.1)	Appropriate volume as required
PEG (MW ~ 3350)	10 % (w/v)
$MgCl_2$	10 mM
$MgSO_4$	10 mM

Note: Adjust the pH of the final solution to pH 6.5, autoclave at 15 lb (121^0C) for 15 min and store at 4^0C.

Table A6. List of oligonucleotide PCR primers

Sl No	Name	Sequence (5'- 3')
1	GAPDH-F	CAAGGTCATCCATGACAACTTTG
2	GAPDH-R	GTCCACCACCCTGTTGCTGTAG
3	AOX-FP1	ATGACTATTCCAGACGAAGTCGACA
4	AOX-RP1	TGAGACCAGGATCCATGCTGGAT
5	AOX-FP2	ACAGTCCCCTCCAAGCCGCT
6	AOX-RP2	TTACAGTCGAGCAAGCCCAGTAAACTC
7	AOX-pET28a-F	GCC**GAATTC**ATGACTATTCCAGACGAAG
8	AOX-pET28a-R	CGC**AAGCTT**CAGTCGAGCAAGCCCAGT

Note: Restriction sites added to the PCR primers are highlighted in bold with its base pairs underlined.

Table A7. Solutions for plasmid isolation

Solutions	Composition	pH
Solution I	50 mM glucose, 25 mM Tris/HCl buffer (pH 8.0), 10 mM EDTA (pH 8.0)	8.0
Solution II	NaOH (freshly diluted from a 10N stock), 1% (w/v) SDS	___
Solution III	60.0 ml Potassium acetate (5M stock), 11.5 ml glacial acetic acid, 28.5 ml ddH_2O	___

Note: Solution I should be prepared in batch of ~100 ml, autoclaved at 15 lb (121^0C) for 15 min and store at 4^0C. Solution II should be prepared fresh and use at room temperature. Solution III should not be autoclaved and stored at 4^0C. Solution I and III should be chilled on ice prior to use.

Table A8. List of restriction enzymes

Restriction Enzyme	Recognition site	100% activity in NEB buffer	Temperature of incubation (^{0}C)	Time of incubation	Heat inactivation (^{0}C)	Heat inactivation time
*Eco*RI-HF (high fidelity)	G/AATTC	Buffer 4	37	5 h	65	20 min
*Bgl*II	A/GATCT	Buffer 3	37	5 h	No	__
*Nde*I	CA/TATG	Buffer 4	37	5 h	65	20 min
*Hind*III-HF (high fidelity)	A/AGCTT	Buffer 4	37	5 h	80	20 min

Table A9. Composition of bacterial lysis buffer

Components	Concentration
Sodium phosphate buffer (pH 7.4)	20 mM
DTT	5 mM
PMSF	1 mM

Note: DTT and PMSF were added just prior to use and no autoclave is required.

Table A10. List of antibiotics

Name	Stock Concentration (mg ml^{-1})	Solvent	Working concentration (µg ml^{-1})
Ampicillin	100	ddH_2O	50-100
Kanamycin	50	ddH_2O	25-50

Note: All the antibiotic was filter sterilized and appropriate aliquots were stored at -20^0C until further use. Repeated freeze/thaw cycles should be avoided.

Table A11. Buffer/solutions for SDS-PAGE

Buffers/solutions	Compositions
30 % acrylamide-bisacrylamide solution (100 ml)	29.2 g acrylamide, 0.8 g bisacrylamide
0.5 M Tris/HCl pH 6.8 (100 ml)	6.06 g of Tris base, pH adjusted to 6.8 with 2 N HCl.
1.5 M Tris/HCl pH 8.8 (100 ml)	18.18 g Tris base, pH adjusted to 8.8 with 2 N HCl.
Tris-glycine SDS gel running buffer	Appendix Table A4
SDS gel loading buffer (2X)	100 mM Tris/HCl (pH 6.8), 4% (w/v) SDS, 0.2% (w/v) Bromophenol blue, 20% (v/v) glycerol, 200 mM DTT or β-mercaptoethanol

Note: DTT if used should be added just prior to use.

Table A12. Blue silver staining solution for SDS-PAGE

Components	Concentration
DdH_2O	Required amount
Ortho phosphoric acid	10 % (v/v)
Ammonium sulfate	10 % (w/v)
CBB G250	0.12% (w/v)
Methanol	20% (v/v)

Note: Add the following components in the order as given in the table. An initial volume of water was taken to dissolve the components and later the volume was make-up to the final desired volume by adding more ddH_2O.

Table A13. Buffers /solutions used for Western Blot

Buffers/solutions	Components
Protein transfer buffer	25 mM Tris base, 39 mM glycine, 20% (v/v) methanol
Phosphate buffer saline (PBS) (1 l), pH7.5	11.5 g Di-sodium hydrogen orthophosphate, 2.96 g Sodium dihydrogen orthophosphate, 5.84 g Sodium chloride
Phosphate buffer saline with Tween 20, washing buffer (PBS-T)	Add 0.05% (v/v) Tween 20 to PBS
Blocking solution	3% (w/v) BSA in PBS-T

Table A14. List of antibodies

Name	Source/Type	Working condition	Working dilution	Use
Anti-poly-histidine antibody	Mouse/monoclonal	RT/2 h	1:3000	Primary antibody in western blot
Anti-mouse IgG (Fab specific)-peroxidase antibody	Goat/monoclonal	RT/1 h	1:6000	Secondary antibody in western blot

Table A15. List of scoring parameters in I-TASSER

Scoring function	Detailed description
Confidence score (C-score)	Confidence score for estimating the quality of predicted models by I-TASSER. Significance of threading template alignments and the convergence parameters of the structure assembly simulations C-score is typically in the range of [-5,2], where a C-score of higher value signifies a model with a high confidence and vice-versa
Template modeling score (TM-score)	Scale for measuring the structural similarity between two structures. The small distance is weighted stronger than the big distance. A TM-score > 0.5 indicates a model of correct topology and a TM-score < 0.17 means a random similarity. The cut off independent of protein length.
Root mean square deviation (RMSD)	Parameter for measuring structural similarity between two structures which are usually used to measure the accuracy of structure modeling when the native structure is known. Where the native structure is not known, distance between the predicted model and the native structure predicts the quality of the modeling prediction. RMSD is an average distance of all residue pairs in two structures.

Table A16. List of plasmid vectors

Name	Company	Use	Promoter	Selection marker (s)	Cloning site
pGEM-T Easy	Promega	T/A cloning vector	T7 lac promoter	Amp^r	*EcoR*I *site*
pET-28a (+)	Novagen	Bacterial expression vector	T7 lac promoter	Kan^r	Multiple cloning site (*BamH*I- *Xho*I)

Figure A1. Vector maps of plasmids used

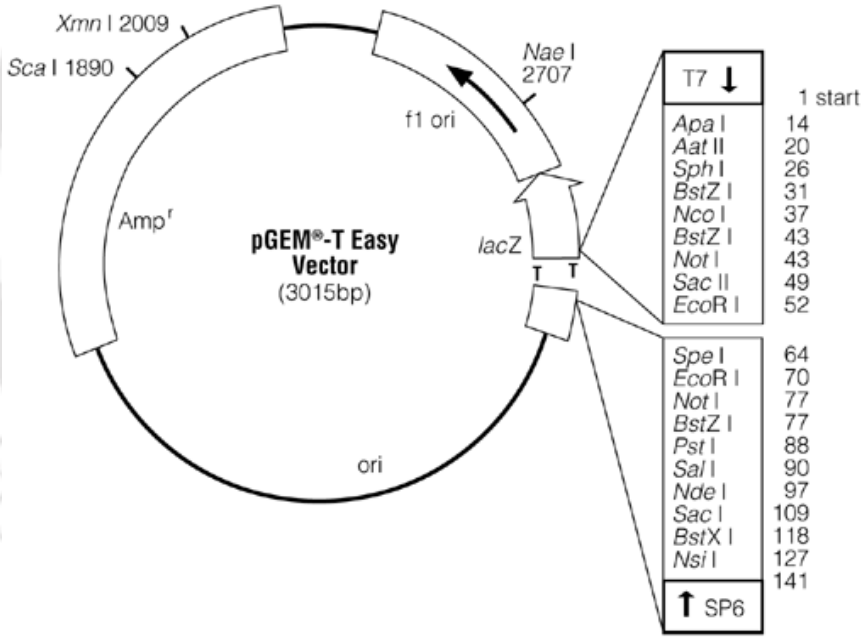

Figure A1.A. Plasmid map of pGEM-T Easy T/A cloning vector (adapted from www.promega.com)

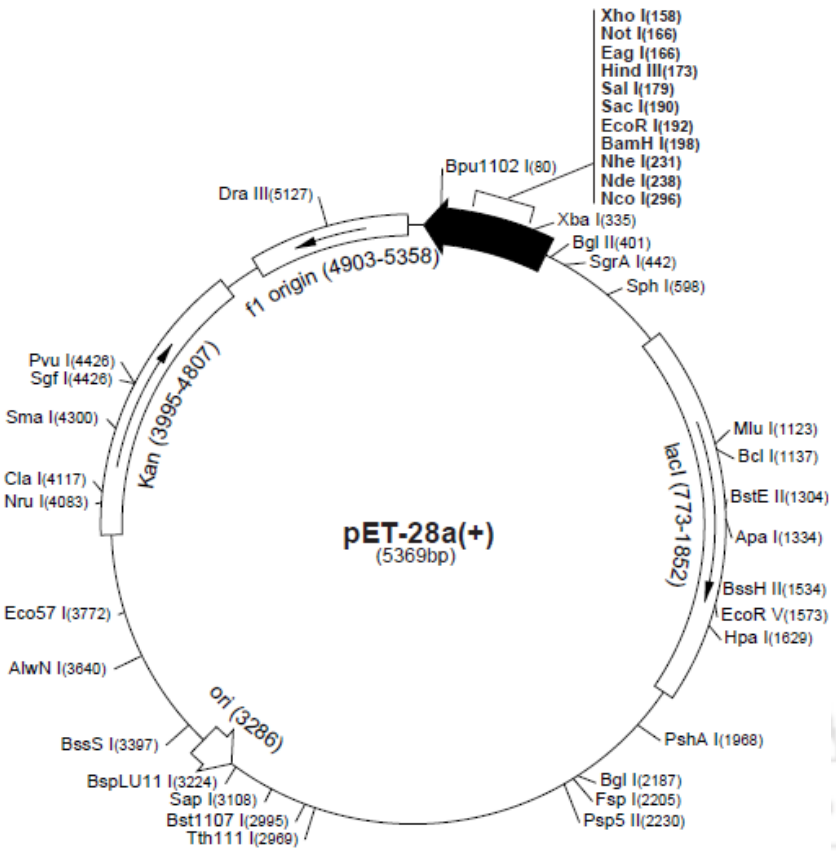

Figure A1.B. Plasmid map of pET28a (+) bacterial expression vector (adapted from www.novagen.com)

Publications

List of Publications

A. In Referred Journals

Chakraborty M, Goel M, Chinnadayyala SR, Dahiya U**,** Ghosh SS, Goswami P (2013) Molecular characterization and expression of a novel alcohol oxidase from *Aspergillus terreus* MTCC6324. *PLoS One (communicated with minor corrections and under review*).

Goswami P, Chinnadayyala SR, **Chakraborty M**, Kumar AK, Kakoti A (2013) An overview on alcohol oxidases and their potential applications. *Appl Microbiol Biotechnol* 13:4842-4849. (*Equal second author contribution*)

Saxena U, **Chakraborty M**, Goswami P (2011) Covalent immobilization of cholesterol oxidase on self-assembled gold nanoparticles for highly sensitive amperometric detection of cholesterol in real samples. *Biosensors and Bioelectronics* 26:3037–3043.

Vatsyayan P, **Chakraborty M**, Bordoloi S, Goswami P (2011) Electrochemical investigations of fungal cytochrome P450, *Journal of Electroanalytical Chemistry* 662:312-316.

B. NCBI/GenBank submission

Chakraborty M, Ghosh SS, Goswami P (2012) *Aspergillus terreus* alcohol oxidase protein (AOx) mRNA, complete cds. GenBank **Acc. #: *JX139751***.

C. Abstracts Published in Conferences

Chakraborty M, Goel M, Ghosh SS, Goswami P (2012) Molecular characterization and structure function relationship studies of a novel alcohol oxidase from *Aspergillus terreus* MTCC 6324. World Congress on Biotechnology, Hyderabad, India. May, 2012, Book of Proceedings, Abstract no: P-88, Pg No: 76. (**adjudged as best poster presentation award**).

Chakraborty M, Ghosh SS, Goswami P (2011) Partial characterization of novel broad Substrate specific alcohol oxidase from *Aspergillus terreus* MTCC 6324 through molecular and in-silico approach. International Conference on New Horizons in Biotechnology and 8th Annual Convention of The Biotech Research Society , India (NHBT-2011), Organized and hosted by NIIST, CSIR, Trivandrum, India. November, 2011. Abstract no: IB-133. Pg No:140.

Saxena U, **Chakraborty M,** Goswami P (2010) Gold nanoparticle based cholesterol biosensor.International. Conference On Frontier in Biological Sciences (InCOFIBS 2010), National Institute of Technology, Rourkela, India. October, 2010. Pg No: 139 **(Adjudged as best paper in the category).**